Ministry of Higher Education & Scientific Research

Ninevah University

College of Electronics Engineering

Communication Engineering Department

Investigation of Frequency Selective Surfaces (FSS) with Absorbing Properties

Amina Jamal Rashid

M.Sc. dissertation

In

Communication Engineering

Supervised by

Prof. Dr. Khalil Hassan Sayidmarie

2022 A.C   **1443A.H**

Investigation of Frequency Selective Surfaces (FSS) with Absorbing Properties

A Dissertation Submitted by

Amina Jamal Rashid

To

The Council of College of Electronic Engineering

University of Nineveh

In Partial Fulfillment of the Requirements
For the Degree of Master of Science

In

Communication Engineering

Supervised by

Prof. Dr. Khalil Hassan Sayidmarie

Supervisor's Certification

I certify that the dissertation entitled (**Investigation of Frequency Selective Surfaces (FSS) with Absorbing Properties**) was prepared by **Amina Jamal Rashid** under my supervision at the Department of Communication Engineering, Ninevah University, as a partial requirement for the Master of Science Degree in Communication Engineering.

Signature: *Sayidmarie*
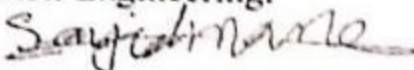
Name: Prof. Dr. Khalil Hassan Sayidmarie

Department of Communication Engineering / Ninevah University

Date: 14 / 3 / 2022

Linguistic Advisor Certification

I certify that the linguistic evaluation of this dissertation entitled **"Investigation of Frequency Selective Surfaces (FSS) with Absorbing Properties"** was carried out by me and it is accepted linguistically and in expression.

Signature: *Salih*

Name: Dr. Salih Abdullah Abdulrahman

Date: /   / 2022

Postgraduate Committee Certification

According to the recommendations presented by the supervisor of this dissertation and the linguistic reviewer, I nominate this dissertation to be forwarded to discussion.
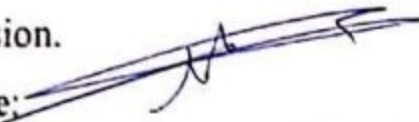
Signature:

Name: Assistant Prof. Dr. Mahmod A. Mahmod

Date: /   / 2022

Department Head Certification

I certify that this dissertation was carried out in the Department of Communication Engineering. I nominate it to be forwarded to discussion.

Signature:
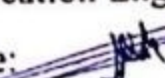
Name: Assistant Prof. Dr. Mahmod A. Mahmod

Date: /   / 2022

Committee Certification

We the examining committee, certify that we have read this dissertation entitled **(Investigation of Frequency Selective Surfaces (FSS) with Absorbing Properties)** and have examined the postgraduate student **(Amina Jamal Rashid)** in its contents and that in our opinion; it meets the standards of a dissertation for the degree of Master of Science in Communication Engineering.

Signature:

Name: Prof. Dr. Jafar R. Mohammed
Head of committee
Date: / 5 / 2022

Signature:

Name: Assist. Prof. Dr. Yasser A. Fadhel
Member
Date: / 5 / 2022

Signature:

Name: Dr. Adham M. Saleh
Member
Date: 8 / 5 / 2022

Signature:

Name: Prof. Dr. Khalil H. Sayidmarie
Member and Supervisor
Date: / 5 / 2022

The college council, in its ………… meeting on   /   / 2022, has decided to award the degree of Master of Science in Communication Engineering to the candidate.

Signature:

Name: Prof. Dr. Khaled Khalil Muhammad

Dean of the College

Date: / /2022

Signature:

Name: Assist. Prof. Dr. Sedki Baker Thenon

Council registrar

Date: / /2022

Acknowledgments

First and foremost, I want to thank Allah, the Almighty, for guiding me through this research. I want to thank everyone who helped completion of this project.

I would also like to express my gratitude to my supervisor Prof. Dr. Khalil H. Sayidmarie for mentoring and inspiring me to accomplish this project, and I am grateful to him for his support and encouragement. His advice was quite helpful in guiding the project on the appropriate path.

I would like to thank the former head of department Dr. Younis Abbosh, and the current head of department Dr. Mahmod for providing the facilities needed for this research, and for their encouragement, and advice.

Furthermore, I would like to thank all of the staff members of the department of communication engineering who assisted me during my study, the support received from my friends and their cooperation. Thanks to everyone who has helped me to finish this research.

Last but not least, I would also like to offer my thanks to my entire family for providing me with the opportunity to study and for supporting me during my education. Importantly, thanks from my heart I present to my father, and my mother for their endless sacrifices and unlimited support throughout my entire life and, for always believing in me. Finally, a special thank goes out to my older brother, who has always boosted my confidence by supporting me in all situations.

Abstract

With the growing use of electromagnetic waves, the problems of electromagnetic interference are becoming more important. An effective electromagnetic wave absorber must be used to absorb a portion of the input wave with minimal reflections. A typical method of avoiding electromagnetic (EM) interference is to utilize materials with high conductivity, such as metals, as shielding, or materials with low resistance. The dissertation investigates the use of frequency selective surfaces (FSS) as an efficient shielding. A single layer of copper rings combined with dielectric and air spacer was proposed. The effects of diameter and air spacer thickness were investigated, showing a small reflection at the operating frequency. The equivalent circuit and estimations for resonance frequencies were derived, as well as the ring impedance. The case of the split ring resonator with four gaps was implemented to demonstrate the effect of gap length on absorption. The modified frequency selective surface absorber (FSSA) that has lumped resistors in each gap shows an improvement in absorption bandwidth when different parameters like the lumped resistors, the thickness of the air spacer, and the width of the ring are changed.

A single layer of a resistive ring and a resistive ground plane was proposed to reduce reflection and increase bandwidth. The effects of diameter and air spacer thickness were investigated, showing better reflection and bandwidth compared to the copper ring. An FSSA of a resistive split ring resonator having two gaps is presented to demonstrate the effect of changing gap length on the absorption band. The development of an FSSA with a resistive strip along the diameter of the ring was studied for two different electric field directions. The effects of resistivity and air spacer thickness were investigated, which is described as an electric field along the strip, the structure exhibited better absorption bandwidth than those when the electric field is perpendicular to the strip.

TABLE OF CONTENTS

LIST OF TABLES

LIST OF FIGURES

LIST OF ABBREVIATIONS

Abbreviation	Name
EM	Electromagnetic
EMF	Electromagnetic field
FDTD	Finite difference time domain
FEM	Finite element method
FBW	Fractional bandwidth
FSS	Frequency selective surface
FSSA	Frequency selective surface absorber
ITO	Indium tin oxide
MA	Metamaterial absorber
ML	Meander lines
MMA	Miniaturized metamaterial absorber
MoM	Method of moments
PET	Polyethylene terephthalate
RCS	Radar cross-section
RF	Radio frequency
RFID	Radio frequency identification
RLC	Resistance-inductance- capacitance
SCR	Split circle ring
UHF-RFID	Ultra high frequency -radio frequency identification
WLAN	Wireless local area network
WiMAX	Worldwide Interoperability for Microwave Access
GSM	Global System for mobile communication

LIST OF SYMBOLS

Symbol	Name
Ae	Effective cross-sectional area
BW	Bandwidth
d	Length of square loop
E	Electric field intensity
E_0	The initial value of electric field intensity
$\overline{E_\iota}, \overline{E_t}, \overline{E_r}$	Incident, transmitted and reflected electric field intensity
$\overline{H_\iota}, \overline{H_t}, \overline{H_r}$	Incident, transmitted and reflected magnetic field intensity
$E_x^{(1)}$	Electric field intensity along X-direction
$H_y^{(1)}$	Magnetic field intensity along Y-direction
E_y	Electric field intensity along Y-direction
d_a	Average diameter of the ring
d_{out}	Outer diameter of the ring
d_{in}	Inner diameter of the ring
D	Electric flux density
f_o	Resonance frequency
g	Gap length
h_1	Substrate thickness
h_2	Air spacer thickness
h	Total thickness

l	Average circumference of the ring.
P	Periodicity of square loop
Q-factor	Quality factor
θ_i	Angle of incidence
θ_t	Angle of transmission
θ_r	Angle of reflected
R_{s1}	Square patch Resistance
R_{s2}	Square loop Resistance
R_{s3}	Spiral shape Resistance
t_1	Square patch thickness
t_2	Square loop thickness
t_3	Spiral shape thickness
V_o	Applied voltage
w	Ring width
Z_e	Equivalent impedance of the ring
Z_{in}	Input impedance
Z_t	Terminated impedance
Z_0	Free space impedance
Z_1	Equivalent impedance of the ground plane
η_1	Intrinsic impedance of the first medium
η_2	Intrinsic impedance of the second medium
β_0	Phase constant

β_1	Phase constant of the first medium
ε_r	Dielectric constant or relative permittivity of the medium
ε_{rc}	Effective dielectric constant for the composite layer
ε_e	Effective relative dielectric constant due to the fringing field
ε_1	Dielectric constant of the first medium
ε_{r_1}	Dielectric constant of substrate
ε_{r_2}	Dielectric constant of air spacer
δ	Skin depth
Γ	Reflection coefficient
γ	Propagation constant
λ_e	Effective wavelength
λ_L	wavelength at Lower frequency
λ_o	Free space wavelength
α_o	Absorption factor
μ_1	Permeability of the first medium
ρ	Resistivity

CHAPTER ONE

INTRODUCTION

CHAPTER ONE
INTRODUCTION

1.1 Overview

Frequency selective surfaces (FSS) are surface structures that can be used to change the phase, amplitude, or polarization of the incident wave. They are a type of periodic structure that can be viewed as a spatial filter for electromagnetic (EM) waves that performs bandpass or bandstop responses. These structures have given a wide spectrum of systems, ranging from low-frequency radio to optical. Frequency-selective surfaces in absorbers have attracted considerable attention because of the increased absorption bandwidth that may be achieved with small structure thicknesses.

A frequency-selective surface absorber (FSSA), in the form of a two-dimensional or three-dimensional array, could absorb undesired electromagnetic wave energy and convert it to heat or other forms of energy. Absorption was widely employed for Radio frequency (RF)/ microwave circuit devices also in commercial, industrial, and military applications. In order to improve the absorber's performance, metallic FSS are proposed for the construction of integrated absorbers that are combined with lumped resistors or resistive materials to add ohmic losses to the FSS.

1.2 Brief History of FSS Absorber

A comprehensive review of the FSS and its application was presented by Ben Munk in 2000 [1]. The Salisbury screen was the first concept for FSS [2, 3] and was employed to make targets invisible to radar. The absorber design was a simple structure that consists of a lossy screen placed at a quarter wavelength distance

above the ground plane. Despite their simplicity, they suffer from a somewhat narrow absorption bandwidth.

The Jaumann absorber is then introduced by using multiple resistive sheets placed in front of a perfectly conducting plane [4,5] which offers wideband absorption but at the expense of increasing overall thickness. Absorbing materials like carbon and ferrite [6–8] provide a compact solution for attenuating reflections, however, this absorber has a narrow bandwidth, bulkiness, breakability, and huge thickness which limits its use to portable applications. The circuit analog absorber is like a Salisbury but incorporates a periodic structure that increases the absorption and enhances the resonance. The development of the design was extended either by using resistive or conductive surfaces with multi-resonance [9–13] and /or multilayer structure [14–17].

1.3 Literature Review

An attempt to describe the resonance behavior of single and double square loops using an equivalent circuit model was reported by Langley and Parker [18, 19] in 1982 and 1983. They described in [18] the equivalent circuit model of the periodic array of a single loop comprising of series LC circuits, on the other hand, that concept is only applicable for a free-standing structure. Shang et al. in 2013, optimize the broadband absorber design for double loop FSS with air spacer using the full-wave simulator [10]. In 2020, Hossain et al. proposed a method for nonmagnetic absorbers employing single and multilayer FSS based on an efficient electric circuit model. The focus of the paper was on the difficult requirements of thin absorbers working at lower microwave frequencies with greater bandwidth [20].

In 2006, Kiani et al. presented a dual absorb/transmit frequency selective surface capable of absorbing 5 GHz wireless local area network (WLAN) signal while passing mobile phone signals [21]. In 2007, Tao et al. investigated FSSA using cross-shaped resistive patches stacked on a single dielectric substrate, which improved the absorbing performance of radar absorbing materials [22]. In the same year, Kiani et al. reported that a dual-layer absorb/ transmit for WLAN was an improvement, which shows better frequency stability for both polarizations under a normal or oblique incident wave [23].

In 2007, Zhang et al. proposed the first design containing lumped resistors, the structure has a single square loop welded with two lumped resistors. The proposed design presented a reflection coefficient below -20 dB, and can cover a frequency band from (6 to 12 GHz) for a thickness of 0.162 λ_L (λ_L wavelength at lower frequency) [24]. In 2010, Costa et al. investigated the lossy frequency selective surface of a resistive square patch placed over a dielectric substrate. The presented intended to a wide bandwidth of reflectance less than -15 dB over a frequency band of (7 - 20 GHz) with a thickness around 0.12 λ_L [25]. In 2011, Rafique et al. designed a two-layer absorber, one with resistive FSS and the other with conducting FSS. The proposed FSS design used for 5 GHz WLAN protection provides absorption for WLAN signals while letting other important RF/microwave signals like mobile phones to pass through. Also, the design exhibits a stable frequency response for oblique incident angles [26].

In 2012, the design of a circular patch and a ground plane separated by a dielectric substrate was described by Liu et al. The results demonstrate that the suggested absorber exhibits strong absorptivity at an absorption bandwidth of (9.65 - 12.45 GHz), with fractional bandwidth (FBW) equivalent to 25.3%, at thickness of 0.026 λ_L [27]. In the same year, Li et al. presented a triple resistive

square loop mounted on dielectric covered by a ground plane. The suggested design exhibited ultrathin and broadband absorbers covering a frequency range of (10.7 - 29 GHz), which is equivalent to 92.2%, with a thickness of 0.071 λ_L [28].

In 2012, Zhang et al. studied a square ring of resistive pattern and a metallic ground plane attached to a single substrate. The proposed FSS shows a fractional bandwidth of 111.6%, covering the range of frequency from (4 to 14.1 GHz) of a thickness of 0.1 λ_L [29]. In 2013, a polarization-insensitive double circular ring metamaterial absorber (MA) working at 10 GHz was proposed by Ayop et al. An absorption bandwidth of 0.47 GHz (9.78 - 10.25 GHz), was achieved at a thickness of 0.057 λ_L [30]. In the same year, Shang et al. designed a single layer using double square loops loaded with lumped resistors. The proposed design revealed three resonances, which exhibited wide absorption fractional bandwidth of about 126% in the range from (2 to 10 GHz) for a thickness of 0.088 λ_L [10].

In 2014, Yuan et al. proposed an electric metal resonator loaded with resistors combined with the dielectric substrate and ground plane. The presented design exhibited broadband absorption less than -10 dB in the frequency range of (2.85 - 5.31 GHz), at a fractional bandwidth of about 60.3% for a thickness of 0.047 λ_L [31]. In 2015, a polarization-independent MA comprising two dielectric substrates has been proposed by S. Bhattacharyya. A two-circular ring is designed as a unit cell on the upper side of both layers. It was found that the structure is polarization insensitive under large angles. The proposed design show bandwidth-enhanced for both C and X bands (6.10 - 7.34 GHz) and (8.36 - 10.28 GHz), respectively, while the thickness was 0.065 λ_L [17]. In the same year, Chen et al. investigated polarization-insensitive double-circle rings connected with lumped resistances over a ground plane. The simulation results reveal that the suggested

absorber provides wide absorption (8.87 - 16.47 GHz), equivalent to 60%, for a thickness of 0.089 λ_L [12].

In 2016, Kundu et al. designed conductive crossed dipoles with lumped resistors. The presented design was imprinted on a dielectric layer and is supported by a ground plane. It offers 104.76% absorption bandwidth from (3.75 to 12 GHz) for a thickness of 0.077 λ_L [32]. In the same year, Liu, and Kim investigated single resistive square loop and ground plane. The dielectric substrate is incorporated between two layers. The proposed design provided a wide bandwidth of 107.89% around the frequency range (4.9 - 16.4GHz), for a thickness of 0.12 λ_L [33]. In the same year, Ghosh et al. reported a multilayer square loop structure with lumped resistors. The proposed design was posted on dielectric substrates separated from the second layer by an air spacer. The simulated result reveals a reflectance of less than -10 dB in the frequency range (4.96 - 18.22 GHz), with a fractional bandwidth of 114.40% under a large incidence angle, with a thickness of 0.076 λ_L [14].

A polarization-insensitive square loop employing lumped resistors was proposed by Ghosh et al, in 2016. The suggested design exhibits a bandwidth covering X and Ku bands from (7.56 to 14.58 GHz) for fractional bandwidth of 63.41%, with an overall thickness of 0.076 λ_L [34].

In 2018, Chen et al. presented a design for a double layer absorber, the proposed design is composed of two lossy layers loaded with resistors, one is a single square loop, while the other is a double square loop, which exhibits five resonance frequencies. The whole design offers a wide bandwidth of 165.5% with a reflectance lower than −10 dB spans from (1.64 to 17.36 GHz), for thickness of 0.1 λ_L [16]. In the same year, Nguyen, and Lim proposed a polarization-insensitive broadband absorber consisting of a fan-shaped splice into four gaps

with inserted four lumped resistors in each gap. The presented absorber is embedded over the dielectric cover with the ground plane, acquiring an absorption bandwidth of about 58.58% in the frequency range of (7 - 12.8 GHz) for a thickness of 0.079 λ_L [35].

In 2018, Ahmad et al. presented a single-layer FSSA constructed from a rectangular loop with lumped resistance coated on the ground plane. The proposed design achieved an absorption bandwidth of 72% between (14.2 - 30.3 GHz) with a thickness of 0.124 λ_L [36]. In the same year, Abdulhakim et al. presented a wideband absorber with polarization-independent circuit analog absorber by using a cross loop with lumped resistor imprinted on a dielectric substrate. The proposed absorber exhibits a 10 dB reduction bandwidth of more than 126.5% over the entire frequency range (4.6 - 20.45 GHz), with a thickness of 0.088 λ_L [37].

In 2019, Haitao et al. proposed a broadband absorber with a resistive circular loop for improvement absorption at low frequency, printed on a magnetic substrate etched on the ground plane. The presented design exhibited an absorption bandwidth of about 82% in the frequency range from (6.76 to 15.97GHz) with a total thickness of 0.045 λ_L [38], thus offering advantages of thin, broadband absorption, and stability over large incident angle. In the same year, Chen et al. presented a polarization insensitive circular ring fed with four lumped resistors combined with a dielectric substrate over the ground plane. The simulation result shows a polarization-insensitive under oblique incident wave. A wide absorption bandwidth of 79.8% was achieved, covering the entire X and Ku bands (7.95–18.5 GHz), for a thickness of 0.066 λ_L [39].

Kalraiya et al. presented in 2019, a polarization-independent design comprising a circular ring and slotted section connected by four lumped resistors

to enhance the absorption bandwidth. An air spacer is incorporated between the dielectric and the ground plane. The proposed design achieved a fractional bandwidth of 91.6% between (3.90 - 10.5 GHz), for a 0.28 λ_L thickness. With its symmetrical arrangement of rings, the absorber is unaffected by the polarization of the incoming wave [40]. In the same year, Youssef et al. reported that the two layers of resistive square loop improved the absorption bandwidth by about 153.85% for the frequency band (4.09 - 31.36 GHz) with a thickness of 0.117 λ_L [41]. Also, in the same year Zhou et al. investigated a resistive frequency selective surface comprising multiple square loops in five different sizes loaded with lumped resistance. The resistive absorber is printed on a substrate separated by an air spacer from the ground plane. The results show an absorption bandwidth of 82% from (7.9 to 18.9 GHz) for a small thickness of 0.074 λ_L [42].

In 2020, Nguyen et al. designed a broadband absorber consisting of a split ring with four lumped resistances printed on a dielectric substrate. The proposed design provided an absorption bandwidth of 47% for the frequency range of (7.8 - 12.6 GHz) for a thickness of 0.083 λ_L [43]. In the same year, Liu et al. described a double layer absorber composed of indium tin oxide (ITO) resistive square loop that makes an absorber insensitive to the polarization and is utilized to build the resonant structure to increase the ohmic loss of the resonances and widen the bandwidth of the resonant frequency ranges. Both of the two layers are coated on a polyethylene terephthalate (PET) substrate and separated from each other by a spacer, thus a wide bandwidth of 116% is achieved between (8–30.3 GHz), with an overall thickness of 0.089 λ_L [44].

In 2020, Khan designed a broadband absorber based single square loop loaded with a lumped resistor and Rogers RT 5880 as the dielectric backed by a copper layer. A wideband absorption response of 65% is achieved, ranging from

(8.508 to 16.701GHz), at a thickness of 0.089 λ_L [45]. A polarization-insensitive wide band based on the absorber conductive ink ring resonators, separated from the ground plane by a dielectric substrate, was introduced by Deng et al. in 2020. They show an absorption of 85.4% across the frequency range (6.58 - 16.38 GHz), with a small thickness of 0.072 λ_L [46].

In 2020, Fan, and Song presented a design of a single layer that consists of a square ring and wire attached to eight lumped resistors over dielectric and air spacer. The proposed design reveals large absorption bandwidth covering S, C, and X bands from (2.55 to 10.07 GHz), corresponding to 119.2% with a total thickness of 0.085 λ_L [47]. In the same year, Hossain et al. investigated two different shapes of FSSA configurations involving square patch and single square loop. The proposed design realized a wideband absorption response for both single and double layers at 126% and 161% fractional bandwidth, respectively [20].

In 2020, Suchu et al. described the design of Minkowski loops FSSA using multi-resonance structure. The proposed design contains two Minkowski loops combined with dielectric and air space over the ground plane. The design is symmetrical in both X and Y-axes, offering a wide absorption bandwidth of 100.45% from (5.5 to 16.6 GHz), for a thickness of 0.084 λ_L [13].

In a recent paper, Santos et al. reported that the transmitter/absorber of a two-layer of resistive and conductive square loop covered by FR4 substrate, produced better attenuation for both reflection and transmission coefficient [48]. In the same year, Singh et al. demonstrated a broadband absorber using two layers of ITO/PET. The absorber structure is in the form of a resistive cross dipole. An air spacer is inserted between the two layers. The proposed design showed greater

absorption bandwidth of 92.16% from (6.61 to 17.91 GHz), for a thickness of 0.088 λ_L [49].

1.4 Aims of the Dissertation

The goal of this project is to explore and analyze the FSSA in order to reduce reflection and increase bandwidth while maintaining a minimum total thickness. As a result, the dissertation includes the following procedures:

1- Designing a single layer of FSSA, investigating, and analyzing the main properties of the absorber. Creating an equivalent circuit of the presented FSSA, and then deriving formulas for the reflection coefficient for assurance impedance matching condition.

2- Investigating the influence of air spacer thickness between the two layers of the proposed absorber.

3- Investigating the split ring FSS absorber example in the circular loop with different gap lengths.

4- Investigating FSSA with lumped resistors, using an equivalent circuit for testing the impedance matching.

5- Studying the single layer FSS, including the resistive loop as an absorber, then investigating the effect of air spacer thickness.

6- Studying the single layer FSS, including the resistive loop with a resistive strip as an absorber, and the effect of its various parameters.

1.5 Dissertation Layout

This dissertation has five chapters. After an introduction, the second chapter focuses on the concept of frequency selective surfaces absorber, as well as their various kinds. The third chapter studies the suggested FSS for single layers absorber that is comprised of three distinct absorber configurations, such as single

circular loop, split ring, and circular loop with lumped resistors and discusses the simulation results and the impacts of the different design parameters using CST software. The proposed FSS's equivalent circuit was provided, along with the mathematical derivation of the reflection coefficient. Chapter four presented a single layer FSSA where two cases of resistive circular loop and resistive circular loop with horizontal strip are applied and investigated the impacts of various design parameters. Chapter five discusses the conclusion as well as future works.

CHAPTER TWO

FUNDAMENTALS OF ABSORBING FREQUENCY SELECTIVE SURFACES

CHAPTER TWO
FUNDAMENTALS OF ABSORBING FREQUENCY SELECTIVE SURFACES

2.1 Introduction

FSS is a thin, repetitive surface designed to reflect, transmit or absorb electromagnetic fields. The response of the surface varies with the frequency of the incident electromagnetic wave and the shape of the periodic pattern on the surface, and to some extent the angle of incidence. The FSS has seen a very wide range of applications, where it is desired to transmit, reflect, or even absorb a certain band of frequency.

Absorbers are spatial filters that do not transmit or reflect electromagnetic signals in a given frequency band. This can be achieved using a very thin metal film to provide absorption by putting resistors in the unit cells of the periodic metallic surface or by printing periodic shapes using resistive ink. By loading lumped resistor elements, or patterned resistive film arrays, an absorption structure could be loaded to absorb the energy of EM waves over a specific range of frequencies.

Absorbers based on the FSS have been widely utilized in both military and commercial applications to reduce the reflectivity of huge equipment such as planes, submarines, tanks, and microwave darkrooms. They have also been employed in a variety of electromagnetic applications, including radio frequency identification (RFID) systems, radomes, and so on. In such applications, the quality factor (Q-factor) of the structure is reduced to obtain broadband absorption, which can be fulfilled by increasing the resistance. The increased resistance offers an additional benefit for dissipating the incident energy and thus leading to minimized reflection over a broad frequency range. For analyzing the

electromagnetic behavior of FSS several mathematical approaches like finite element method (FEM), finite difference time domain (FDTD) codes or dedicated method of moments (MoM) approaches are commonly employed. By engineering the structure and choosing the proper material. Therefore, both transmission and reflection are minimized and a large loss results in. The following sections discuss various theoretical concepts that explain the operation of the FSS, followed by a brief review of the various designs of the FSS that have been presented in recent years.

2.2 Reflection of Electromagnetic Waves

A simple example of the reflection coefficient is when the uniform plane wave strikes the boundary between two dielectrics with no surface-charge density, the incident and reflected wave are described by relative permittivity and permeability of material as indicated in Fig. 2.1. The electric field intensity in X-direction is the sum of incident plus reflected waves as follows [50]:

$$E_x^{(1)} = E_0(e^{-j\beta_1 Z} + \Gamma e^{j\beta_1 Z}) \qquad (2.1)$$

While the magnetic field intensity in Y-direction:

$$H_y^{(1)} = \frac{E_0}{\eta_1}(e^{-j\beta_1 Z} - \Gamma e^{j\beta_1 Z}) \qquad (2.2)$$

Where E_0 is the initial intensity of the electric field intensity. The quantity β_1 represents the phase constant of the first medium in radians per meter and is also known as wave number.

$$\beta_1 = \omega\sqrt{\varepsilon_1 \mu_1} \qquad (2.3)$$

Where ω represent the angular frequency. μ_1 and ε_1 represent the permittivity and permeability of the first medium.

$$\eta_1 = \sqrt{\frac{\mu_1}{\varepsilon_1}} \hspace{8cm} (2.4)$$

η_1 is the Intrinsic impedance of the first medium.
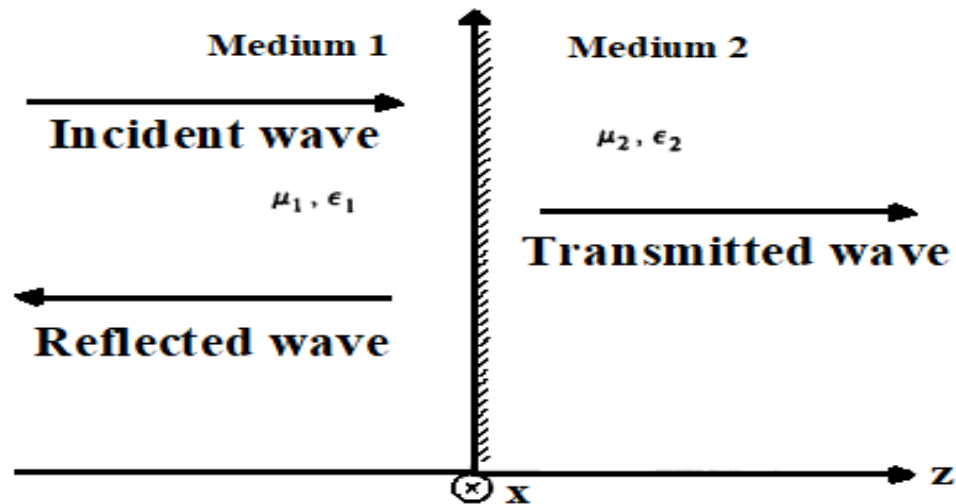
Figure 2.1: Reflection of a normally-incident wave at the boundary [50].

The amount of reflected radiation is measured by the reflectivity of a surface. The reflectivity depends upon the polarization of the radiation, the angle of incidence, and the electromagnetic properties of the materials at the boundary surface. These properties can be changed for different wavelengths of radiation. Reflecting materials are split into two groups: transparent materials and imperfect conducting materials. Transparent materials are also known as dielectrics. Radiation that passes through a transparent medium propagates almost unattenuated whereas radiation that passes through an imperfect conducting medium is significantly attenuated.

2.2.1 Reflection and Transmission at a Dielectric media

In the case of an electromagnetic wave struck on a dielectric medium the reflection and transmission coefficients are related to the direction of the electric field. The polarization can be split into two types. The reflection and transmission coefficients will be different for the following cases:

2.2.1.1 Parallel Polarization

As observed in Fig. 2.2 when the incident, reflection, transmitted electric field vectors are parallel or lying in the plane wave formed by the direction of incidence and normal to the boundary, the case is known as parallel polarization.

If the incident electric field intensity has magnitude $\bar{E}_i$ and the electric field vector is in the XZ-plane, the reflected wave must be at the same angle as the incident wave, since the incident, reflected, and transmitted fields must match across the boundary [50].

The reflection coefficient can be expressed as:

$$\Gamma_{//} = \frac{\eta_2 cos\theta_t - \eta_1 cos\theta_i}{\eta_2 cos\theta_t + \eta_1 cos\theta_i} \qquad (2.5)$$

Where η_2 is the intrinsic impedance of the second medium.

θ_i = angle of incidence.

θ_t = angle of transmission.

While the transmission coefficient is:

$$T_{//} \frac{2\eta_2 cos\theta_i}{\eta_2 cos\theta_t + \eta_1 cos\theta_i} \qquad (2.6)$$
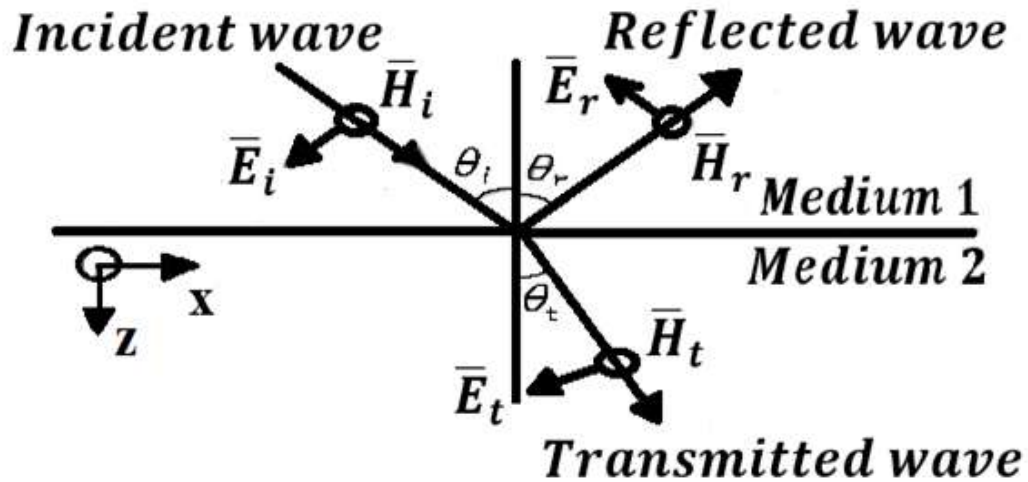
Figure 2.2: Parallel polarization, reflection, and transmission of a plane wave [50].

2.2.1.2 Perpendicular-Polarization

When the electric field vectors of the incident, reflected, and transmitted waves are perpendicular to the plane of incidence the polarization is known as perpendicular-polarization as shown in Fig. 2.3.
Following the same procedure of applying the boundary condition at the interface, the reflection and transmission coefficients can be given by [50]:

$$\Gamma_{\perp} = \frac{\eta_2 \cos\theta_i - \eta_1 \cos\theta_t}{\eta_2 \cos\theta_i + \eta_1 \cos\theta_t} \qquad (2.7)$$

$$T_{\perp} = \frac{2\eta_2 \cos\theta_i}{\eta_2 \cos\theta_i + \eta_1 \cos\theta_t} \qquad (2.8)$$
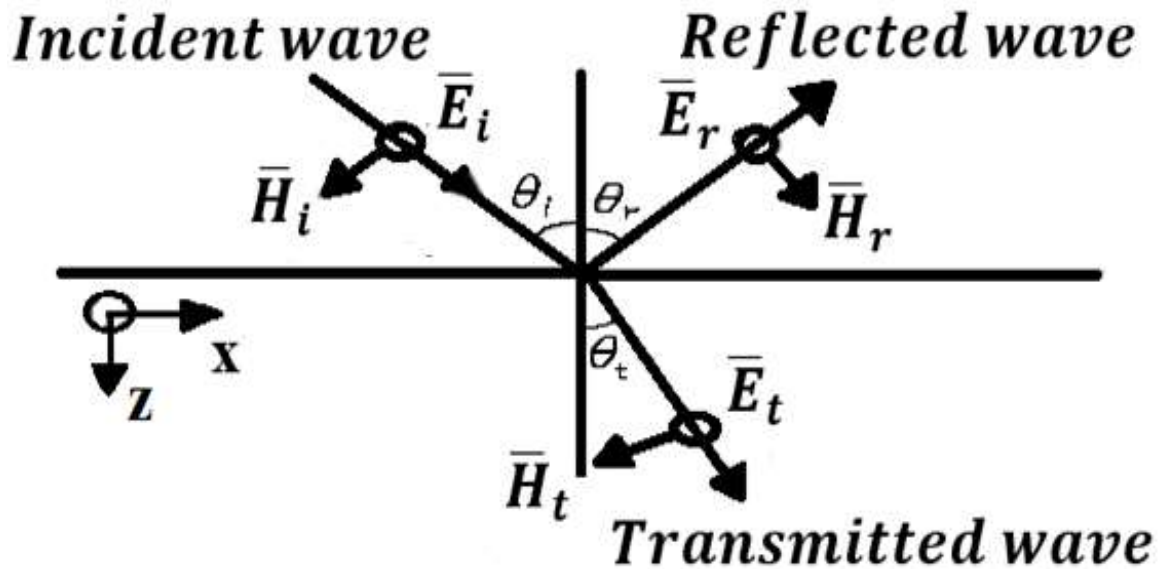
Figure 2.3: Perpendicular polarization, reflection, and transmission of a plane wave [50].

2.2.2 Reflection at Perfect Electrical Conductors

For a good conductor, the characteristic impedance is very small as the conductivity approaches infinity. The tangential component of the electric field must be zero, therefore all the incident energy is reflected, thus

$$\Gamma_{\parallel} = \Gamma_{\perp} = \Gamma = -1. \qquad (2.9)$$

2.3 Frequency selective surfaces (FSS)

Those surfaces are formed of periodic resonant structures, which act as a spatial filter are known as frequency selective surfaces. These structures, which act as a wave barrier, can either reject or pass electromagnetic waves of a given frequency, based on the geometry of the elements. The FSS have potential applications such as selective frequency shielding for room windows to stop radio

waves from leaking into and out of rooms, stealthy radome [51],[1], sidewalls of microwave ovens to avoid EM field leakage, and in radar cross-section (RCS) reduction [52]. Designing an FSS for a specific resonant frequency relies upon several parameters like conductive-element, dimensions and thickness. The dielectric supporting material also affects the operating frequency. The dimensions of the conductive elements have the main influence on the operating frequency. Finding the appropriate FSS element and array geometry required to exactly produce a desired frequency response. An FSS of aperture and patch periodic array elements are shown in Fig. 2.4. The slot and patch elements are complementary to each other. The FSS element in the form of aperture reflects low frequencies while transmitting high frequencies (has a similar response to the high-pass filter). The FSS element of a patch shape transmits low frequencies while reflecting high frequencies (much like a low-pass filter). The application of FSS has generated new areas of research in the designing of electromagnetically absorbent surfaces, resulting in improved properties exhibited in better bandwidth/thickness ratio as well as the modifiability of the absorbing bandwidth narrowband, multi-band, wideband, ultra-wideband for the wanted applications.
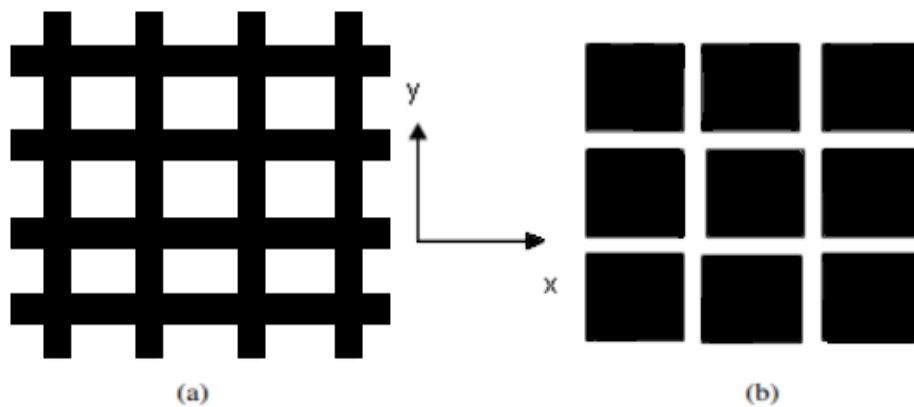
Figure 2.4: FSS element (a) Aperture type, (b) patch type.

2.4 Interference theory

The absorption mechanism in the FSS is quantitatively analyzed using the multiple interference theory that was presented in [53]. Figure 2.5 depicts the three-interference model for the FSSA. The FSS interface, the air spacer interface, and the copper ground plane. The FSS and air spacer function as a part of the reflective surface, reflecting and transmitting a portion of the incident wave. The copper ground plane works as a perfect reflector with a reflectance of $r_{23} = -1$ thus the transmission through the FSS is zero.
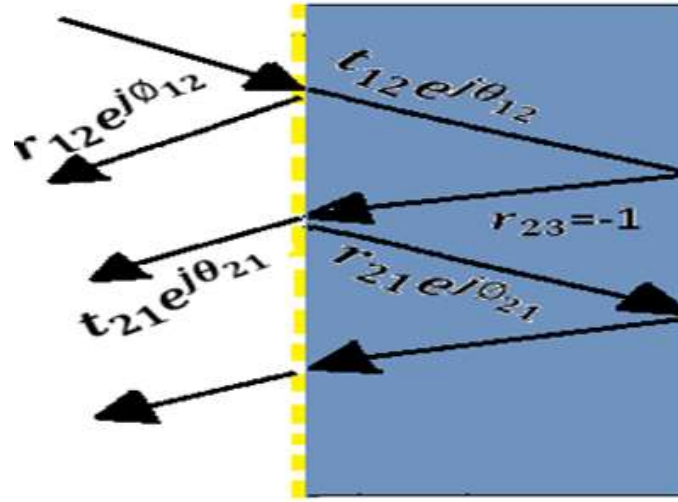
Figure 2.5: Interference model of the FSSA [53]

At the air spacer interface in the design of a cross resonator array as illustrated in the inset of Fig. 2.5, the incoming wave has become partially reflected back to air with a reflection coefficient $\tilde{r}_{12} = r_{12} \, e^{j\varphi_{12}}$ and partially transmitted into the spacer with a transmission coefficient $\tilde{t}_{12} = t_{12} \, e^{j\theta_{12}}$. The latter keeps propagating whenever it approaches the ground plane, with a complex propagation constant $\gamma = \alpha_o + j\beta_o$, where $\alpha_o = 0$ is the absorption factor, and $\beta_o = 2\pi/\lambda_o$ is the phase constant for the air spacer (free space). The value of λ_o is represented the free space wavelength. After the wave is reflected at the ground plane and added to another propagation phase β, partial reflection and transmission tend to happen again at

the air spacer interface with coefficients $\tilde{r}_{21} = r_{21}\,e^{j\varphi_{21}}$ and $\tilde{t}_{21} = t_{21}\,e^{j\theta_{21}}$. Thus, the total reflection is the sum of the individual reflections [53]:

$$\tilde{r} = \tilde{r}_{12} - \frac{\tilde{t}_{12}\tilde{t}_{21}e^{j2\tilde{\beta}}}{1 + \tilde{r}_{21}e^{j2\tilde{\beta}}} \qquad\qquad (2.10)$$

Where the term is due to the direct reflection the cross-resonator array, while the second term, with its "−" sign, is the reflection originating from the sum of individual reflections between the cross-resonator array and ground plane. The absorption obtained using $A(\omega) = 1 - /\,r(\omega)\,/^2$, Since the transmission is zero.

Another observation is that when an incident wave hits the surface of the ground plane, the reflected electric field at the ground plane has a phase of 180 degrees differing from that of the incident electric field due to the boundary condition. The boundary condition states that the tangential component of the total electric field at the ground plane has to be zero [54], thus the incident and reflected field should be out of phase.

2.5 Types of FSS absorbers

In many applications it is required that certain surfaces have reduced reflection, thus the FSS surfaces have been used to offer small reflection. This result can be achieved if the FSS is designed to absorb part of the incident wave.

A comparative review of several forms of FSSA is offered here to create better knowledge of the operation of FSSA structures. The way these elements are grouped in the array format is also part of the design work for the FSSA array element, which represented one of the major parameters in the response of the designing FSSA. The elements are shaped to be resonant at or near the operating frequency. The current behaves as an electromagnetic source depending on how it

is distributed, resulting in a scattered field. The total field in the space surrounding the FSS is made up of the scattered field plus the incident field [55]. As a result of managing the scattered field, the desired filter response is obtained. Element shapes can be spliced into different types included basic element type FSSA, convoluted/meandered FSSA, as well as fractal FSSA. More detailed explanations are included in this section.

2.5.1 Types of Basic FSSA Elements

FSSA can be categorized into different types based on the geometry of the elements that are used. These can have the shape of circular ring, cross dipole, square shape as depicted in Fig. 2.6. Other types of FSSA are of fractal geometry or convoluted/meandered. One or more shapes can be combined together on single or multiple layers to achieve the desired absorber.
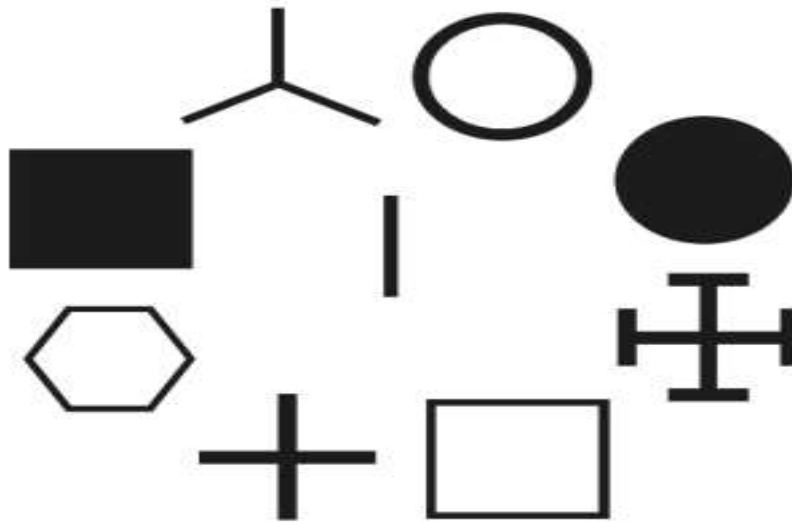
Figure 2.6: Common FSSA shapes [55].

2.5.2 Convoluted or Meandered FSSA

The use of miniaturized FSS having a convoluted array of square loop elements was the first introduced in [56], since the large unit cell size associated with previously proposed band-absorptive materials may result in unstable frequency response when subjected to oblique incidence. Reducing the unit cell size by using a curved shape, or spiral can be made resonant frequency relatively stable to the angle of incidence. Miniaturized metamaterial absorber (MMA) with an incurved square loop fed by lumped resistors was considered to have better absorption properties in the worldwide ultra high frequency -radio frequency identification (UHF-RFID) in [57]. The suggested design's geometry is shown in Fig. 2.7. The air layer close to the ground metallic layer has a thickness of 20 mm. The four lumped resistors are optimized to be 82 Ohm. The simulated results indicate that the MMA has better absorbing property in the band (860–960 MHz) that is used by UHF-RFID. In this dissertation circular ring will be investigated.
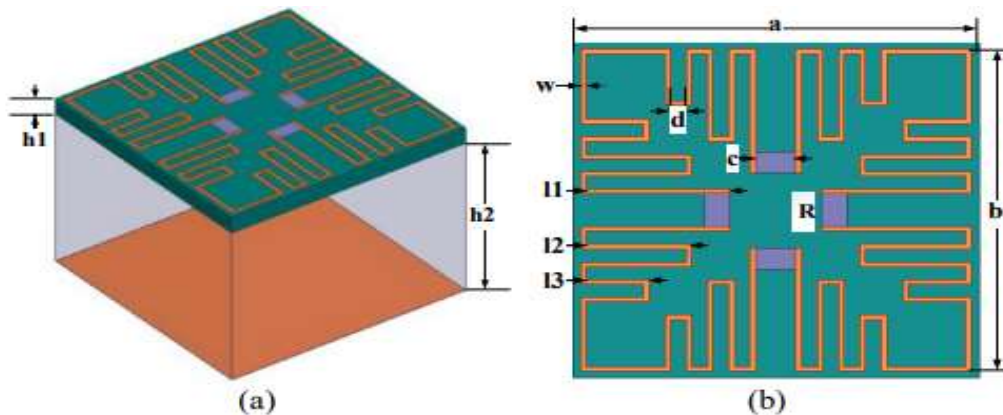
Figure 2.7: (a) Three dimensions of MMA, (b) unit cell structure [57].

Another miniaturized MA comprising meander lines (ML), and magnetic materials (MM) layers, supported by a conducting ground was demonstrated in [58]. The two sets of ML split square rings are joined in series by four metal vias to form the so-called "2.5-dimensional" design. The suggested absorber has a unit

cell dimension of 0.019 $\lambda_L \times$ 0.019 λ_L, making it stable over a wide range of polarization states and incidence angles. Good absorption was achieved from (0.8 to 3.2 GHz). In this dissertation, circular ring will be investigated.

2.5.3 Fractal FSSA

The self-similarity aspect of fractal geometry is considered to be the most important feature of fractal geometry. The geometry replication at a different scale inside a structure. The FSS Minkowski fractal design technique, which incorporates four lumped resistor printing on FR4 dielectric substrate is shown in Fig. 2.8. The resistors tend to absorb the energy of the incident EM wave, resulting in broadband behavior as described in [59].

The simulation results demonstrated that the absorption bandwidth covers the entire C-band (4–8.12 GHz) with a 0.288 λ_L thick absorber.
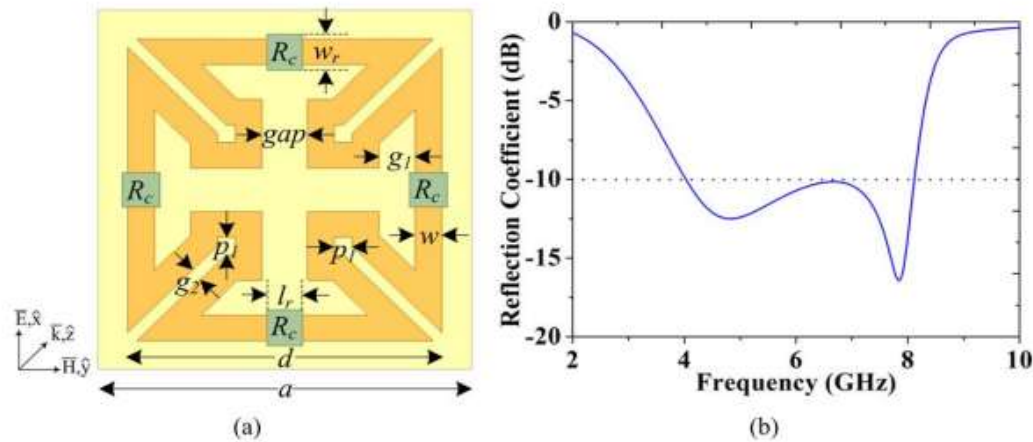
Figure 2.8: (a) Unit cell structure, (b) simulation result [59].

2.6 FSS with absorbing properties

FSSA is a property of a repeated 2D periodic array printed on a dielectric substrate layer. The filter design can provide absorption of the wave with minimum reflection. FSSA can be categorized into two types of losses either in

the substrate (dielectric loss) or in the conductive (ohmic loss). The structure of the design might be a single, double, multi. The main advantage is to optimize the EM absorption across the wanted frequency band. The important factors influencing the response of the FSSA are the shape and dimensions of the element. The basic principle operation of the absorber is based on matching the impedance of the absorber layer to the free space impedance.

FSSA, in general, have many common shapes and geometries, such as a square loop [28,29],[33], [60], [61], ring [26], cross dipole [21,22], fractal [62], and hexagonal ring [63]. These surfaces have potential design applications. This approach could be useful in designing an absorber for a microwave oven, wireless security, absorption of WLAN 802.11a/n signals, although other bands (like WLAN 802.11b/g or global System for mobile communication (GSM)) can go through with no absorption. [26]. Also, they are employed to make military aircraft and targets invisible to radars.

2.6.1 Single-layer absorbers

A simple FSSA structure can be represented by a square shape loop as shown in Fig. 2.9. An example of an absorber design that uses a square loop printed on 0.15 mm thick FR4 plate and backed by a copper ground plane to eliminate the transmission coefficient. The square ring FSS is represented by a serial resistance-inductance-capacitance (RLC) circuit in Fig. 2.9 (c). These components are dependent on the unit cell shape (Fig. 2.9 (b)). When the resistance is zero, the design obtains perfect reflection (unity reflection). The inductance (L) is caused by the current passing through the square loop, which is proportional to the periodicity of square loop's and width. The capacitance (C) is attributed to the dielectric material between the conducting sections of the FSS, the value of

resistance of the copper ring is equal to $R = \rho \frac{l}{Ae}$, where ρ is the resistivity in units of ohm-meter, Ae is the effective cross-sectional area of the conducting strip, whereas l is the average circumference of the ring.
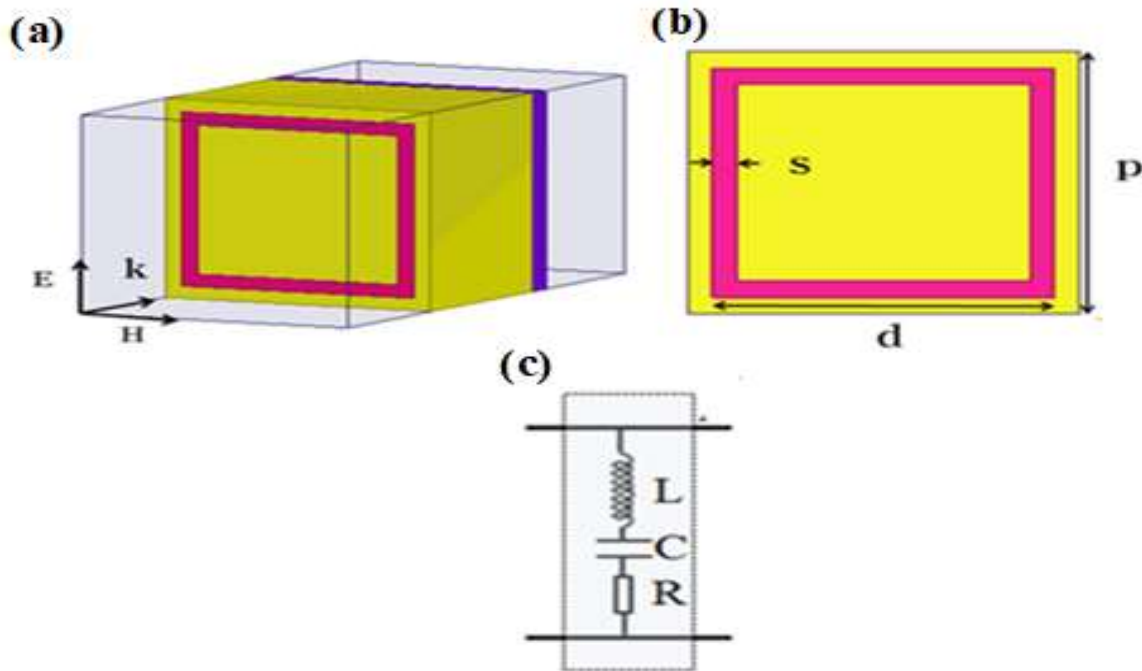
Figure 2.9: (a) Square loop-FSSA, (b) geometry of unit cell, (c) equivalent circuit model [33].

Another design in Fig. 2.10(a) of the incident wave along Z-direction consists of a split circle ring (SCR) loaded with four lumped resistors printed on FR4 substrate of 3.2 mm thickness. The four resistors are placed symmetrically at four sides of the circular ring. Placing resistors is responsible for realizing the broadband absorber by introducing ohmic loss. The value of the inductance is affected by the variation of the radius and the width of the ring.
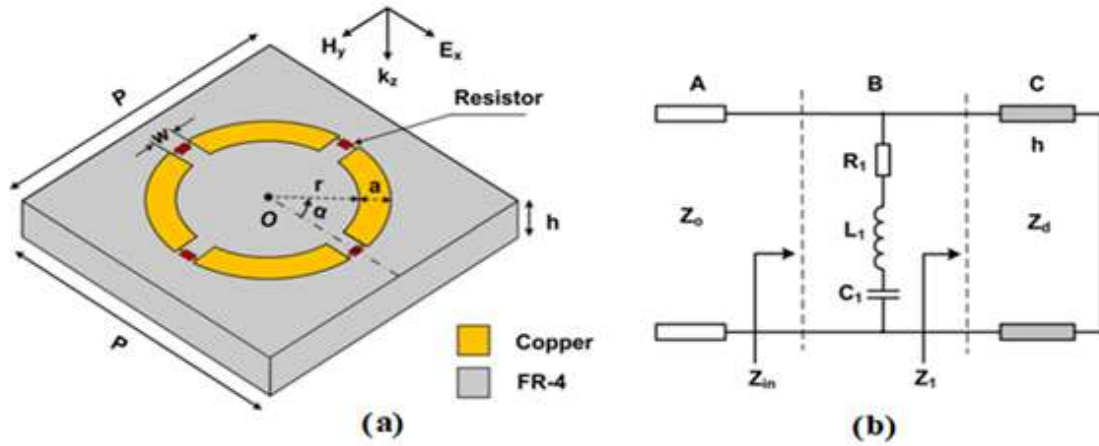
Figure 2.10:(a) Three dimension of MMA, (b) equivalent circuit model [43].

2.6.2 Double-layer absorbers

Figure 2.11(b) presents the design of two dielectric layers between a copper sheets. The circular ring MA has strong absorbance for typically occurring EM waves and is insensitive to all polarization states due to its geometric characteristic.
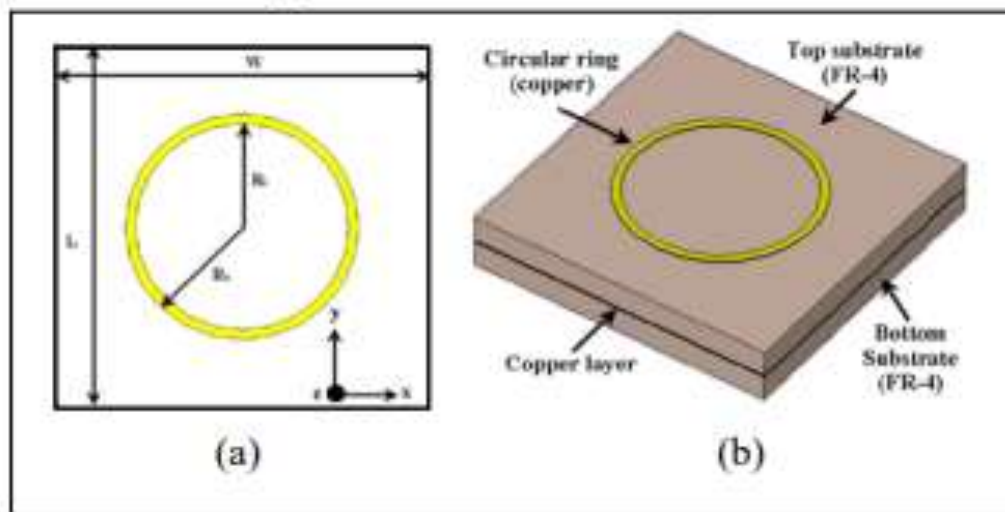
Figure 2.11: (a) Unit cell of a circular ring, (b) double-layer MA [30].

The simulated result in Fig. 2.12 is expressed in terms of S_{11} (reflection coefficient) and S_{21} (transmission coefficient). The transmittance, reflectance, and absorbance may all be calculated using these two quantities. The combination of different FSS patterns for designing the ultra-wide bandwidth absorbers is illustrated in Fig. 2.13. The presented design of two FSS combinations square patch/loop (FSS_1/FSS_2) achieves low-reflectivity absorbers in a broader frequency band.
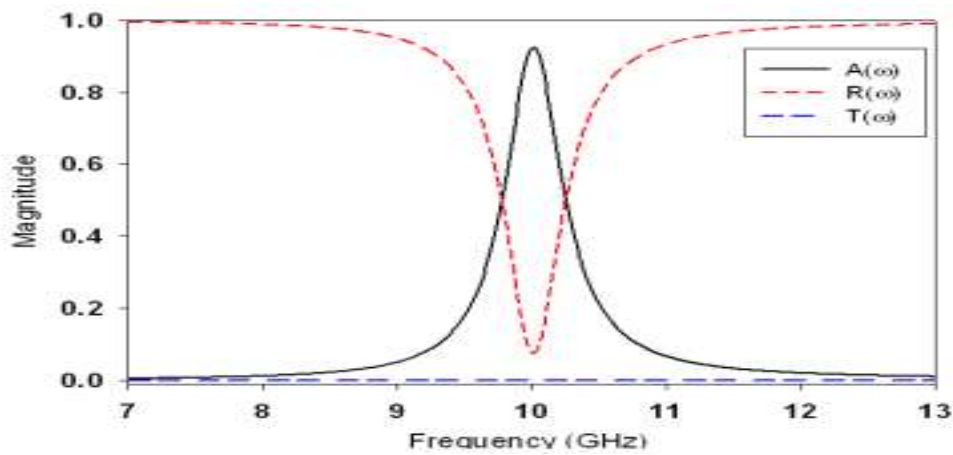
Figure 2.12: Simulated reflectance, transmittance, and absorbance [30].
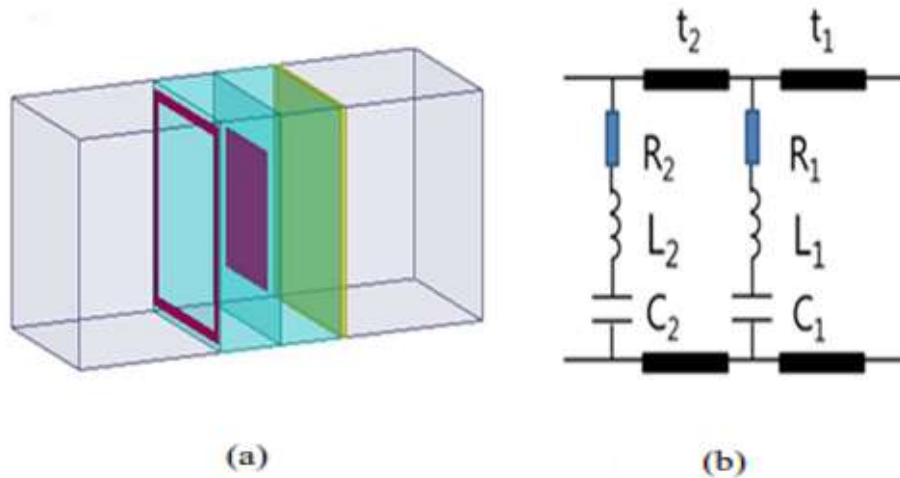
Figure 2.13 :(a) Double-layered FSSA, (b) equivalent circuit model of a combination of (FSS_1/FSS_2) [64].

At the values R_{s1} =100 Ohm/sq, R_{s2} =20 Ohm/sq, t_1= 2.0 mm and $t_2 = 3.5$ mm. The reflection coefficient was reduced below than -10 dB, which exhibits ultra-wide absorption bandwidth from 6.3 GHz to 40.0 GHz that was achieved at a relatively thin total thickness of 0.115 λ_L as shown in Fig. 2.14.
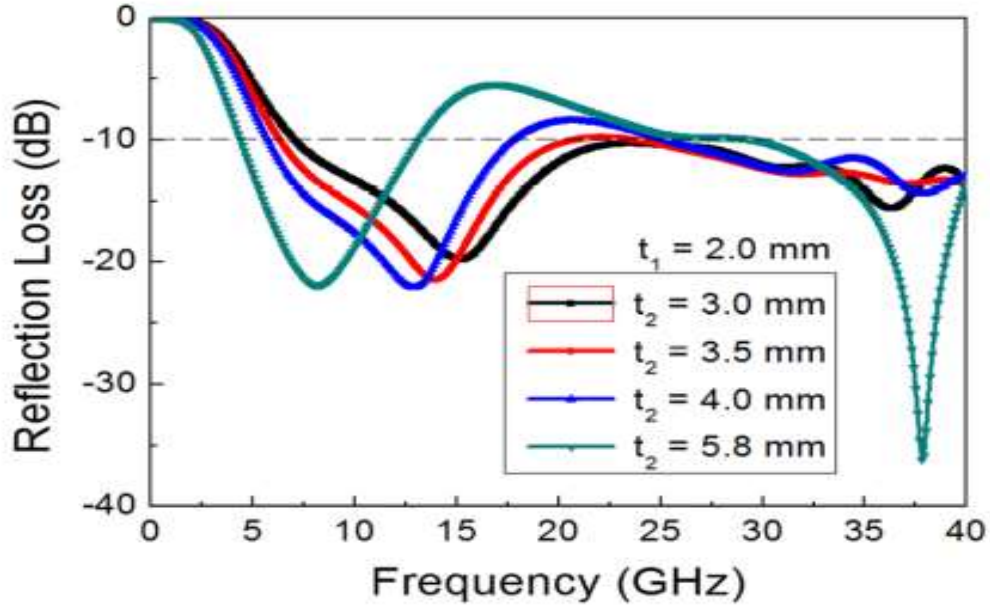
Figure 2.14. Variation of the reflection coefficient for the double-layered absorbers having a square patch/loop (FSS_1/FSS_2) combination for various values of second substrate thickness (t_2), and $t_1 = 2.0$ mm [64].

2.6.3 Triple-layer

Fig. 2.15(a) displays a design for wide-bandwidth triple-layer FSSA using a combination of three resistive FSS layers. The model comprising a square loop placed in the middle of the design between spiral and patch shapes with the equivalent circuit shown. The dimensions of the unit cell of a square loop (FSS_2) chosen as the period p=6.0 mm, length d=5.6 mm, and the width w=0.3 mm, the thickness of t_2=3 mm with value of resistance R_{s2}=20 Ohm/sq, and R_{s3}=250 Ohm/sq for spiral shape (FSS_3) with thickness $t_3 = 2$ mm. The square patch has

resistance $R_{S1} = 100$ Ohm/sq, thickness $t_1 = 2.0$ mm. The overall design total thickness was set to be equal to $0.109 \ \lambda_L$.
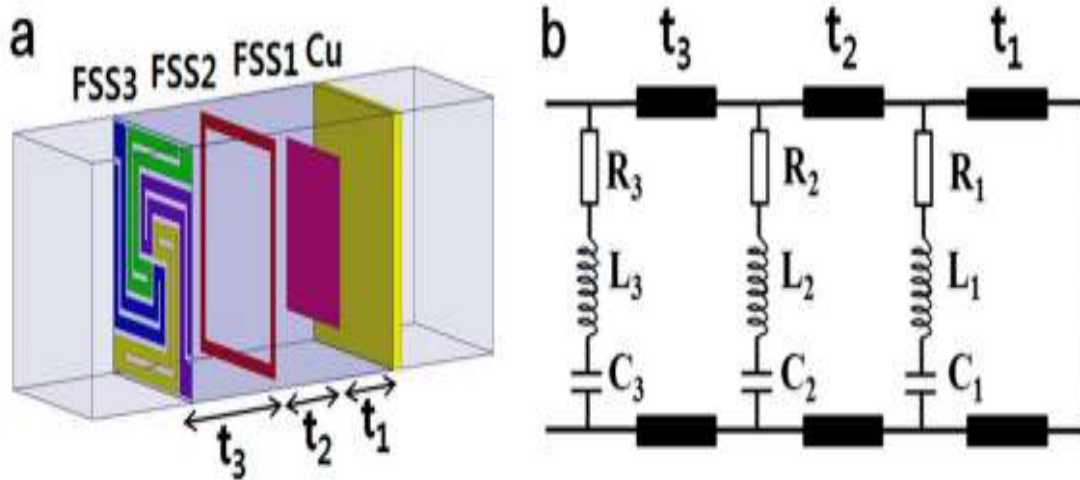
Figure 2.15: (a) Triple layer FSSA, (b) equivalent circuit model [61].

The simulation results as seen in Fig. 2.16 demonstrated ultra-wide absorption bandwidth found in the frequency range which is located between (4.7 –56.4 GHz) at a smaller thickness.
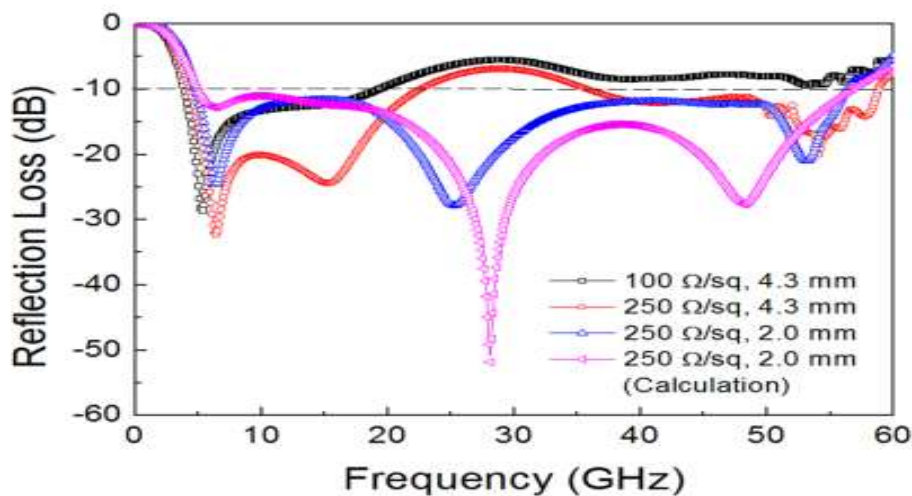
Figure 2.16: Variation of reflection coefficient for the triple-layer FSSA at resonance for FSS_3, where other parameters of FSS_1 and FSS_2 are fixed [61].

A square loop supported by FR4 substrate over an air layer can be presented in the design of the triple-band absorber with lumped resistors on top layer [65,66]. The metallic loop as shown in Fig. 2.17 has been inserted in the middle of the design between meandered cross dipole and ground plane. The width of the ring can be represented as the inductive. Variation of the width also can affect the resonant frequency. The problem of unsharp reflection for stop band or limited absorption band was mitigated due to the effect of square loop. This effect is demonstrated in Fig. 2.18. The simulation shows that two absorption bands are present in the frequency ranges (2.12 to 4.15 GHz) and (6.08 to 9.58 GHz), where notch band reflection is extended from (4.3 to 5.65 GHz). The total thickness of the FSS is 0.143 λ_L.
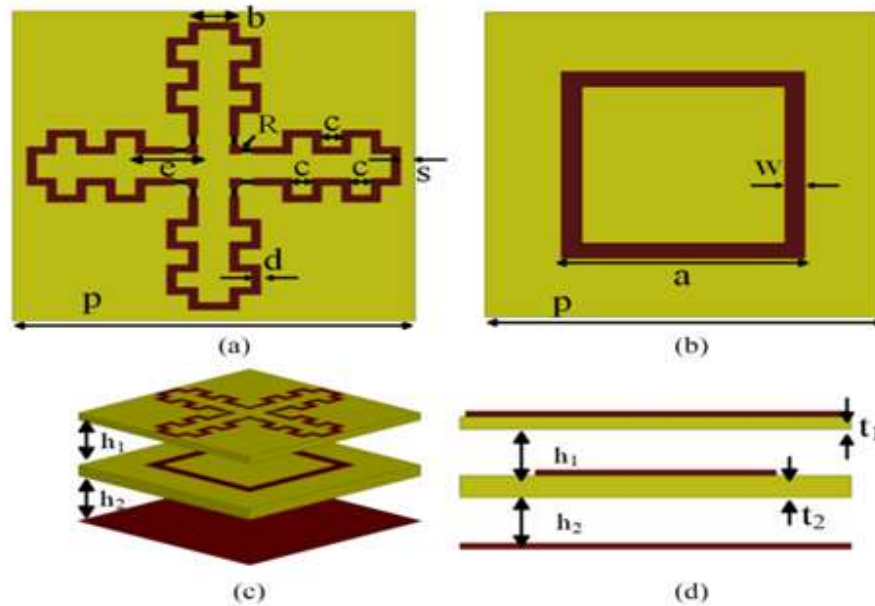
Figure 2.17: Geometry of the unit cell of the absorber: (a) Top layer, (b) middle layer, (c) three-dimensional view, and (d) side view [65].
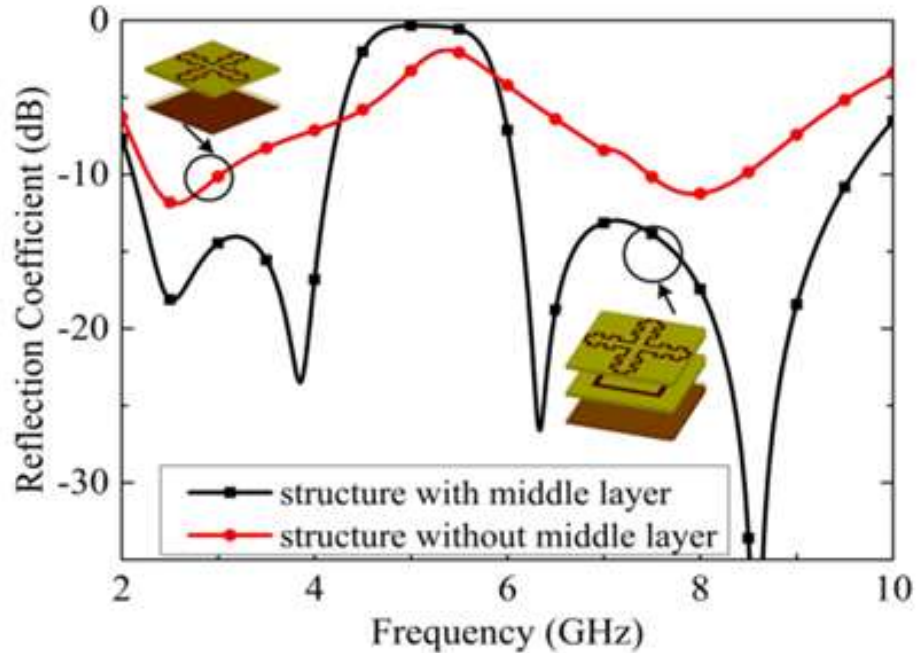
Figure 2.18: Variation of reflection coefficient (a) With, and (b) without the middle layer [65].

2.6.4 Absorber using Complementary Layer

Figure 2.19 shows the geometry of the proposed design by Bhardwaj et al. in [67], where a double complementary structured layer of ITO deposited PET film is used. This design is insensitive to the polarization of the incident wave and has better absorption even at oblique incidence. This absorber was based on surface resistances, where the top complementary layer has larger sheet resistivity (200 Ohm/sq) and bottom complementary layers has 10 Ohm/sq. The spacing between each layer is 4 mm. The simulation results showed more than 90% absorption in the S band from (2 to 4.5 GHz), while the total thickness of the 4-layers FSS is 0.084 λ_L [67].
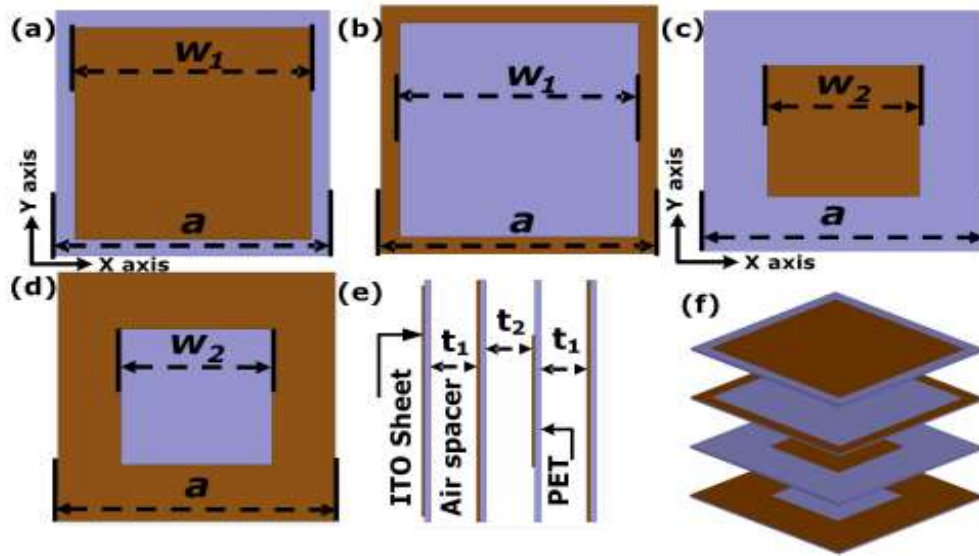
Fig. 2.19: (a), (b) Top view of first and second layers, (c), and (d) second set of complementary layers. (e), and (f) side view, and three-dimensional view of the suggested geometry [67].

CHAPTER THREE

ANALYSIS OF ABSORBING FSS WITH CIRCULAR RING AND LUMPED RESISTORS

CHAPTER THREE
ANALYSIS OF ABSORBING FSS WITH CIRCULAR RING AND LUMPED RESISTORS

3.1 Introduction

The FSS have found increasing applications, where the incident electromagnetic wave is wanted to be absorbed with a small reflection. Moreover, it is desirable that minimal transmission through the FSS is achieved. With the later requirement, most absorbing FSS have a conducting ground plane layer. The main considerations in improving the performance of the FSSA are reducing the reflection coefficient at the desired frequencies, and increasing the bandwidth of the FSS. Thus, better operational performance can be achieved. In this chapter, the FSS characteristics are investigated with the emphasis on improving the absorbing performance. The proposed FSSA have lumped resistors that were used to absorb the incident electromagnetic power is also investigated.

3.2 Analysis of FSS with circular ring backed by an air layer

The suggested FSS design is composed of a circular conducting ring printed on a dielectric substrate that is separated by a certain distance from the backing ground plane. The circular ring was chosen due to insensitivity over wide incidence angles. The geometry of the FSS design is depicted in Fig. 3.1. The conducting ring is made of copper, and the substrate is FR4 with relative permittivity of 4.3, loss tangent of 0.025, and thickness of 1.6 mm. The design frequency was chosen to be 3 GHz in the band of (2 - 4 GHz) for microwave ovens, Bluetooth, WLAN, and WiMAX absorption. The FSSA is investigated using the CST software Suite, where the unit cell approach is used.

(a) FSS layer   (b) Side view   (c) Ground plane
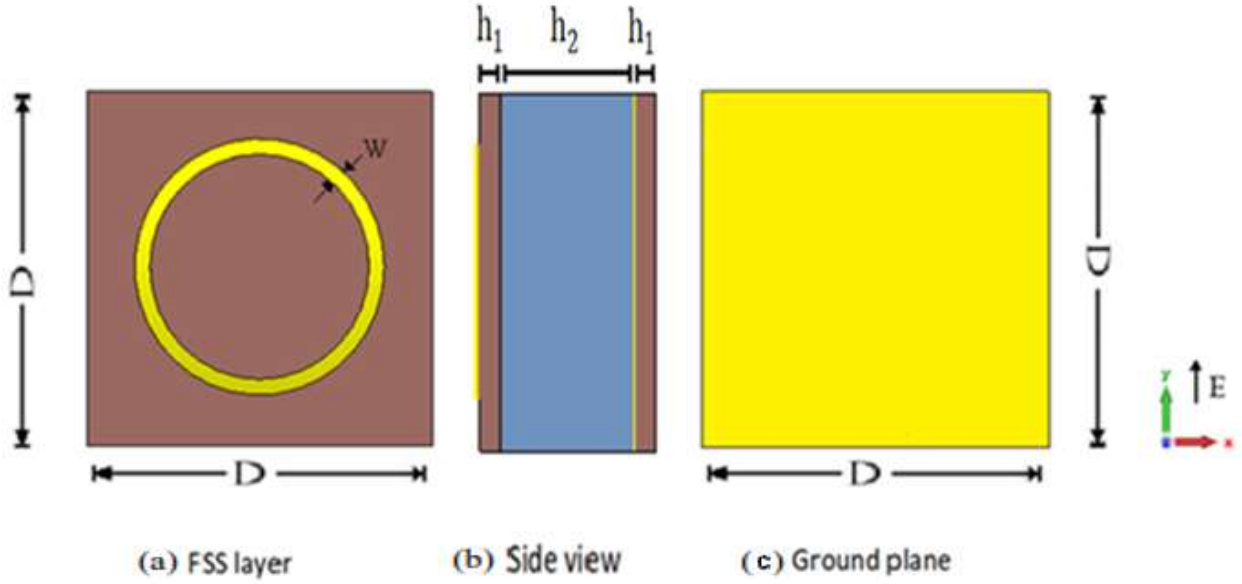
Figure 3.1: Geometry of the proposed FSS and ground plane; (a) Top view of FSS layer, (b) side view, and (c) top view of the ground plane.

The design parameters of the FSS cell can be chosen to achieve operation at the desired band of frequencies if the effective dielectric constant of the assumed configuration is determined. In the design shown in Fig. 3.1, there are two layers of air and FR4 substrate underneath the conducting ring. For the double dielectric substrate used here, the total thickness h is the sum of the substrate thickness h_1 and the air spacer thickness h_2. The value of the effective dielectric constant ε_{rc} is the combination of ε_{r_1} and ε_{r_2} due to the FR4 and air layers respectively. So, the resultant dielectric constant that can be derived by applying the static condition of constant electric flux density (D=εE) through the two dielectric layers from $V_o = h\,E_y$ applied voltage. Where E is the electric field intensity, E_y is electric field intensity along Y-direction, and ε is the dielectric constant of the medium [68].

$$v_0 = h_2 (D/\varepsilon_0 \varepsilon_{r_2}) + h_1 (D/\varepsilon_0 \varepsilon_{r_1}) = (h_2 + h_1)(D/\varepsilon_0 \varepsilon_{r_c}) \tag{3.1}$$

Where h_1, ε_{r_1} are the thickness and dielectric constant for the substrate, and h_2, ε_{r_2} are the thickness and dielectric constant for the air spacer. Then the value of the effective dielectric constant ε_{rc} for the composite layer can be found as [69]:

$$\varepsilon_{r_c} = \frac{(h_2+h_1)(\varepsilon_{r_2}\varepsilon_{r_1})}{(h_2\varepsilon_{r_1}+h_1\varepsilon_{r_2})} \qquad (3.2)$$

Then for the used FR4 substrate (h_1= 1.6 mm, ε_{r1}= 4.3), and assuming air layer thickness h_2=10 mm, the effective dielectric constant will be:

$$\varepsilon_{r_c} = \frac{(h_2+h_1)(\varepsilon_{r_2}\varepsilon_{r_1})}{(h_2\varepsilon_{r_1}+h_1\varepsilon_{r_2})} = 1.118$$

Since the thickness of the air spacer is larger as compared to that of the dielectric substrate, then the expected effective dielectric constant is closer to the dielectric constant of the air. Thus, the above result (1.118) is closer to unity than to (4.3).

From another point of view, the circular ring is now assumed over an equivalent substrate of thickness 10+1.6= 11.6 mm and an effective dielectric constant of 1.118. In such case, there will fringing effect of the electric field, and this can be accounted for by assuming an effective relative dielectric constant due to the fringing field which can be obtained as [68]:

$$\varepsilon_e = \frac{\varepsilon_{rc}+1}{2} + \frac{\varepsilon_{rc}-1}{2} \frac{1}{\sqrt{1+\frac{10h}{w}}} \qquad (3.3)$$

Where w is the ring width, and h is the total thickness of the two-layer substrate. Therefore, for the parameters of the above assumed design, and assuming w=2 mm, the effective relative dielectric constant is:

$$\varepsilon_e = \frac{1.118+1}{2} + \frac{1.118-1}{2} \frac{1}{\sqrt{1+\frac{10\times11.6}{2}}} = 1.067$$

Thus, at the frequency of 3 GHz, the effective or guide wavelength will be:

$$\lambda_{e=}\frac{\lambda_0}{\sqrt{\varepsilon e}} \tag{3.4}$$

Which for the considered case gives:

$$\lambda_{e=}\frac{\lambda_0}{\sqrt{\varepsilon e}} = \frac{\lambda_0 \, k}{\sqrt{1.067}} = 97 \text{ mm}$$

The closed ring resonates when its circumference is equal to ½ the effective wavelength. By proper choice of the values of outer and the inner diameters of the ring, one can obtain the values of the circumference of the ring and set it equal to or half of the effective wavelength and its multiple. Thus choosing 16.6 mm and 14.6 mm for the outer and inner diameters of the ring respectively, the average circumference l will be:

$$d_a = \frac{(d_{out}+d_{in})}{2} = \frac{(16.6 + 14.6)}{2} = 15.6 \text{ mm} \tag{3.5}$$

$$l = \pi \, d_a = \pi \times 15.6 = 49 \text{mm} \tag{3.6}$$

Having obtained the parameters of the ring the unit cell was chosen to be a square of side dimension of 23 mm. At these dimensions, the unit cell size is 23/97 = 0.24 λ_e. The parameters of the design are tabulated in Table 3.1.

Figure 3.2 displays the variations in the reflection coefficient with the incident wave's frequency when the air spacer is 10 mm thick., and other parameters are as listed in Table 3.1. It can be seen that there is a small decrease in the reflection coefficient at 3 GHz, while there is twice the reduction in the reflection coefficient at 7.65 GHz frequency.

Table 3.1: Parameters of the design for the copper ring FSS.

h_1	1.6
ε_{r_1}	4.3
ε_{r_c}	1.118
ε_e	1.067
Resonance frequency (f_o)	3 GHz
λ_o	100 mm
λ_e	97
Outer diameter of the ring d_{out}	16.6 mm
Inner diameter of the ring d_{in}	14.6 mm
w	2 mm
Thickness of air spacer h_2	10 mm, and other values

Examining the results of Fig. 3.2, the resonant frequency acquired from the CST simulated result is that which gives a small reflection coefficient. Thus, this frequency is 3 GHz, which corresponds to a wavelength of

$$\lambda_0 = \frac{c}{f} = \frac{3 \times 10^8}{3 \times 10^9} = 100 \text{ mm}.$$

Then, according to Eq. (3.4), the effective wavelength is

$$\lambda_{e=} \frac{\lambda_0}{\sqrt{\varepsilon e}} = \frac{\lambda_0}{\sqrt{1.067}} = 97 \text{ mm}.$$

But the average circumference of the ring is 49 mm according to Eq. (3.6), which means:

$$\frac{\lambda e}{l} = \frac{97}{49} = 1.979$$

This means that the average circumference of the ring is half the effective wavelength.
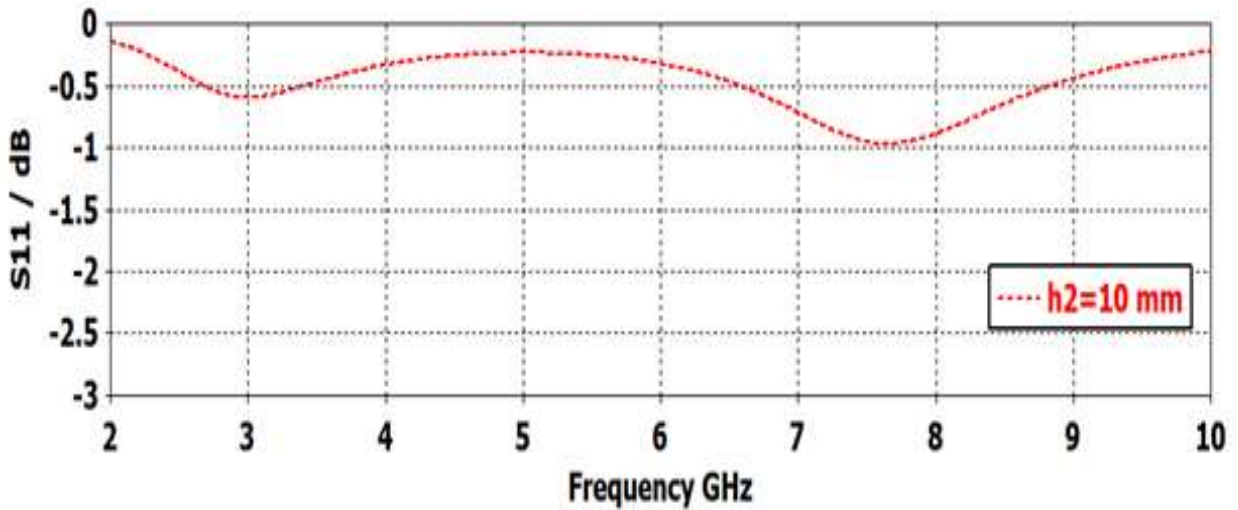
Figure 3.2: Variation of the reflection coefficient S_{11} with frequency for 10 mm air spacer thickness.

3.2.1 Effect of ring diameter

Figure 3.3 shows the results obtained for various values of the ring diameter, where it can be seen that as the diameter of the ring is increased the reflection coefficient of the first resonance frequency decreased.

In addition, it can be observed that increasing the diameter of the ring further led to the appearance of another resonance frequency (high order mode) between (10 and 11 GHz).
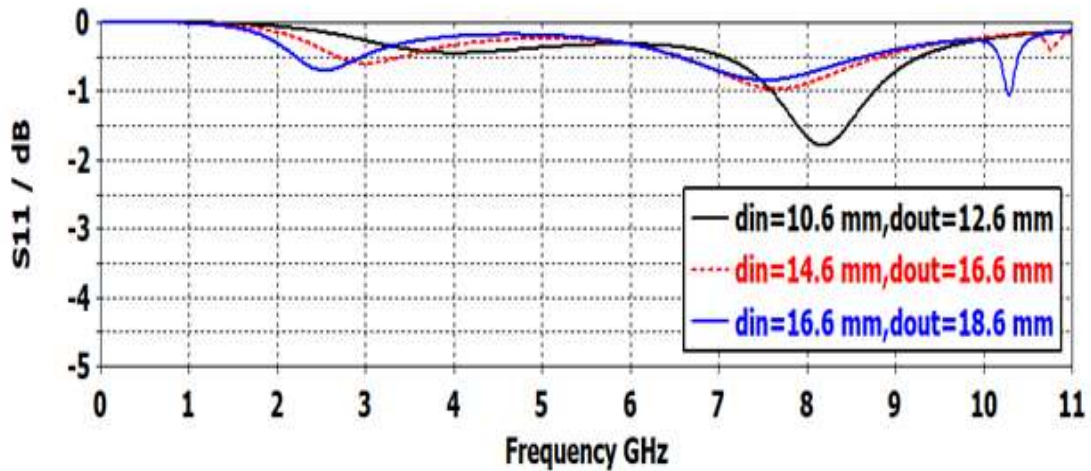
Figure 3.3: Variation of the reflection coefficient S_{11} with frequency for various
ring diameters, and with 10 mm air spacer thickness.

3.2.2 Effect of air spacer thickness

The effects of varying the air spacer thicknesses between the dielectric substrate and ground plane was investigated. The purpose of this investigation is to examine the effects of changing the spacing on the reflection coefficient of the FSS, getting minimum reflection as much as possible to achieve better absorption. Figures 3.4 and 3.5 show the variation of the reflection coefficient of the FSS with frequency for various values of the air spacer thickness. The figures show that there is a resonance case indicated by a small reflection coefficient at frequencies in the range of 3-3.8 GHz. As the thickness of the air spacer h_2 is changed, then the effective permittivity of the two layers (air+ FR4) will change according to Eq. (3.2) and Eq. (3.3). Thus, the effective wavelength given by Eq. (3.4) results in changing the resonance frequency. The other note on the results of these Figures is that at 10 mm spacer thickness there is another resonance frequency at higher of around 8 GHz. there is a third resonance frequency at a 5 mm air spacer. From Figs. 3.4 and 3.5 it can also be seen that the increase in the air spacer thickness results in reducing the reflection coefficient with a lower shifting of the second

38

resonance frequency. However, the reflection coefficient needs to be further reduced for the FSS to function as a good absorber.
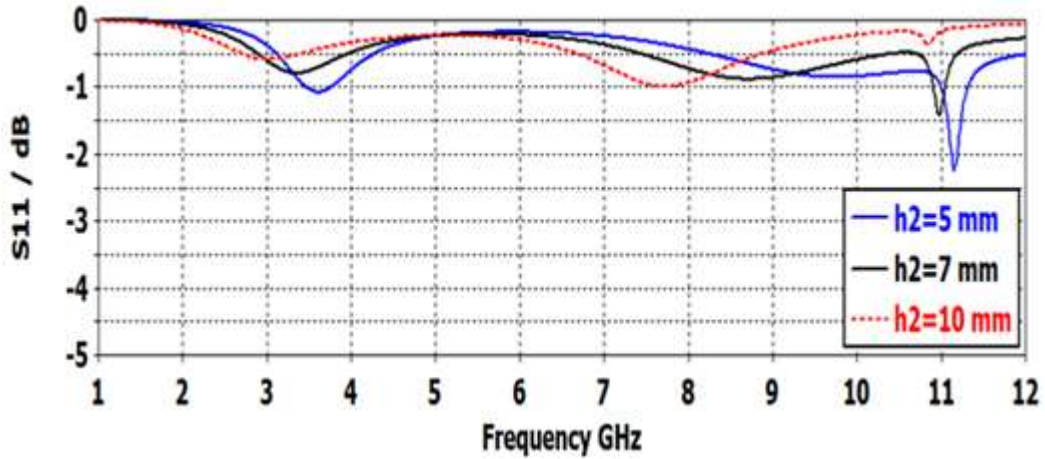
Figure 3.4: Variation of the reflection coefficient S_{11} with frequency for various air spacer thicknesses h_2, when $d_{in}= 14.6$ mm, $d_{out}= 16.6$ mm.
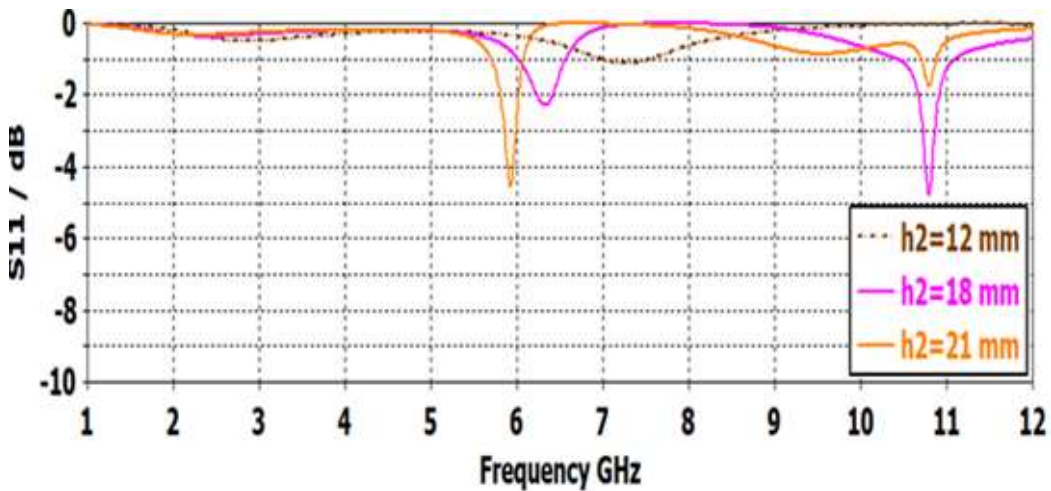
Figure 3.5: Variation of the reflection coefficients S_{11} with frequency for various air spacer thicknesses h_2, when $d_{in}= 14.6$ mm, $d_{out}= 16.6$ mm.

Table 3.2 shows the resonance frequencies found from the CST results, compared to those estimated from the determined effective dielectric constant, where the average circumference of the ring is given by Eq. (3.6):

$l = \pi \ d_{a =} \ \pi \times 15.6 = 49$ mm

Then the estimated frequency is found as:

$$\lambda_e = 2 \ l = C \ / \ [f \ \sqrt{\varepsilon e}] \tag{3.7}$$

$f = C \ / \ [2 \ l\sqrt{\varepsilon e}]$

Thus, for an average circumference of 49 mm, Eq. (3.6) results in :

$f = C \ / \ [2 \ l\sqrt{\varepsilon e}] = f = 3.1/\sqrt{\varepsilon e}$ GHz.

Table 3.2: Reflection coefficients at resonance for various values of the air spacer thickness h_2, when d_{in}= 14.6 mm, d_{out}= 16.6 mm.

Air spacer thickness (h_2) (mm)	ε_e from Eq. (3.3)	Resonance f From Eq. (3.7)	Resonance f_1(GHz) From CST	Reflection (S_{11}) (dB)
4	1.167	2.87	3.70	-1.34
5	1.134	2.91	3.55	-1.09
7	1.096	2.96	3.31	-0.80
10	1.067	3	3	-0.59
12	1.055	3.02	2.80	-0.51
15	1.044	3.03	2.55	-0.43
18	1.037	3.04	2.38	-0.37
21	1.031	3.05	2.19	-0.32

It can be seen that the resonant frequency changes slightly as the air spacer is increased. This is due to the decrease in the value of the composite permittivity as

the air-spacer is increased. Table 3.2 compares the values of the resonance frequency that were obtained from the CST simulation results with those estimated from the Eq. (3.7). It can be observed the accuracy of the estimated is better when the thickness of the air spacer is around 10 mm.

3.2.3 The equivalent circuit

In the analysis of the unit cell of the FSSA, the structure of the design consists of a circular ring printed on a dielectric substrate that has been set at a certain distance from the plane of the ground. The absorber's overall thickness (dielectric + air spacer) is approximately 0.12 λ_e. The suggested absorber's operation could be described by equivalent circuit model. As shown in Fig. 3.6, the suggested absorber's equivalent circuit includes three sections: section 1 of an RLC circuit parallel to a short transmission line, The RLC component represented by the continuous ring and the shorted transmission line for section 2 of length h_1 corresponding to the dielectric substrate. Section 3 of a short transmission line section has a length of h_2, which denotes the air spacer thickness backed by the ground plane. When such an absorber is subjected to incident microwaves, the metal background prevents transmission, therefore the incident microwave power could either be reflected or absorbed.

The equivalent impedance of this circuit as a function of frequency can be given by:

$$Z_e = R + j\omega L + \frac{1}{j\omega C} \tag{3.8}$$

The series inductance and capacitive of continuous ring in section 1 act as a short-circuit at resonance.

$$Z_e = R \text{ at resonance}$$

For the air spacer of thickness (h_2) that is backed by copper ground plane, the equivalent impedance can be expressed as [45]:

$$Z_1 = j\, Z_0 \tan(\beta_0 h_2) \tag{3.9}$$

$$Z_1 = j\, Z_0 \tan\left(\frac{2\pi f_o}{c} h_2\right)$$

Where j is the imaginary unit, Z_0 is the characteristic impedance of the free space, f_o and c represents the incident electromagnetic wave's frequency and velocity of light, respectively.

At 3GHz frequency and air spacer of 10 mm, the impedance Z_1 shown in Fig. 3.6 will be:

$$Z_1 = j\, Z_o \tan\left(\frac{2\times\pi\times3\times10^9}{3\times10^8} \times 0.01\right) = \; j\, 0.727 Z_o \text{ Ohm.}$$

The equivalent impedance Z_1 is transformed to Z_t after passing through the substrate, since the substrate of a small thickness compared to the air gap, then the following approximation can be adopted.

$$Z_t = Z_1 \tag{3.10}$$
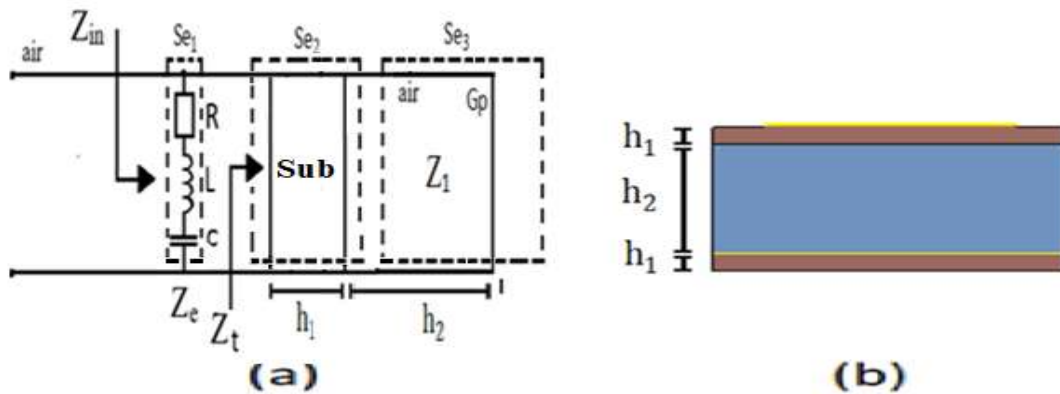
Figure 3.6: (a) Equivalent circuit model of the FSS continuous ring absorber. (b) proposed design for FSSA.

$$Z_{in} = Z_e // Z_t \qquad\qquad (3.11)$$

At resonance, the RLC circuit (equivalent circuit of the ring) will have an impedance R, then the input impedance Z_{in} of the FSS structure will be:

$$Z_{in} = R // Z_t$$

Then the reflection coefficient at resonance for the incident wave is:

$$\Gamma = \frac{Z_{in} - Z_o}{Z_{in} + Z_o} \qquad\qquad (3.12)$$

$$\Gamma = \frac{\dfrac{Z_1 R}{Z_1 + R} - Z_0}{\dfrac{Z_1 R}{Z_1 + R} + Z_0}$$

$$\Gamma = \frac{-RZ_0 + Z_1 (R - Z_0)}{RZ_o + Z_1 (R + Z_0)}$$

But $Z_1 = j\,0.727Z_0$ then

$$\Gamma = \frac{-RZ_0 + j0.727Z_0(R - Z_0)}{RZ_o + j0.727Z_0(R + Z_0)}$$

$$\Gamma = \frac{-R + j0.727(R - Z_0)}{R + j0.727(R + Z_0)}$$

Since the left side of the above relation is a real value, then right side is converted into polar form and its magnitude is equated to Γ as follows:

$$\Gamma^2 = \frac{(R^2 + [(0.727(R - Z_0)]^2)}{(R^2 + [0.727(R + Z_0)]^2)}$$

$$\Gamma^2 = \frac{R^2 + 0.529(R^2 - 2RZ_0 + Z_0{}^2)}{R^2 + 0.529(R^2 + 2RZ_0 + Z_0{}^2)}$$

From Table 3.2 when the reflection coefficient is -0.59 dB at air spacer thickness h_2=10 mm the impedance of the continuous copper ring is calculated as:

$$(0.935)^2 = \frac{R^2 + 0.529(R^2 - 2RZ_0 + Z_0{}^2)}{R^2 + 0.529(R^2 + 2RZ_0 + Z_0{}^2)}$$

$R = 12.824$ or 3832.21 Ohm.

This value of resistance $R = 12.824$ Ohm is substituted in the above equation for obtaining reflection coefficient using MATLAB program. It was found that the reflection coefficient ($\Gamma = 0.7526$) is not conformed to that simulated from CST.

Then the input impedance calculated from Eq. (3.12) will be:

$Z_{in} = 0.726 < 1.51°$ Ohm.

From this result, it is shown that there is no impedance matching, so the design is not suitable for obtaining high absorption.

3.2.3 Impedance calculation

The resistance of the ring can be obtained by taking the cross-sectional area of the copper ring as depicted in Fig. 3.7, So it is computed as:

$$R = \rho \, \frac{l}{Ae} \tag{3.13}$$

At 3 GHz the skin depth is:

$$\delta = \sqrt{\frac{\rho}{\pi f_o \mu}} \tag{3.14}$$

44

$$\delta = \sqrt{\frac{1.72\times 10^{-8}}{\pi \times 3\times 10^9 \times 4\pi \,x10^{-7}}} = 1.2\times 10^{-6} \text{ m.}$$

So, the effective area of multiplying width with thickness can be evaluated as:

$$\text{Ae} = \text{width} \times \text{thickness} - [(\text{width} - 4\delta) \times (\text{thickness} - 4\delta)]$$

$$= 2\times 10^{-3} \times 0.035 \times 10^{-3} - [(2 \times 10^{-3} - 4 \times 1.2 \times 10^{-6}) \times$$

$$(0.035 \times 10^{-3} - 4 \times 1.2 \times 10^{-6})]$$

$$\text{Ae} = 0.97 \times 10^{-8} \text{ m}^2.$$

then $R = \rho \dfrac{l}{\text{Ae}} = 1.72\times 10^{-8} \dfrac{0.097}{0.97\times 10^{-8}\, m^2} = 0.17$ Ohm.

Where the voltage is assumed and the current is various along circular copper ring.

$$I = \frac{V}{R} \tag{3.15}$$

Then the electromagnetic lost power can be obtained as $P_{loss} = I^2 \times R.$
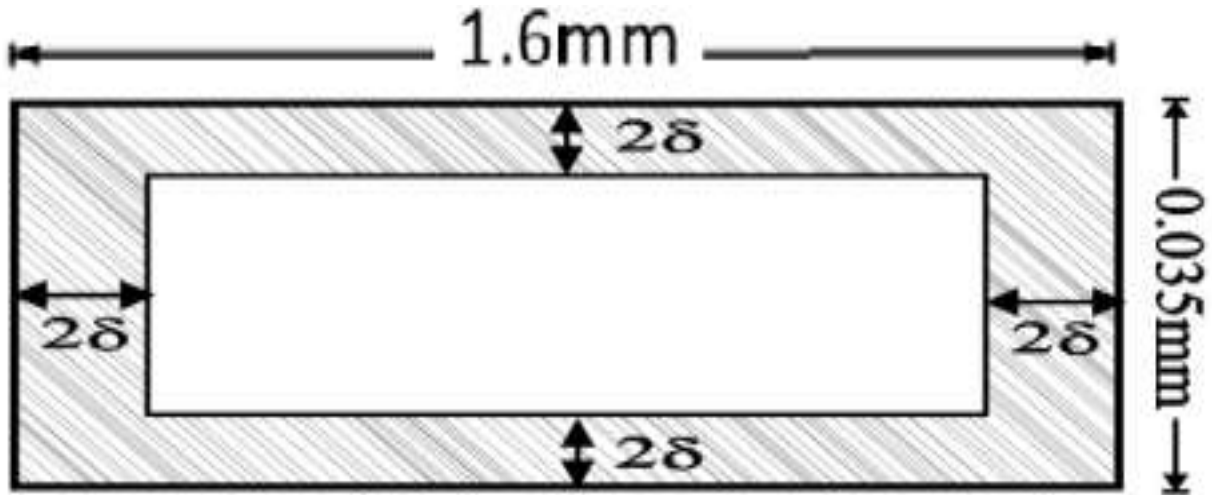
Figure 3.7: Concentration of current (shaded area) across the cross-section of the strip forming the circular loop. The current is effectively assumed to be at twice the skin depth.

3.3 Analysis of a circular ring FSS with lumped resistors

In the development of the performance of the FSSA, it was suggested to use lumped resistors to provide absorption of the power of the incident wave, so that the reflected power and reflection coefficient are reduced.

The incident wave induces an electromotive force (EMF) voltage in the ring leading to a circulating RF current.

If a resistor is placed in the path of this current, then ohmic losses in the form of I^2R will lead to reduced reflected power and a smaller reflection coefficient. This idea is implemented and explained in the next section.

3.3.1 The Conductive of Split ring resonator

The proposed FSS unit cell comprises a split ring having four equal parts, where four lumped resistors are placed across the resulting four gaps. The design of the FSS ring with four split parts is depicted in Fig. 3.8. The split ring is embedded on the FR4 substrate at a 10 mm distance from the ground plane. The length of each of the four gaps was initially set at 2 mm.

(a) FSS layer   (b) Side view   (c) Ground plane
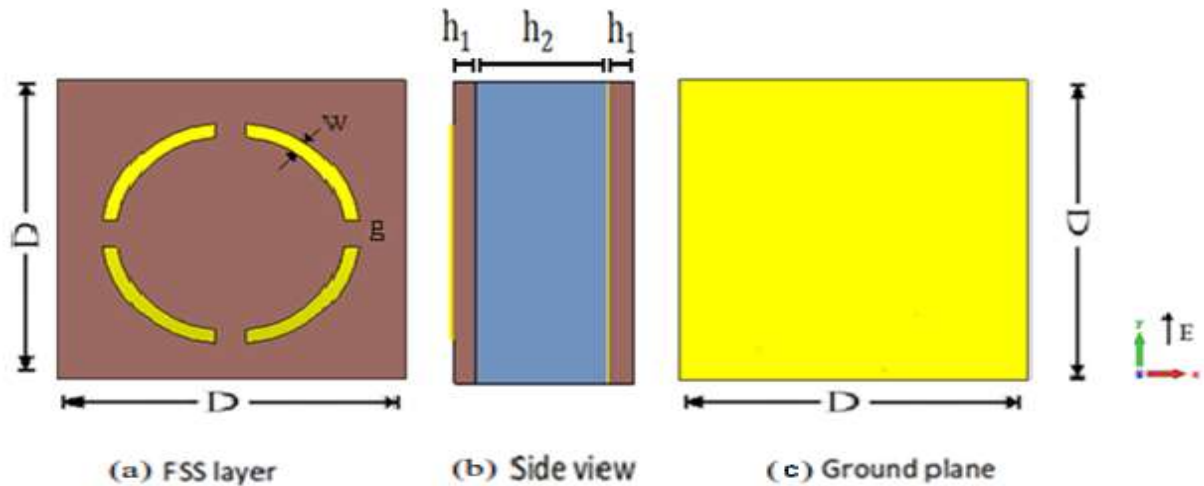
Figure 3.8: Geometry of the proposed FSS with split ring and ground plane; (a) top view of FSS, (b) side view, and (c) top view of ground plane.

The effect of the variation of gap length on resonance frequency and reflection were simulated using an average diameter of the ring of 49 mm, (d_{in}= 14.6 mm, d_{out}= 16.6 mm). The obtained results are shown in Fig. 3.9 and Table 3.3, where the four parts of the ring are not connected with resistors. It can be seen that when the gap length is zero (continuous ring), then the resonance frequency is about 3 GHz. However, when the ring is spliced into four parts. The first resonance frequency increased to higher values between (4 and 5 GHz), whereas the second resonance increased between (8.5 - 11.5 GHz). As each part of the ring can resonate at a frequency corresponding to its length, one should take into account the effect of the gap between any two adjacent segments.

This gap can be considered as a capacitance connecting the two adjacent parts of the ring. As the length of the gap is increased, the capacitance due to the gap decreased with a gradual increase in the reflection coefficient while reducing the reflection coefficient at the second resonance.
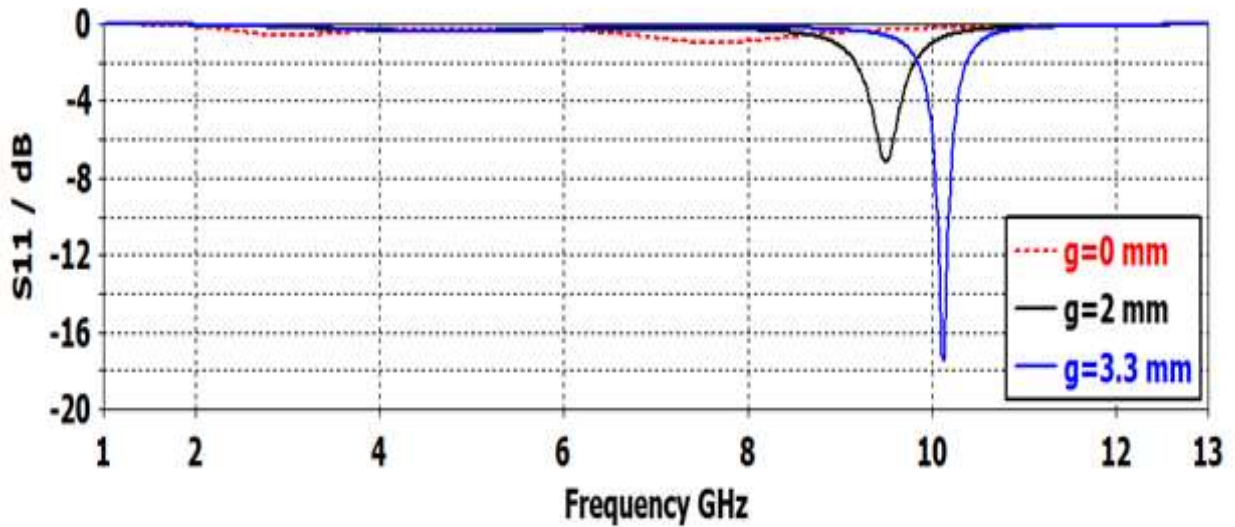
Figure 3.9: Variation of the reflection coefficients S_{11} with frequency for the 4-segment ring for various gap lengths.

In Table 3.3 as the gap length increases, the bandwidth increases, and larger bandwidth is achieved when the gap length is increased to 3.3 mm, which is located between (10.05 -10.18 GHz) with minimum reflection equal to -17.36 dB, but there is poor reflection indicated at first resonance response at operational frequency.

Table 3.3: Reflection coefficients at resonance for the 4-segment ring for various values of the gap length.

Gap length (mm)	Frequency f_1(GHz)	Reflection (S_{11}) dB	Frequency f_2(GHz)	Bandwidth (GHz)	Reflection (S_{11}) dB
0	3	-0.59	7.76	---	-0.96
0.5	4.28	-0.42	8.86	---	-3.48
2	4.63	-0.38	9.49	---	-7.17
3.2	4.76	-0.36	10.06	0.12	-15.63
3.3	4.69	-0.35	10.12	0.13	-17.36
3.4	4.78	-0.35	10.19	0.12	-20.84
4	4.67	-0.34	10.56	0.1	-16.93
4.5	5.06	-0.34	11.09	---	-8.25

3.3.2 Absorption FSS

This section investigates the influence of adding lumped resistors to the circular ring on the electromagnetic wave absorption. The incident wave produces a certain current in the loop, which results in I^2R loss in each of the lumped

resistors. In the investigated design, the ring was split into four parts, and four resistances were added at the resulting gaps as shown in Fig. 3.10. The gap length was chosen as 2 mm.
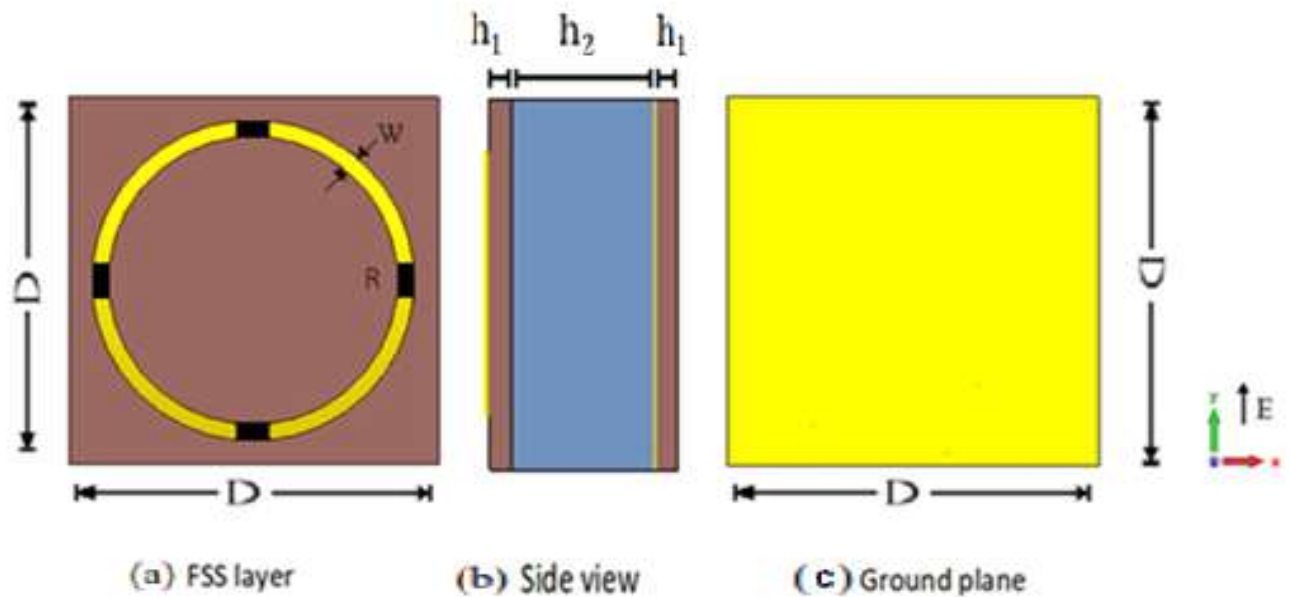
Figure 3.10: Geometry of the proposed FSS with four resistances and a ground plane; (a) Top view of absorption FSS, (b) side view, and (c) top view of the ground plane.

3.3.2.1 Effect of the ring diameter and resistances

The effect of the variation in the diameter of the ring is shown in Fig. 3.11. The ring's diameter is increased to tune the resonance frequency, whereas the resistance is varied to achieve a better response with less reflection and a wider bandwidth.
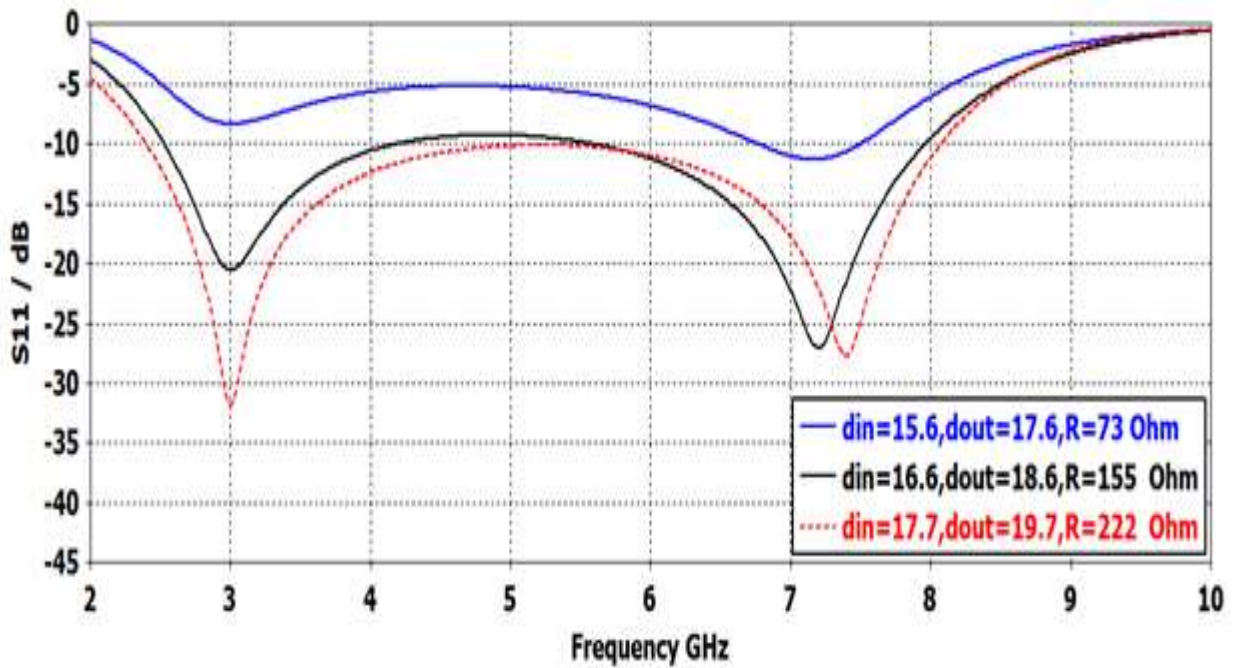
Figure 3.11: Variation of the reflection coefficient S_{11} with frequency for various values of the ring diameters and resistors, when $h_2=10$ mm.

The results of the performed simulations are listed in Table 3.4. From this table, it can be seen that as the diameter of the ring increases, the required resistance to get better response increases as well.

The largest achieved bandwidth is 5.68 GHz when the diameters of the ring are $d_{in}=17.7$ mm, $d_{out}=19.7$ mm.

The minimum reflection obtained in this bandwidth is -31.80 dB. These findings represent a considerable improvement compared to the case without the lumped resistors. The influence of the resistor values is studied in the next section.

Table 3.4: Bandwidth and reflection coefficients at resonance for 10 mm air spacer thickness at various values of the resistances and ring diameter.

d_{in} (mm)	d_{out} (mm)	Resistances (R) (Ohm)	Resonance f_1 (GHz)	Bandwidth (GHz)	Reflection (S_{11}) (dB)
14.6	16.6	1	3.03	---	-0.72
15.4	17.6	73	3	---	-8.37
16.6	18.6	155	3	1.68	-20.54
17.7	19.7	222	3	5.68	-31.80
16.6	18.6	155	3	1.68	-20.54
18.6	20.6	266	3	5.60	-21.03

3.3.3 Comparison between continues ring and lumped resistance

Comparison of FSS with four resistance and continuous ring are shown in Fig. 3.12, The figure shows that much better absorption has been achieved as compared with the case of the continuous ring (without the resistors).

Lower reflection coefficient has been achieved, and it extends over a wider range of frequencies.

The blue color represents the reflection coefficient for the ring, while the red dash color is for the case of spliced ring with 222 Ohm resistors.

It can be observed higher value of reflection occurred for R=0 Ohm (continuous ring). By adding resistances, a smaller value of reflection coefficient is obtained at 3 GHz frequency.

These high absorptions are mainly due to the ohmic losses at this frequency. Minimized reflection is caused by decreased current in the copper ring due to the presence of resistances.
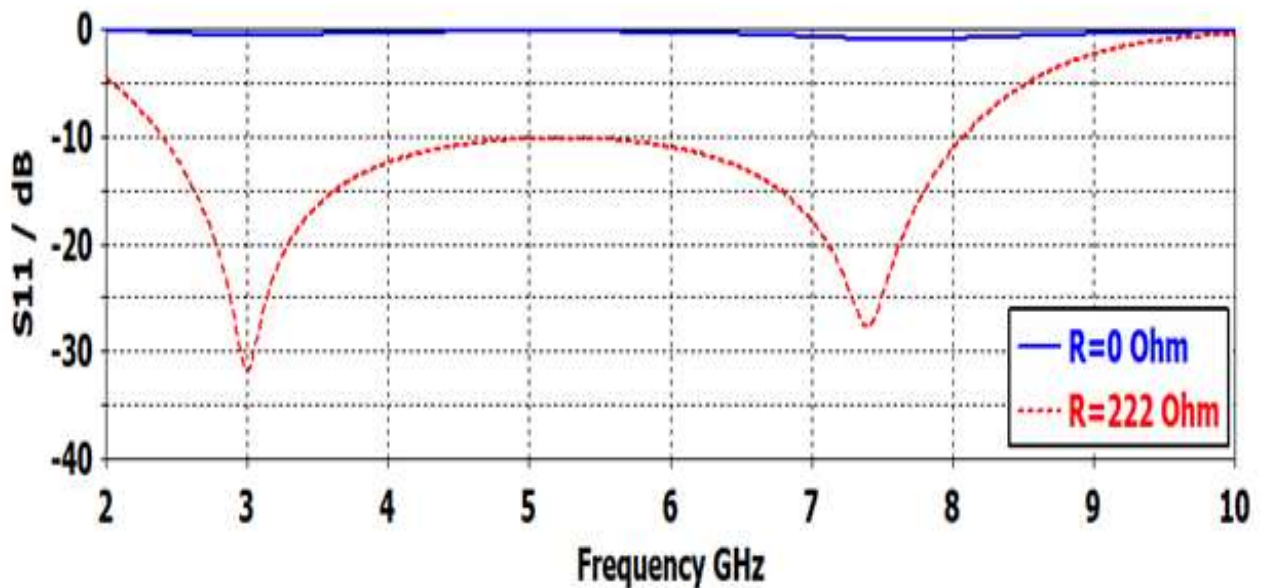
Figure 3.12: Variation of the reflection coefficient S$_{11}$ with frequency for a continuous ring and that with the four resistances, when h_2=10 mm, d_{in} =17.7 mm, d_{out} =19.7 mm.

The existing current distributions in Fig. 3.13 show the current density of both four resistances ring and continuous ring without resistance. It can be seen that intensity of current density for the continuous ring (green color) is 60 A/m.

By adding four resistances of 222 Ohm, the intensity of the current (blue color) is reduced by approximately 3 times from that continuous ring with no resistances.
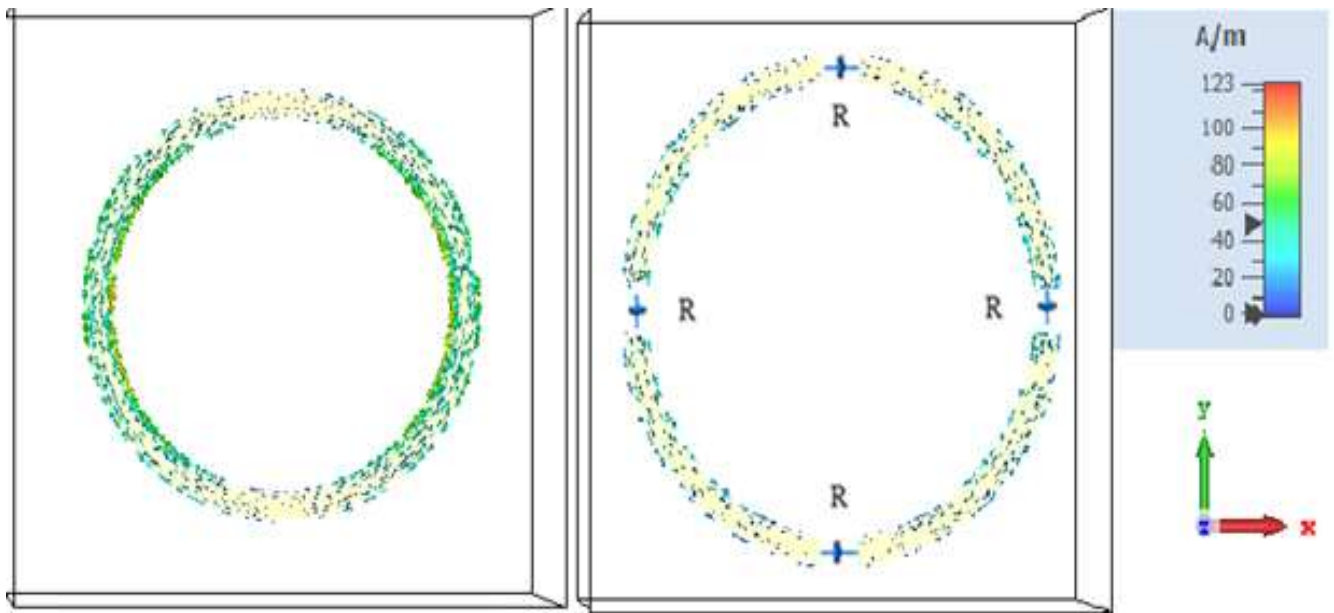
Figure 3.13: Current distribution at 3 GHz, (a) Continuous ring without resistances; (b) With resistances.

3.3.4 Effect of the lumped resistors

The influence of the value of the resistances on the performance of the FSSA was investigated by trying to optimize the resistor value. Figure 3.14 displays the reflection coefficient with frequency change for different resistors values, and the parameters of the obtained results are compared in Table 3.5.

The table shows that as the lumped resistances are increased from 50 Ohm to 550 Ohm, the frequency of minimum reflection changes slightly. The -10dB bandwidth increased with the increase of the resistance and then decreased. Thus, the performance of bandwidth-reflection coefficient can be optimized by a proper change of the lumped resistors.

The increase in the bandwidth can be attributed to the fact that the Q-factor of the resonating ring.

The Q-factor decreases as the resistance is increased. The bandwidth is related to the Q-factor by [43]:

$$BW = \frac{f_o}{Q} = \frac{R}{2\pi L} \qquad\qquad (3.16)$$

Where R is resistance, f_o is the resonant frequency and L is the inductance of ring.
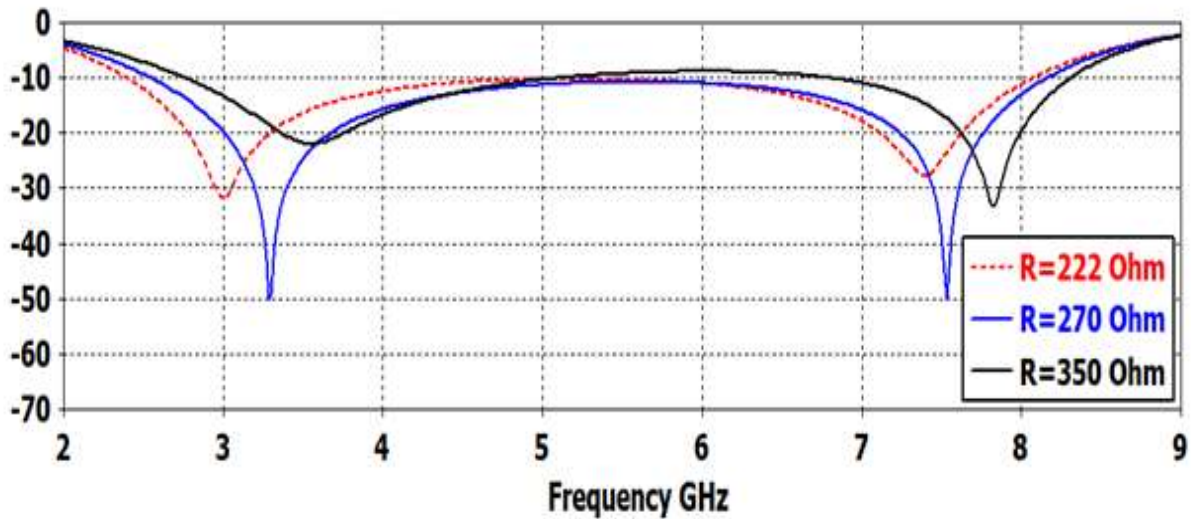
Figure 3.14: Variation of the reflection coefficient S_{11} with frequency for various values of the resistors, when $h_2=10$ mm.

Higher bandwidth of 5.68 GHz is obtained when the resistances equal to 222 Ohm, which is located between (2.39-8.07 GHz).

The results also show that the best reflection coefficient is obtained for the resistance value of 222 Ohm.

Further increasing the resistance raises the reflection coefficient towards unity, which is not recommended, resulting in a decrease in absorption to zero.

Table 3.5: Bandwidth and reflection coefficients at resonance for 10 mm air spacer thickness at various values of the resistances, when d_{in} =17.7 mm, d_{out} =19.7 mm.

Resistances (R) (Ohm)	Resonance f_1 (GHz)	Bandwidth (GHz)	Reflection (S_{11}) (dB)
50	2.41	---	-7.42
100	2.49	0.64	-15.57
220	2.99	5.65	-31.77
221	2.99	5.67	-31.73
222	3	5.68	-31.80
223	3.01	5.65	-31.90
230	3.05	5.63	-32.41
240	3.12	5.62	-33.83
250	3.18	5.67	-36.07
260	3.24	5.62	-40.29
270	3.28	5.61	-50.03
280	3.33	5.63	-43.31
290	3.36	3.02	-35.24
300	3.42	5.58	-32.15
350	2.54	2.35	-21.96
400	3.65	2.35	-17.76
550	3.80	1.06	-11.69

3.3.5 Equivalent circuit model

This section attempts to derive formulas for FSS ring with four lumped resistors. The transmission line analysis together with equivalent circuit models for the (FR4+air spacer) can be used to find the input impedance of the structure. The FSSA can be modeled by a three-section transmission line as shown in Fig. 3.15. The copper ring in Section 1 is made up of resistance (4R) capacitance (C) and inductance (L). The four lumped resistances have total value that exceeds the resistance of the copper ring, thus the latter was neglected, while in Fig. 3.6 the resistance R represents the resistance of the copper ring. Section 2 shows the top FR4 layer, which has a thickness of h_1, and section 3 shows the air spacer layer, which has a thickness of h_2. The ground plane is modeled here as a short circuit connected to section 3 of the transmission line. The absorbing structures are backed by a metal plate in practical applications to eliminate the absorption characteristics' dependence on environmental factors that are located behind the absorber. The series inductance and capacitive of section 1 of Z_e impedance, act as a short- circuit at resonance, so the effect of four resistance has to be taken into account so Eq. (3.8) will be:

$$Z_e = 4R + j\omega L + \frac{1}{j\omega C}$$

$Z_e = 4R$ at resonance.

As a result, to achieve broadband microwave absorption, the input impedance Z_{in} must match the air characteristic impedance Z_0 over a wide frequency range. Perfect absorption can be achieved when the overall impedance of the FSSA matches the impedance of free space [70].
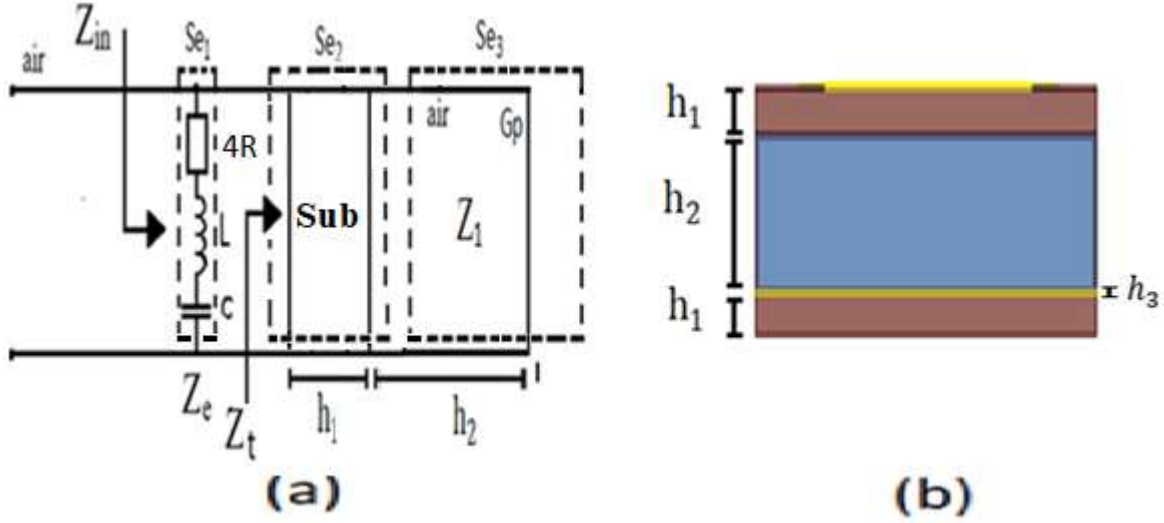
Figure 3.15: (a) Equivalent circuit model of the FSS with lumped resistors absorber. (b) proposed design for FSSA.

The air spacer of thickness (h_2) that is backed by copper ground plane can be considered as short-circuited transmission line, thus the impedance can be expressed as Eq. (3.9):

$$Z_1 = jZ_0 \tan(\beta_0 h_2)$$

Then at 3 GHz frequency and air spacer of 10 mm, the impedance Z_1 shown in Fig. 3.12 (a) will be:

$$Z_1 = j Z_o \tan(\frac{2 \times \pi \times 3 \times 10^9}{3 \times 10^8} \times 0.01) = j\, 0.727\, Z_o$$

The small thicknesses of the substrate (h_1) was neglected as Eq. (3.10):

$$Z_t = Z_1$$

The proposed FSS (Z_{in}) input impedance can be obtained as parallel connection between equivalent impedance Z_e of the ring and the terminated impedance Z_t:

At resonance, the FSS equivalent circuit produces a resistive value 4R parallel to the Z_t so the Eq. (3.11) will be

$$Z_{in} = 4R // Z_t \qquad\qquad (3.17)$$

Then the reflection coefficient at resonance for the incident wave is:

$$\Gamma = \frac{Z_{in} - Z_o}{Z_{in} + Z_o}$$

$$\Gamma = \frac{\frac{Z_1 \times 4R}{Z_1 + 4R} - Z_0}{\frac{Z_1 \times 4R}{Z_1 + 4R} + Z_0}$$

$$\Gamma = \frac{-4RZ_0 + Z_1 (4R - Z_0)}{4RZ_o + Z_1(4R + Z_0)}$$

But $Z_1 = j\,0.727 Z_o$ then

$$\Gamma = \frac{-4RZ_0 + j0.727Z_0(4R - Z_0)}{4RZ_o + j0.727Z_0(4R + Z_0)}$$

By finding the magnitude of numerator and denominator i.e.

$$\Gamma^2 = \frac{(16R^2 + [(0.727(4R - Z_0)]^2)}{(16R^2 + [0.727(4R + Z_0)]^2)}$$

At small reflection -31.80 dB when lumped resistance equal to 222×4 from Table 3.5 the impedance of lumped resistance can be evaluated as:

$$(0.026)^2 = \frac{16R^2 + 0.529(16R^2 - 8RZ_0 + Z_0{}^2)}{16R^2 + 0.529(16R^2 + 8RZ_0 + Z_0{}^2)}$$

R= 55.42<0.94° or 55.42< (-0.94)° Ohm.

The value of reflection coefficient from MATLAB program is equal to $\Gamma = 0.5096$.

Then, the input impedance for 55.42< (-0.94)° calculated from Eq. (3.12):

$Z_{in} = 0.734 < 1.56\degree$ Ohm.

3.3.6 Effect of the air spacer thicknesses on ring with four resistors

The simulation results for adding four resistances of 222 Ohm on copper ring with various values of air spacer thicknesses are shown in Fig. 3.16. The simulation shows that there is a shifting happened in the frequency to the lower values when the air spacer thickness increased.
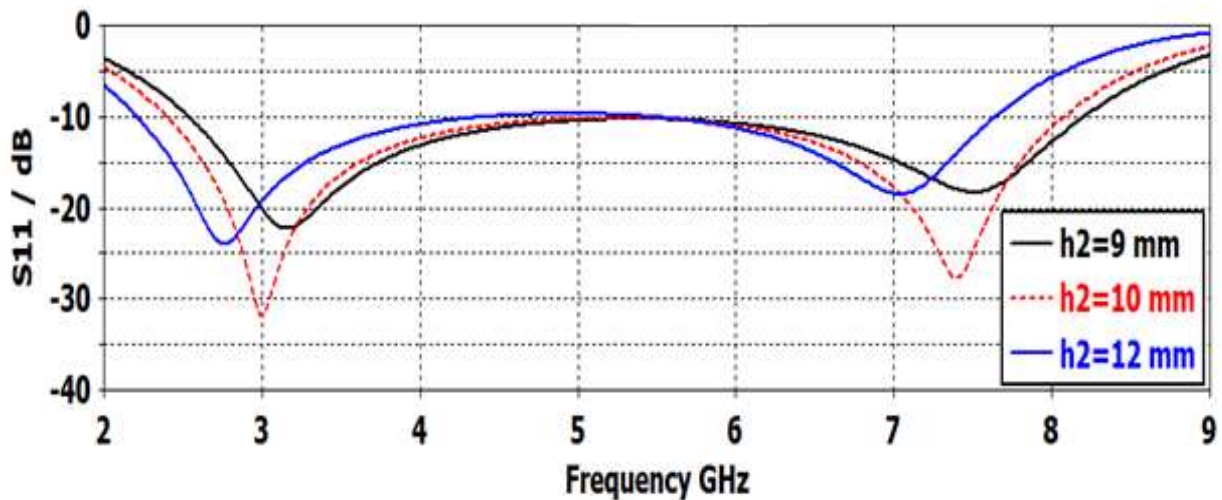
Figure 3.16: Variation of the reflection coefficient S_{11} with frequency for various air spacer thicknesses, when R=222 Ohm.

Table 3.6 demonstrates the reflection coefficient and bandwidth of different thicknesses. The reflection coefficient at resonance changes as the spacer thickness is changed.

The bandwidth changes slightly when the air spacer thickness changed. High bandwidth can be found at the case of h_2=10 mm spacer thickness, which is equal to 5.68 GHz where the small reflection coefficient -31.80 dB which is located at (2.39 -8.07GHz).

Table 3.6: Bandwidth and reflection coefficients at resonance for 222 Ohm resistances at various values of the air spacer thicknesses, when d_{in} =17.7 mm, d_{out} =19.7 mm.

Air spacer thickness (h_2) (mm)	Resonance f_1 (GHz)	Bandwidth (GHz)	Reflection (S_{11}) (dB)
5	4	---	-9.18
6	3.73	1.29	-11.51
7	3.51	1.94	-14.16
8	3.32	2.44	-17.53
9	3.15	5.66	-22.29
9.9	3.02	5.66	-30.04
10	3	5.68	-30.81
10.1	2.98	5.67	-33.64
11	2.87	2.72	-33.79
12	2.75	2.21	-23.97
15	2.49	1.43	-15.18
18	2.27	0.80	-11.72
21	2.10	---	-9.60

3.3.7 Effect of the ring width

Figure 3.17 demonstrates how the S_{11} reflection coefficient changes with frequency at 10 mm air spacer for various widths of the ring in the presented of four resistances of 222 Ohm, where the average circumference of the ring was kept

constant. The results show that the bandwidth of the response is affected by the width of the ring.

Larger bandwidth of the ring is obtained when w=2 mm However, the frequency of minimum reflection coefficient is also affected by the width of the ring. The minimum value of the reflection coefficient changed as the ring width is increased.

It can be observed that the minimum value of reflection coefficient is shown at w=2 mm is equal to -31.80 dB, however, larger width results in a small reflection coefficient at the resonance frequencies.
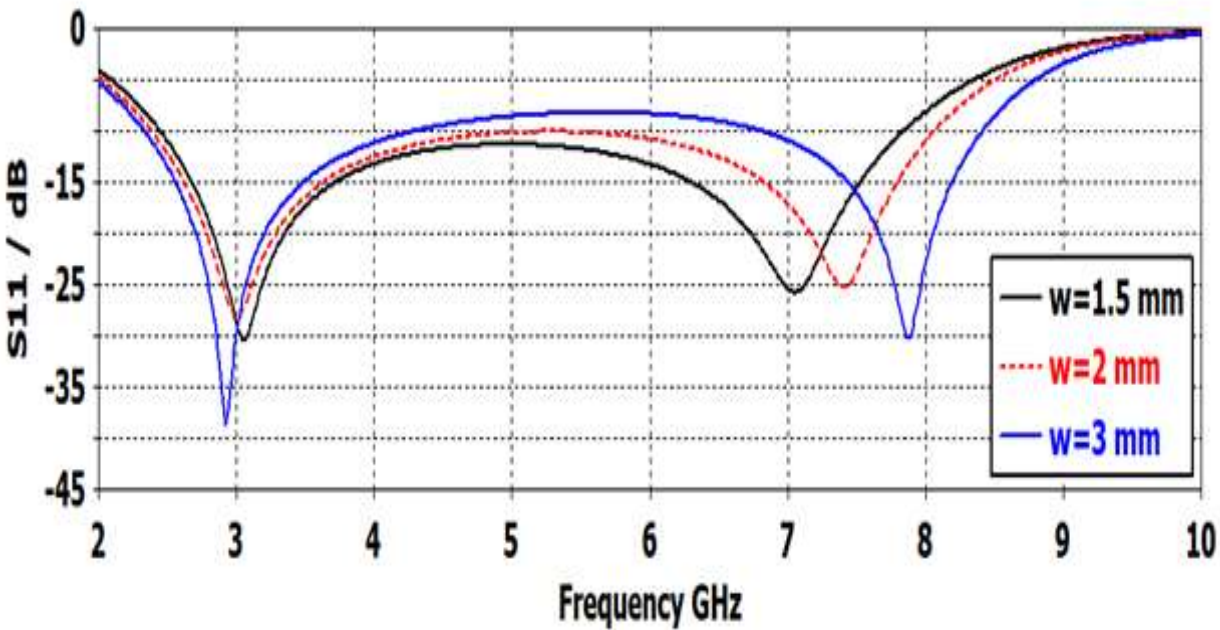
Figure 3.17: Variation of the reflection coefficient S_{11} with frequency for various values of widths, when h_2=10 mm, and R=222 Ohm.

Table 3.7: Bandwidth and reflection coefficients at resonance for 10 mm air spacer thickness at various values of the ring width.

Width (w) (mm)	Resonance f_1 (GHz)	Bandwidth (GHz)	Reflection (S_{11}) (dB)
0.5	3.09	4.50	-25.34
1	3.06	5.05	-26.99
1.5	3.05	5.39	-30.34
1.8	3.01	5.57	-30.93
1.9	2.98	5.62	-30.07
2	3	5.68	-31.80
2.1	3	2.74	-33.77
3	2.92	1.96	-38.69
4	2.85	1.75	-42.87
5	2.75	1.59	-40.94
6	2.65	1.47	-34.33
7	2.53	1.36	-27.47
9	2.40	1.25	-21.41

3.3.8 Impedance calculation

The impedance of the microstrip line forming the ring is affected by the width of the ring, height of substrate FR4+air space as well as the effective relative permittivity. It should be noted that in this design, the ring is backed by an FR4 layer of 1.6 mm thickness, and an air layer of 10 mm thickness. Thus, the impedance of its two-layer substrate has to be calculated properly. From determining the ratio of the width to height $\frac{w}{h} \leq 1$ so the impedance can be calculated as [70]:

$$Z_c = \frac{60}{\sqrt{\varepsilon e}} \ln\left[\frac{8h}{w} + \frac{w}{4h}\right]$$ (3.18)

At w=2 mm, and h_2=10 mm.

$$Z_c = \frac{60}{\sqrt{1.067}} \ln\left[\frac{8 \times 11.6}{2} + \frac{2}{4 \times 11.6}\right] = 222.9 \text{ Ohm}.$$

Table 3.8: Impedance of copper ring at resonance for 10 mm air spacer thickness and 222 Ohm lumped resistors at various values of the width.

Width (w) (mm)	Impedance Calculated (Ohm)	Resonance f_1 (GHz)	Bandwidth (GHz)	Reflection(S_{11})(dB)
0.5	303.4	3.09	4.50	-25.34
1	263	3.06	5.05	-26.99
1.5	239.6	3.05	5.39	-30.34
1.8	229	3.01	5.57	-30.93
1.9	225.9	3.02	5.63	-32.42
2	222.9	3	5.68	-31.80
2.1	220	3	2.74	-33.77
3	199.5	2.92	1.96	-38.69
4	182.8	2.85	1.75	-42.87
5	170	2.75	1.59	-40.94
6	159.6	2.65	1.47	-34.33
7	150.8	2.53	1.36	-27.47
9	136.6	2.40	1.25	-21.41

From Table 3.8 above, it can be noted that the value of the ring impedance is nearly equal to the lumped resistance 222 Ohm, indicating that matching impedance occurred at this resistance.

3.4 Comparison with the previous work

Table 3.9 Compares this work with former studies on FSSA. It can be been shown that the proposed structure bandwidth has been significantly improved

Table 3.9: Performance comparison of the suggested absorbers with earlier works.

Reference	FBW [%]	Thickness [mm]	Unit cell characteristics
[10]	126.8%	$0.088\ \lambda_L$	Single layer, spacer-8 resistors
[57]	10.99%	$0.062\ \lambda_L$	Single layer, spacer-4 resistors
[14]	114.4%,	$0.076\ \lambda_L$	Two layer, 12 resistors
[36]	72 %	$0.124\ \lambda_L$	Single layer+spacer-4 resistors
[40]	91.6%.	$0.098\ \lambda_L$	Single layer+ spacer-4 resistors
[37]	126.5%	$0.084\ \lambda_L$.	Single layer +Spacer, 4 resistors
[65]	127.52%	$0.084\ \lambda_L$	Triple-layered+2 Spacer, 4 resistors
[66]	132.7%	$0.085\ \lambda_L$	Triple-layered+2 Spacer, 4 resistors
Presented work	108.6%	$0.092\ \lambda_L$	Two layer, 4 resistors

Summary

1. The proposed conducting ring design resonates at half effective wavelength along the ring's circumference. The air spacer thickness also affects the FSS's resonance frequency.

2. From the analysis by the equivalent circuit model, and computed input impedance it was found that there is no perfect impedance matching.

3. The calculated impedance of the ring using the skin effect formulas agrees well with the estimated impedance from the CST simulation.

4. The comparison of continuous rings with and without lumped resistors reveals a significant reduction in reflection coefficient and an increase in bandwidth.

5. When air spacer thickness and ring width is considered, they all had the same absorption bandwidth of 108% and reflection coefficient.

6. The ring's impedance was computed using the microstrip line's characteristic impedance equation and compared to that estimated from the CST simulation.

CHAPTER FOUR

ANALYSIS OF ABSORBING FSS WITH CIRCULAR RING AND RESISTIVE STRIP

CHAPTER FOUR
ANALYSIS OF ABSORBING FSS WITH CIRCULAR RING
AND RESISTIVE STRIP

4.1 Introduction

This chapter investigates the enhancement of FSSA, where the attention is confined to the response of FSSA. The proposed design is based on the use of a resistive sheet instead of the copper for the metallic parts of the absorber. The suggested unit cell shape is a circular ring as that used in the former chapter. Then, a resistive strip is added with the intent of decreasing reflection and increasing in the bandwidth.

4.2 Analysis of a circular ring FSS with an air layer

The suggested FSSA is in the form of a resistive circular loop printed on the substrate. The substrate is backed by a ground plane that is separated by a certain layer of air as shown in Fig. 4.1. The circular loop is chosen so that there is no sensitivity to the direction of the incident electric field. In the investigated design, the effect of the air layer thickness is also considered. The substrate is made of FR4, which has a thickness of 1.6 mm, relative permittivity of 4.3 and loss tangent of 0.025. The circular ring is made of ohmic sheet of 0.035 mm thickness. The circular ring has a surface resistivity of 10 Ohm/sq. The outer diameter of the ring is 16 mm and while the inner diameter is 14 mm. The unit cell has dimensions of 18.2 mm×18.2 mm.
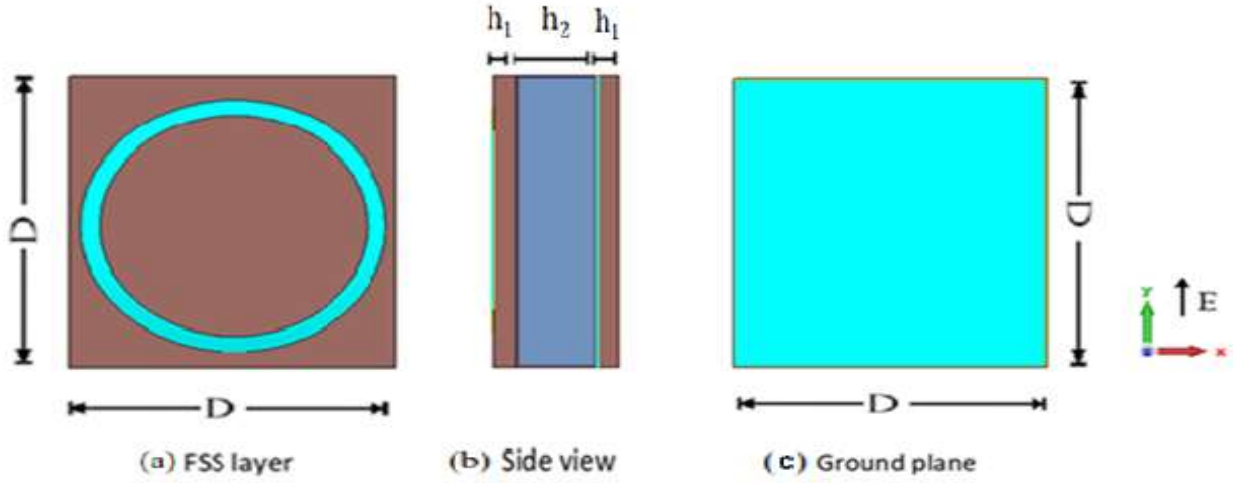
Figure 4.1: Geometry of the proposed FSS resistive ring and ground plane;
(a) Front view, (b) side view, and (c) back view showing the ground plane.

The parameter values of the design are listed in Table 4.1. The effective value of the permittivity ε_{rc} for the composite layer of the FR4 substrate and air is defined from Eq. (3.2).

$$\varepsilon_{rc} = \frac{(h_2+h_1)(\varepsilon r_2 \varepsilon r_1)}{h_2 \varepsilon r_1 + h_1 \varepsilon r_2}$$

$$\varepsilon_{rc} = \frac{(h_2+h_1)(\varepsilon r_2 \varepsilon r_1)}{h_2 \varepsilon r_1 + h_1 \varepsilon r_2} = 1.229$$

Which for the FR4 substrate and assuming a 5 mm layer of air, ε_{rc} becomes 1.229

The equivalent relative permittivity is due to the fringing effect is calculated from Eq. (3.3):

$$\varepsilon_e = \frac{\varepsilon_{rc}+1}{2} + \frac{\varepsilon_{rc}-1}{2} \frac{1}{\sqrt{1+\frac{10h}{w}}}$$

$$\varepsilon_e = \frac{1.229+1}{2} + \frac{1.229-1}{2} \frac{1}{\sqrt{1+\frac{10\times6.6}{2}}} = 1.134$$

Which for the equivalent layer ($\varepsilon_{rc} = 1.229$) will be equal to 1.134.

Thus, at the frequency of 3 GHz it is calculated from Eq. (3.4):

$$\lambda_{e=}\frac{\lambda_0}{\sqrt{\varepsilon e}} = \frac{\lambda_0}{\sqrt{1.134}} = 93.90 \text{ mm}$$

When the inner and outer diameters of the ring are 14 and 16 mm, then the average diameter from Eq. (3.5) will be :

$$d_a = \frac{(d_{out}+d_{in})}{2} = \frac{(16+14)}{2} = 15 \text{ mm}$$

So, the average circumference according to Eq. (3.6) will equal to:

$$l = \pi \, d_a = \pi \times 15 = 47.12 \text{ mm}$$

 The ring will resonate when its circumference is equal to half the effective wavelength, so the frequency is estimated from Eq. (3.7) :

$$f = C / [2 \, l\sqrt{\varepsilon e} \,] = f = 3.183/\sqrt{\varepsilon e} \qquad \text{GHz}$$

Table 4.1: Parameters of the design for resistive ring FSSA.

h_1	1.6
ε_{r_1}	4.3
ε_{r_c}	1.229
ε_e	1.134
f_o	3 GHz
λ_o	100 mm
λ_e	93.90
d_{out}	16 mm
d_{in}	14 mm
w	2 mm
Thickness of air spacer h_2	5 mm, and other values

The ring resonates when the value of circumference is equal λe /2. The design frequency was chosen to be 3 GHz, then $\lambda_o = 100$ mm, and according to Eq. (3.4), $\lambda_e = 93.90$ mm. To achieve resonance at this frequency, then according to Eqs. (3.6) and (3.7) the outer and inner diameters of the ring were set at $d_{in}=14$ mm, and $d_{out} =16$ mm respectively.

The simulation starts by considering a resistive ring, i.e, without the strip, and the obtained results are shown in Fig. 4.2, where the thickness of the air layer was assumed at 5 mm. It can be seen that there are two resonance frequencies, one at 3 GHz and the other at 9.47 GHz frequency. The upper frequency can be attributed to the third harmonic. It is observed from these results a higher dip in the reflection coefficient of about -29.39 dB at the first resonance frequency. It can be seen that as the diameter of the ring increases the resonance frequency decreases, while the diameter of 17 mm produces the smallest reflection coefficient.
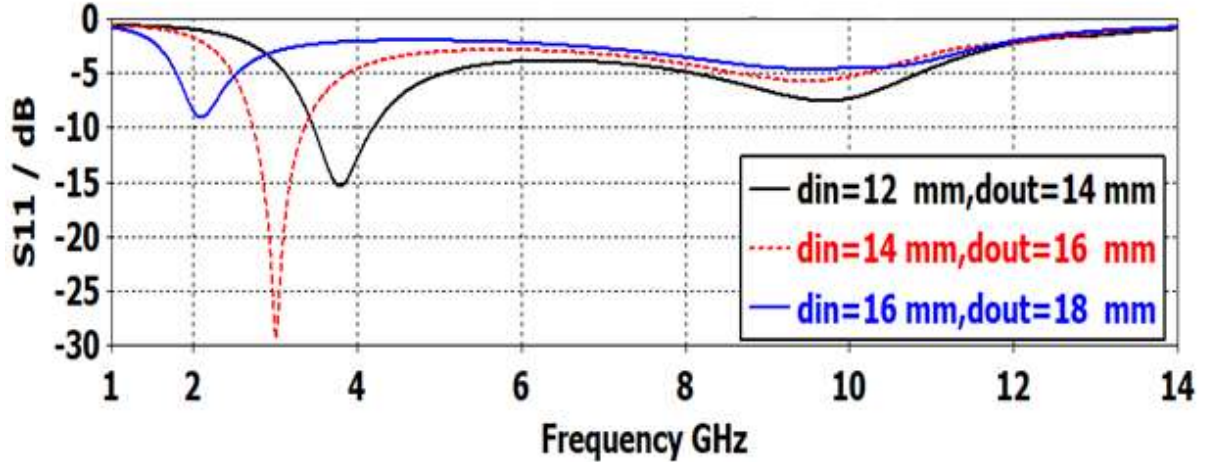
Figure 4.2: Variation of the reflection coefficient S_{11} with frequency for various ring diameters, and with 5 mm air spacer thickness.

4.2.1 Effect of air spacer thickness

In order to better understand the impact of air spacer thickness on the absorption of the unit cell, the air spacer thickness was varied between 5 mm and

21 mm, and the obtained results are shown in Figs. 4.3 and 4.4. The lowest reflection coefficient was obtained for a 5 mm thickness.
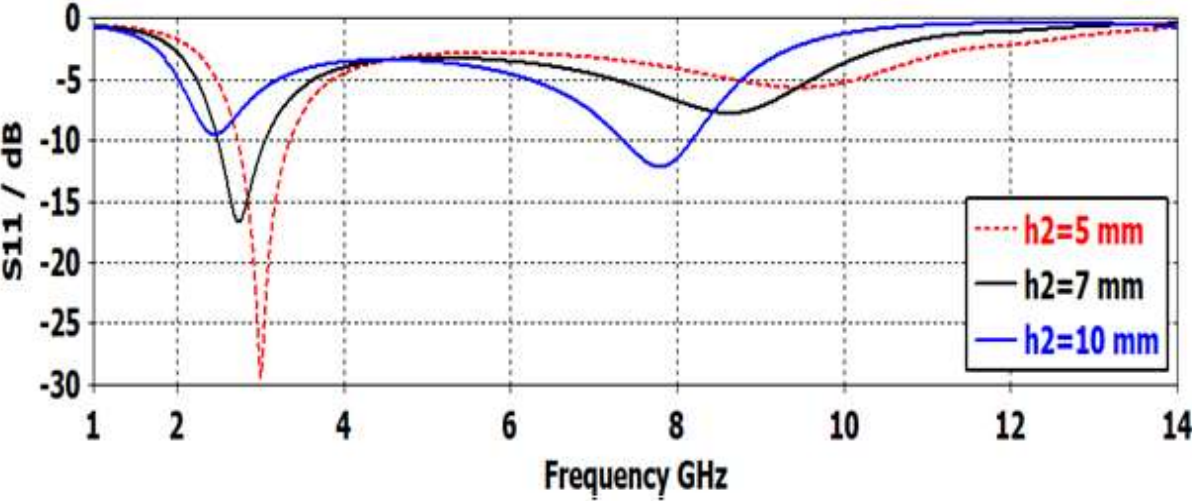
Figure 4.3: Variation of the reflection coefficient S_{11} with frequency for various air spacer thicknesses h_2, when $d_{in}=$ 14 mm, $d_{out}=$ 16 mm.
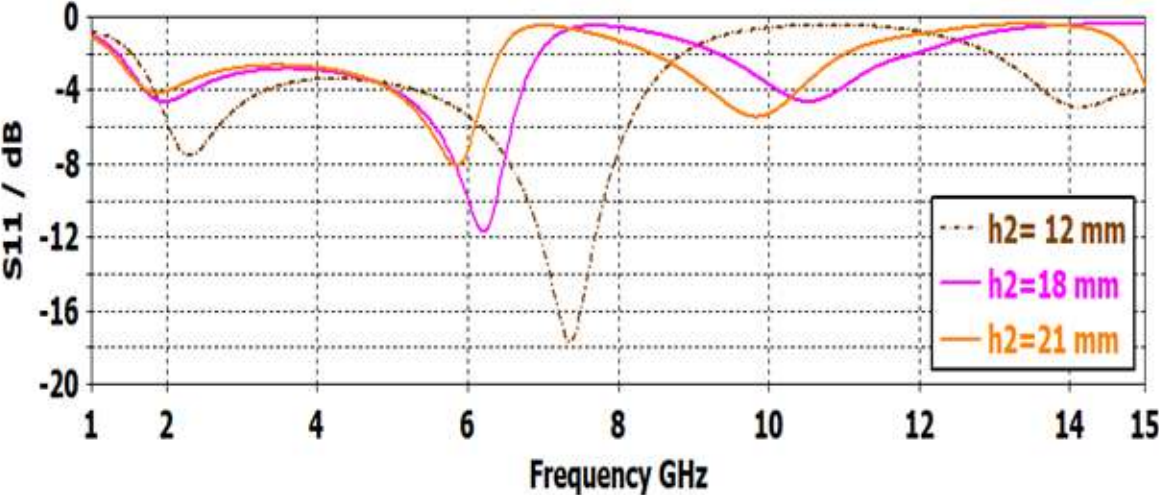
Figure 4.4: Variation of the reflection coefficient S_{11} with frequency for various air spacer thicknesses h_2, when $d_{in}=$ 14 mm, $d_{out}=$ 16 mm.

Figure 4.4 shows the obtained results for larger values of the air spacer, where it can be seen that the same trend of decreasing frequency with the increase in the value of the air-spacer. It was shown in Table 4.2, that the composite

permittivity and the effective permittivity, decrease as the air layer thickness is increased. Thus, the effective wavelength according to Eq. (3.4) will change and this will yield a slight reduction in resonance frequency. It can be noted that for larger spacer values, higher resonance also starts to appear at frequencies between 6 GHz and 8 GHz, where these can be attributed to the third mode of resonance.

Table 4.2: Reflection coefficients at resonance for various values of the air spacer thickness h_2, when d_{in}= 14 mm, d_{out}= 16 mm.

Air spacer thickness (h_2) (mm)	ε_e from Eq. (3.3)	Resonance f_1 from Eq. (3.7)	Resonance f_1 (GHz) From CST	Bandwidth (GHz)	Reflection (S_{11}) (dB)
4	1.167	2.95	3.14	0.54	-16.31
5	1.134	3	3	0.62	-29.3
7	1.096	3.04	2.73	0.56	-16.67
10	1.067	3.08	2.45	---	-9.55
12	1.055	3.09	2.30	---	-7.55
15	1.044	3.12	2.12	---	-5.64
18	1.037	3.13	1.96	---	-4.62
21	1.031	3.14	1.86	---	-4.14

4.3 Comparison between copper and resistive ring

To compare the results obtainable when using a copper ring, Fig. 4.5 shows that the resistive ring resulted in a smaller reflection coefficient of -29.39 dB. This means that the resistive ring performs much better than the copper ring because its

higher resistance leads to larger I^2R loss, and consequently small reflection coefficient.
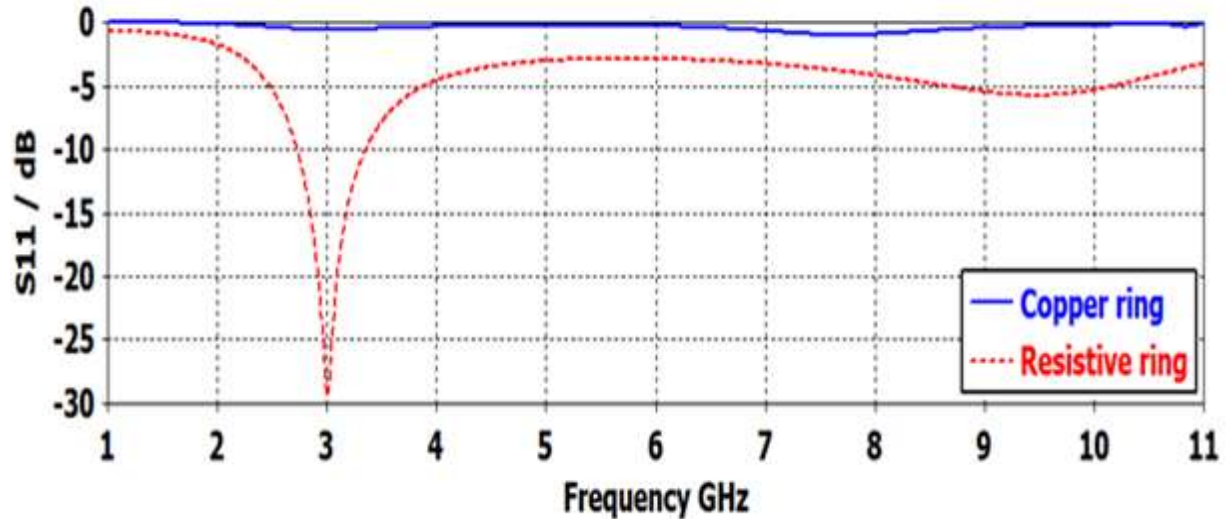
Figure 4.5: Variation of the reflection coefficients S_{11} with frequency for circular resistive ring (ρ = 10 Ohm/sq), compared to that for a copper ring.

4.4 The Resistive Split ring resonator

In this section, a split ring resonator is investigated where the ring is cut into two equal pieces, with small gaps as shown in Fig. 4.6. Figure 4.7 presents the variation of the reflection coefficient with frequency for the continuous ring and the split ring for various gap lengths. It can be seen the frequency of minimum reflection at 3 GHz has changed to about 6 GHz, as the length of each of the two arcs has become half the circumference of the ring. Moreover, another frequency above 10 GHz has appeared when the ring is cut into two pieces. This frequency represents the third order resonance compared to the continuous ring. On the other hand, the gap between the two strips forms some capacitor, whose value slightly affects the resonance frequency, as can be seen from Fig. 4.7, and the listed results in Table 4.3.

(a) FSS layer   (b) Side view   (c) Ground plane
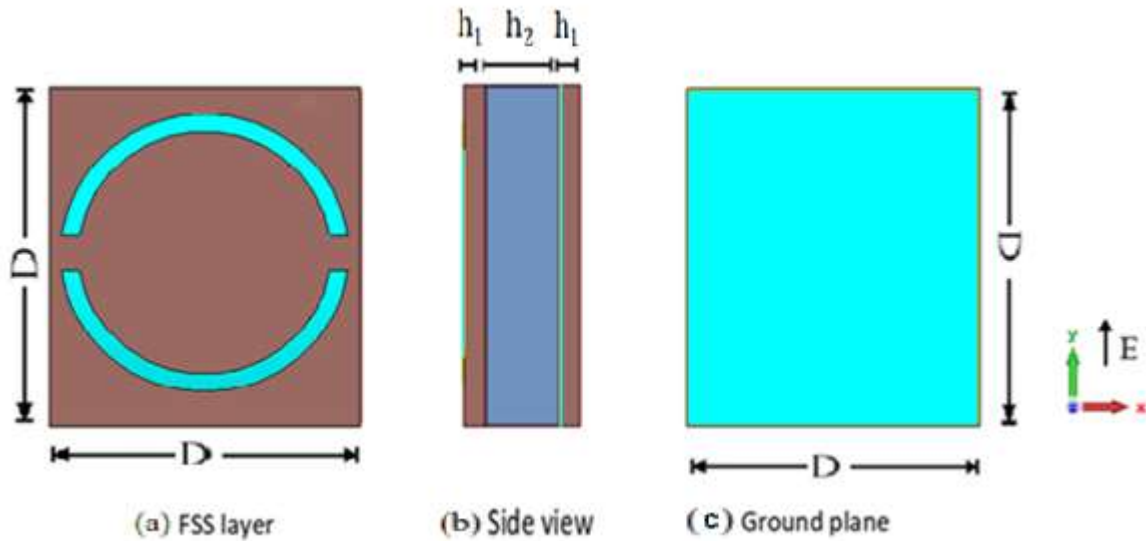
Figure 4.6 Geometry of the proposed FSS with split ring and ground plane; (a) Top view of FSS, (b) side view, and (c) top view of ground plane, h_2= 5 mm.
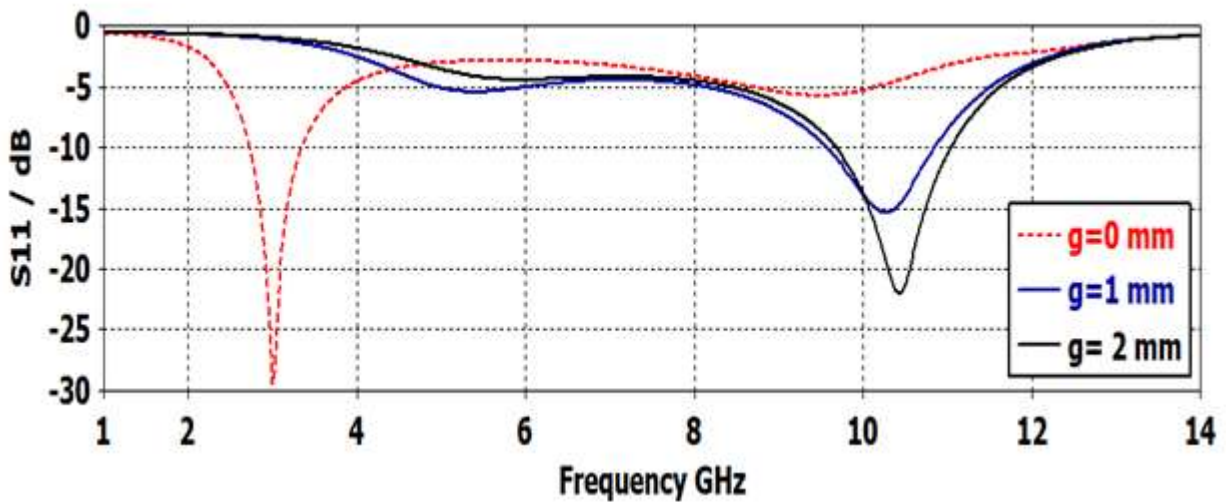
Figure 4.7: Variation of the reflection coefficients S_{11} with frequency for the 2-segment ring for various gap lengths, compared to a continuous ring.

From Table 4.3 it can be seen that the maximum bandwidth is obtained in the range of frequency of 10 GHz when the gap length is between 2 mm and 2.3 mm, where the reflection coefficient is -25.69 dB.

Table 4.3: Reflection coefficients at resonance for the 2-segment ring for various values of the gap length.

Gap length (mm)	Frequency f_1(GHz)	Reflection (S_{11}) dB	Frequency f_2(GHz)	Bandwidth (GHz)	Reflection (S_{11}) dB
0	3	-0.58	7.74	---	-0.99
0.5	5.13	-6.03	10.20	1.08	-12.90
2	5.98	-4.45	10.42	1.37	-22
2.1	6	-4.39	10.16	1.37	-23.05
2.3	6.10	-4.25	10.46	1.37	-25.69
3	6.71	-3.82	10.57	1.30	-38.1
4	7.03	-3.33	10.74	1.15	-19.27
5	7.27	-2.84	10.95	0.83	-13.51

4.5 Absorption FSS consisting of ring and resistive strip

To enhance the performance of the FSS, a resistive strip was added to the ring, where the strip was oriented horizontally along the diameter of the ring as shown in Fig. 4.8. The resistive strip is intended to absorb power from the incident wave and thus will lead to lower reflection coefficient. The width of the strip was chosen to be equal to 2 mm. Two cases were considered regarding the polarization of the incident plane wave. The first is that when the electric field is in the Y-direction (perpendicular to the strip), while in the other, the field is along the X-axis (parallel to the strip) that can be presented in the next section.
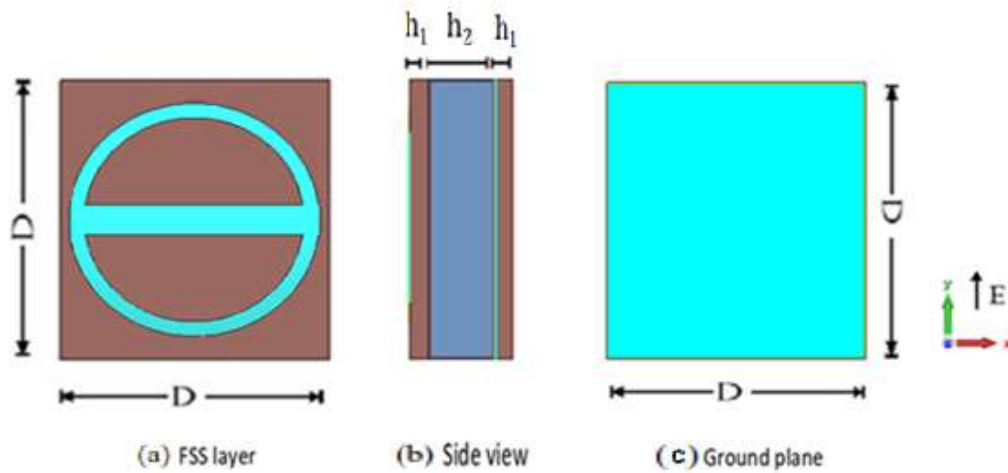
Figure 4.8: Geometry of the proposed FSS resistive ring and strip; (a) front view of FSS layer, (b) side view, and (c) back view of the ground plane.

4.5.1 Effect of the air spacer thickness on ring with resistive strip

The effect of the thickness of the air spacer on absorption is investigated, by varying its thickness from 3 mm to 18 mm, as shown in Fig. 4.9.
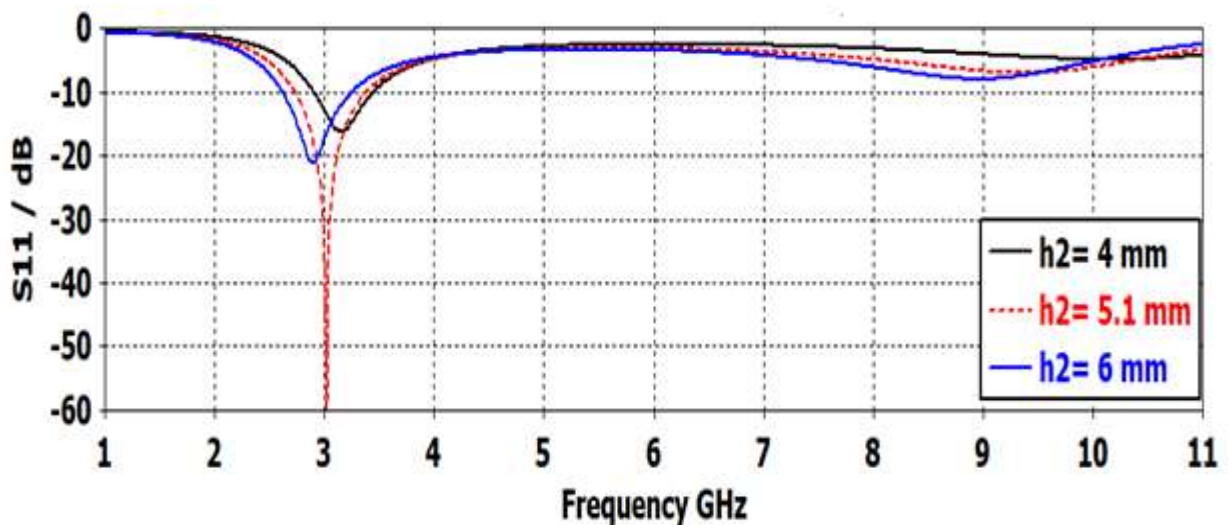
Figure 4.9: Variation of the reflection coefficient S_{11} with frequency for various air spacer thicknesses, when $\rho = 10$ Ohm/sq.

where it can be seen that there are changes in the minimum reflection coefficient as the spacer thickness is changed. A small reflection coefficient was obtained at a spacer of 5.1 mm. As illustrated in Table 4.4 it can be seen that the largest bandwidth of absorption is 0.65 GHz (2.72GHz-3.37GHz), and it was achieved at 5.1mm air spacing.

Table 4.4: Bandwidth and reflection coefficients at resonance for 10 Ohm/sq resistivity at various values of the air spacer thicknesses, when d_{in}= 14 mm, d_{out}= 16 mm.

Air spacer thickness (h_2) (mm)	Resonance f_1. (GHz)	Bandwidth (GHz)	Reflection (S_{11}) (dB)
3	3.35	0.32	-11.25
4	3.18	0.58	-17.63
4.5	3.10	0.63	-23.2
4.8	3.05	0.65	-29.5
4.9	3.04	0.65	-32.8
5	3.03	0.65	-39.9
5.1	3.01	0.65	-59.7
5.2	3	0.65	-40.07
5.3	2.98	0.65	-33.7
6	2.89	0.63	-21.1
7	2.77	0.55	-15.27
10	2.46	----	-9.01
15	2.13	----	-5.83
18	1.97	----	-4.38

4.5.2 Effect of the resistivity on ring with resistive strip pluses ground plane

In Fig. 4.10, the effect of resistivity for the ring with resistive strip and ground plane is shown. It can be seen from the figure and the results listed in Table 4.5, at the value of air spacer thickness of 5.1 mm that there is a small increase in resonance frequency to the higher values. The maximum bandwidth is attained for resistivity values between ρ =16.1 Ohm/sq and ρ =16.2 Ohm/sq.

The absorption bandwidth reaches a maximum of 0.75 GHz with reflection lower than -10 dB at those values of resistivity. The electric field is along Y-axis (perpendicular to the strip) for this case.
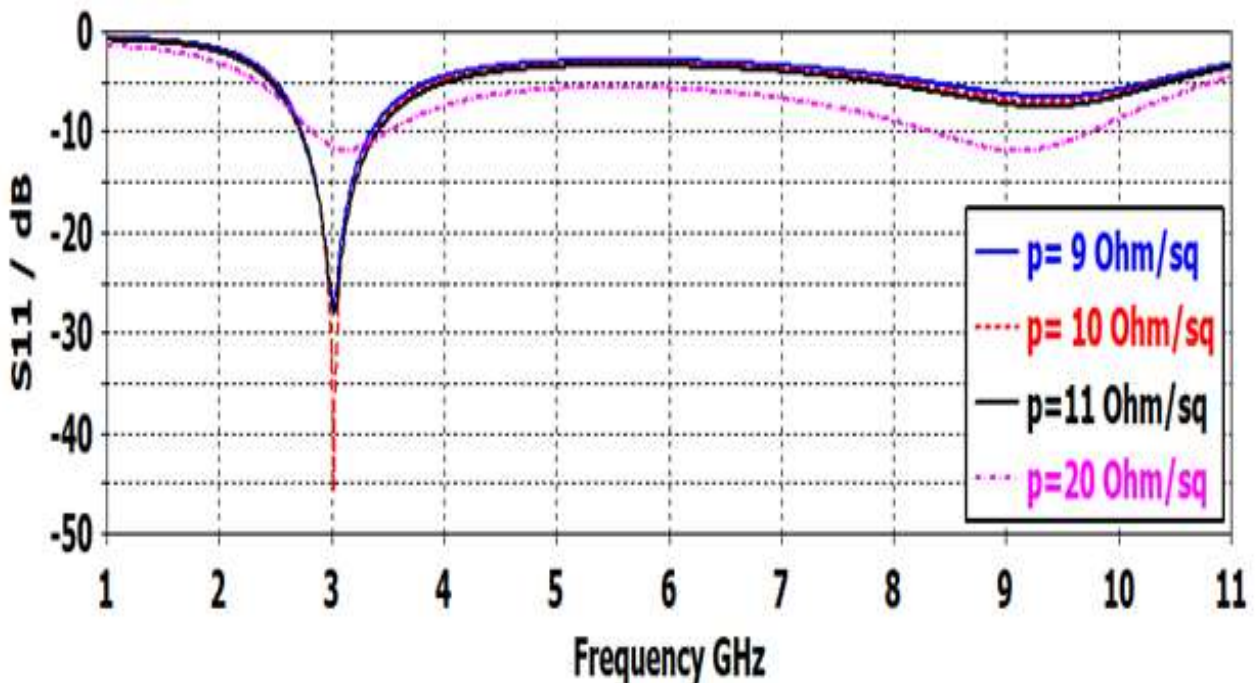
Figure 4.10: Variation of the reflection coefficient S_{11} with frequency for various values of resistivity, when the electric field is along the Y-axis (perpendicular to the strip).

Table 4.5: Bandwidth and reflection coefficient at resonance for various resistivity values, when h_2=5.1 mm, d_{in}= 14 mm, d_{out}= 16 mm, and the electric field is along Y-Axis (perpendicular to the strip).

Resistivity (Ohm/sq)	Resonance f_1 (GHz)	Bandwidth (GHz)	Reflection (S_{11}) (dB)
7	3	0.48	-16.9
8	3	0.55	-21
9	3.01	0.60	-27.55
9.9	3.01	0.80	-49.7
10	3.01	0.65	-56.68
10.1	3.01	0.66	-45.9
11	3.02	0.69	-27.98
12	3.03	0.71	-22.61
13	3.03	0.71	-19.57
15	3.05	0.74	-16
16	3.06	0.74	-14.81
16.1	3.07	0.75	-14.31
16.2	3.07	0.75	-14.61
17	3.08	0.73	-13.87
20	3.42	0.66	-11.85
30	3.40	----	-9.09

4.5.3 Effect of the diameter and resistivity at electric field along the X-axis

The simulation results when the electric field is along X-axis are shown in Fig. 4.11. The results show that there is reflection coefficient of about -10 dB at 3.25 GHz resonance frequency.
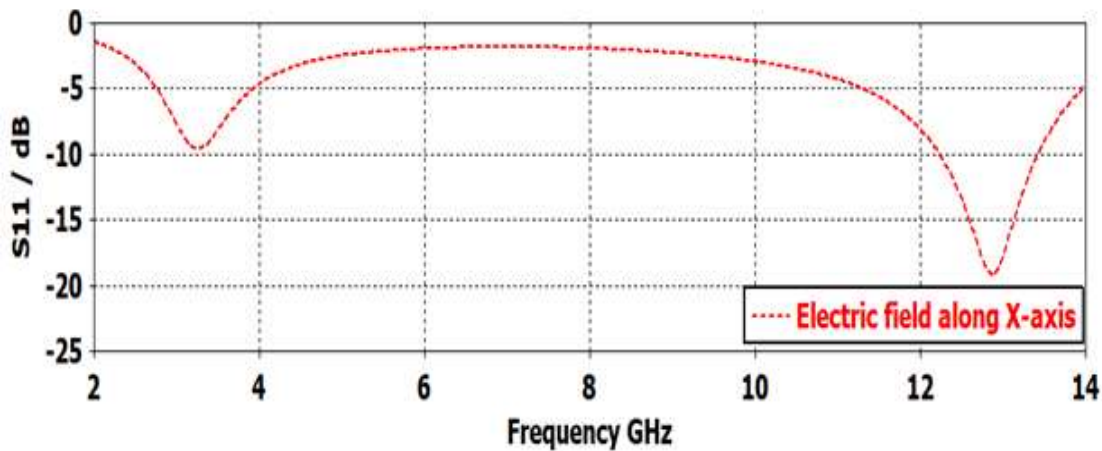
Figure 4.11: Variation of the reflection coefficients S_{11} with frequency, when the electric field is parallel to the strip.

In order to tune the resonance frequency, the ring's diameter is expanded, while the resistance is altered to provide a better response with less reflection and a wider bandwidth, these effects can be seen in Figure 4.12. An illustration of the effect of ring diameter change is provided in Table 4.6. It was found that as the diameter and the resistance is increased the absorption level increased, then decreased on the other hand the bandwidth also tend to increase. Higher bandwidth is achieved when ρ =29 Ohm/sq equal to 0.94 GHz which is located between (2.58GHz-3.52GHz).
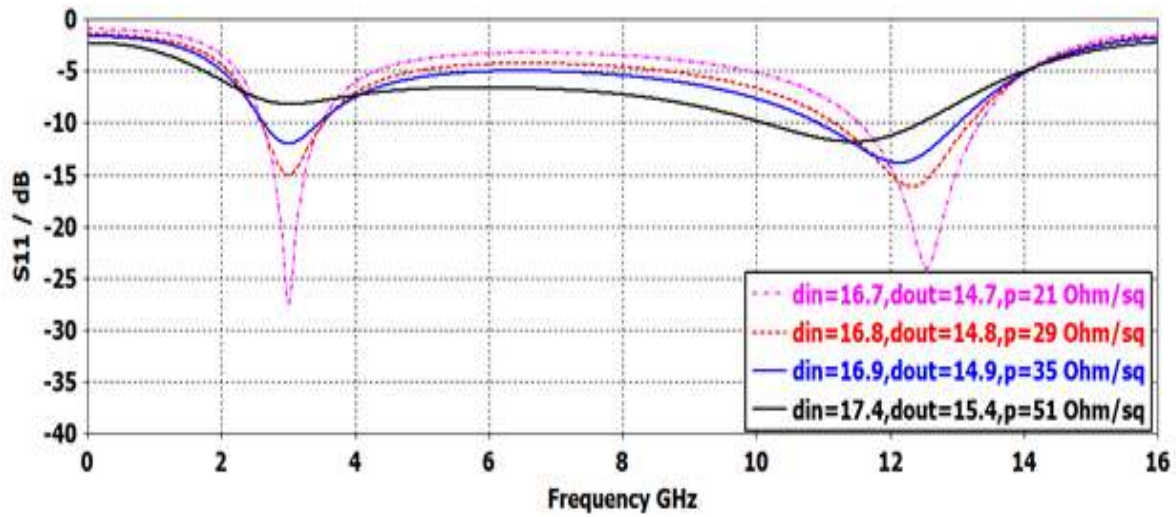
Figure 4.12: Variation of the reflection coefficient S_{11} with frequency for various values of the ring diameters and resistors, when $h_2=5$ mm.

Table 4.6: Bandwidth and reflection coefficients at resonance for 5 mm air spacer thickness at various values of the resistances and ring diameter.

d_{in} (mm)	d_{out} (mm)	Resistivity (Ohm/sq)	Resonance f_1 (GHz)	Bandwidth (GHz)	Reflection (S_{11}) (dB)
16	14	1	3.25	---	-2.05
16.6	14.4	1	3	---	-2.10
16.7	14.7	21	3	0.88	-27.48
16.8	14.8	29	3	0.94	-15.65
16.9	14.9	35	3	0.82	-12
17	15	40	3	0.51	-10.48
17.4	15.4	51	3	---	-8.18

4.5.4 Effect of the resistivity of the ring with resistive strip pluses the ground plane at electric field along the X-axis

The influence of the resistivity for the ring with resistive strip and ground plane on reflection coefficient is shown in Fig. 4.13. It can be seen that as the resistivity is increased, there is a slight shift up in the reflection coefficient at both of the resonance frequencies, while the reflection coefficient at the center of the band tend to decrease. The bandwidth increased then decreased as observed in Table 4.7. The bandwidth of the second resonance frequency is increased to infinity. Higher bandwidth of 0.94 GHz is obtained when ρ =29 Ohm.
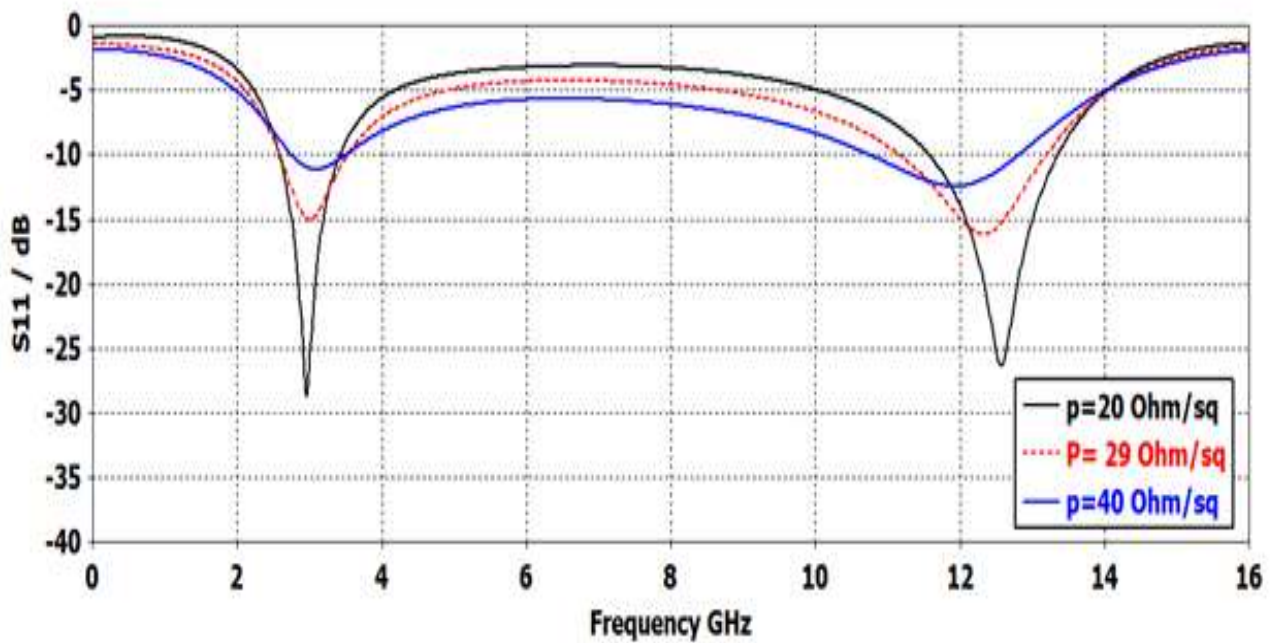
Figure 4.13: Variation of the reflection coefficient S_{11} with frequency for various values of resistivity, when the electric field is along the X-axis (parallel to the strip).

Table 4.7: Bandwidth and reflection coefficient at resonance for various resistivity values, when h_2=5 mm, d_{in}= 14.8 mm, d_{out}= 16.8 mm, and the electric field is along X-axis (parallel to the strip).

Resistivity (Ohm/sq)	Resonance f_1 (GHz)	Bandwidth (GHz)	Reflection (S_{11}) (dB)
5	2.94	---	-6.23
10	2.93	0.36	-12.15
15	2.94	0.68	-21.63
20	2.95	0.83	-28.71
28	2.98	0.93	-15.65
29	3	0.94	-15.03
30	3	0.93	-14.47
40	3.11	0.75	-11.11
50	3.22	---	-9.70

4.5.5 Effect of the Electric field direction on ring with resistive strip

The comparison between the results when the electric field is parallel and perpendicular to the strip is displayed in Fig. 4.14. When the electric field is perpendicular to the strip, the reflection coefficient is smaller than that for the case when the electric field is parallel to the strip. The difference in values of the reflection coefficients is about 15 dB at the first resonance frequency, whereas the bandwidth is smaller than the electric field along X-axis.

The current density on the ring was calculated by the CST program and the obtained results for the two cases are shown in Fig. 4.15. It can be seen that small

current density has resulted for the case of parallel electric field, and this means higher I^2R loss and lower reflection coefficient.
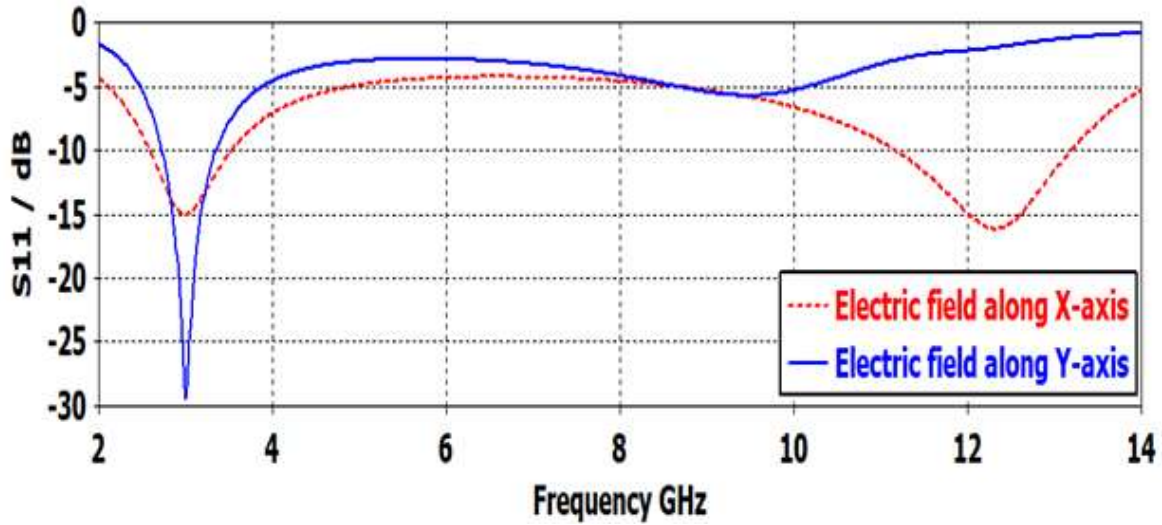
Figure 4.14: Variation of the reflection coefficients S_{11} with frequency, when the electric field is parallel and perpendicular to the strip.
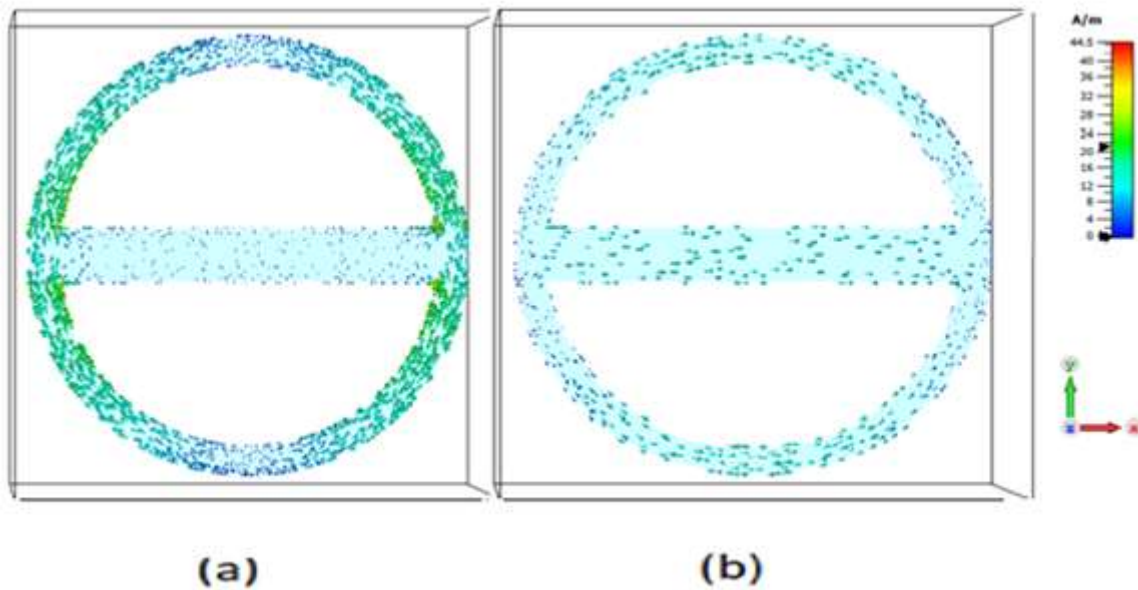
Figure 4.15: The current distribution on the ring of the FSSA; (a) The electric field is perpendicular to the strip, (b) the electric field is parallel to the strip.

4.5.6 Effect of the air spacer thickness on ring with resistive strip at electric field along the X-axis

Figure 4.16 indicates the effect of four different air spacer thickness on reflection coefficient and frequency.

From this figure it can be observed that the absorption peak gradually shifts toward the lower frequency with the increasing of h_2. The calculated absorption bands are provided in Table 4.8. The results show better absorption bandwidth is 1.01 GHz in the frequency range (2.31GHz-3.32GHz) for a thickness of 6.4–6.5 mm.
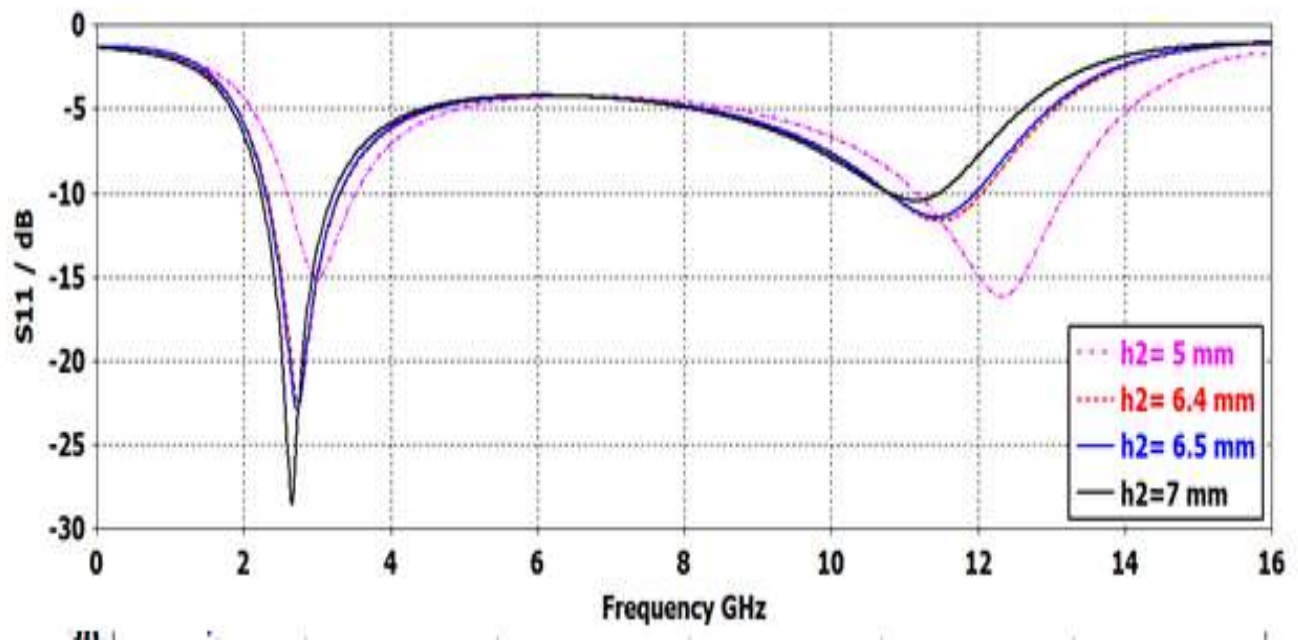
Figure 4.16: Variation of the reflection coefficient S_{11} with frequency for various air spacer thicknesses, when ρ =29 Ohm/sq, and the electric field is along X-axis (parallel to the strip).

Table 4.8: Bandwidth and reflection coefficients at resonance for 29 Ohm/sq resistivity at various values of the air spacer thicknesses, when d_{in}= 14.8 mm, d_{out}= 16.8 mm.

Air spacer thickness (h_2) (mm)	Resonance f_1 (GHz)	Bandwidth (GHz)	Reflection (S_{11}) (dB)
3	3.95	---	-9.36
4	3.19	0.63	-11.41
5	3	0.94	-15.03
5.1	2.97	0.95	-23.40
5.5	2.90	0.98	-17.15
6.4	2.73	1.01	-22.42
6.5	2.72	1.01	-22.85
6.6	2.71	1	-24.16
7	2.65	0.99	-28.53
10	2.28	0.80	-18.69
12	2.10	0.63	-14.19
18	1.73	---	-8.65

Summary

1. The FSS of a resistive circular ring printed on a substrate with an air spacer resonates when the ring circumference equals half effective wavelength.

2. The diameter of the ring and the thickness of the air spacer have an effect on the resonance frequency and band of absorption. An increase in each of them leads

to a decrease in the reflection coefficient, as well as a smaller shift in the resonance frequency.

3. A ring with a resistive strip along the diameter improves its bandwidth The absorption band is around 21% at the lowest reflection coefficient of -59.07 dB when h_2 = 5.1 mm and less than -10 dB for resistivity between 16.1 and 16.2 Ohm/sq, besides shifting in resonance frequency, whereas 36% at electric field a long X-axis.

CHAPTER FIVE

CONCLUSIONS AND FUTURE WORK

CHAPTER FIVE
CONCLUSIONS AND FUTURE WORK

5.1 Conclusions

FSS can be represented by a simple array of elements constructed in unique patterns to manage absorption bandwidth and resonant frequencies, which can be supported by corresponding circuit models. The dissertation investigated a single layer of conductive FSSA having three different configurations, as well as a resistive FSSA, a split resistive ring, and then included a resistive strip for absorption enhancement. The goal is to provide broad absorption of electromagnetic waves. The obtained conclusions are stated as follows:

1. An array of conducting rings placed on a substrate over an air spacer and the ground plane forms a simple FSS, which resonates at an effective wavelength equal to twice the circumference of the ring. The simulations in CST studio has confirmed this relation.

2. The resonance frequency of the FSS depends on the diameter of the rings and the thickness of the air spacers.

3. In the analysis of FSSA containing a single ring by the equivalent circuit model, and calculated the reflection coefficient using MATLAB program, it was found that there is no perfect impedance matching to the free space, so the design is not suitable for obtaining high absorption.

4. The impedance of the ring was calculated using the skin effect formulas and compared to that estimated value from the CST simulation.

5. Adding four lumped resistors to the ring leads to enhanced absorption. Both diameter and lumped resistors influenced the resonance frequency and absorption band, which exhibited a wide absorption bandwidth of 108% with a reflection lower than -30 dB.

6. A comparison of the FSSA with lumped resistors and a copper ring reveals that a wide absorption band was attributed to lost power in the resistors.

7. The air spacer thickness and width of the ring influence the resonance frequency and absorption band. At the same resistances and ring diameters, they all had the same absorption bandwidth of 108% and reflection coefficient. The impedance of the ring was calculated using the characteristic impedance equation of the microstrip line and compared to that estimated from the CST simulation.

8. The FSSA of a resistive circular ring printed on a substrate over a ground plane by an air spacer, resonates when the effective wavelength equals the circumference of the ring.

9. The diameter of the ring and air spacer thickness affect the resonance frequency and absorption band. The increase of each of them causes a decrease in the reflection coefficient with shifting to a lower resonance frequency.

10. From the comparison of the resistive ring and copper ring, a smaller reflection coefficient of -29.39 dB was achieved for the resistive ring.

11. A resistive strip is etched on the ring along its diameter to enhance its bandwidth. By taking into account the air spacer thickness and the resistivity of the metal, the absorption band was optimized to about 21% at the smallest reflection coefficient of -59.07 dB when $h_2 = 5.1$ mm and less than -10 dB at resistivity between 16.1 and 16.2 Ohm/sq, plus shifting lower case in resonance frequency.

5.2 Future work

The future work on this project can be focused on the development of wide absorption and a decrease in the total thickness of the absorber as well.

1. Design of an FSSA with a double square loop and optimization with a genetic algorithm.

2. Enhancemet of the absorption using semiconductor devices for controlling absorption and transmission.

3. Investigation of two layers FSS having fractal geometry as a unit cell, and using lumped resistors.

REFERENCES

References

[1] B. A. Munk, "Frequency Selective Surfaces, Theory and Design," Hoboken, NJ, USA: Wiley, 2000.

[2] W. W. Salisbury, "Absorbent body for electromagnetic waves," U.S. Patent No.: 2599944, 1952.

[3] R.L. Fante, M.T. Mccormack, "Reflection properties of the Salisbury screen, IEEE transactions on antennas and propagation, No.36, Vol.10, pp.1443-1454, 1988.

[4] Du Toit, L. J, and J. H. Cloete, "A design process for Jaumann absorbers," In Proceedings of the Digest on Antennas and Propagation Society International Symposium, San Jose (USA), pp. 1558–1561, 1989.

[5] J. Leendert, and Du Toit, "The design of Jaumann absorbers," IEEE Antennas and Propagation Magazine, " Vol. 36, No. 6, pp. 17–25, 1994.

[6] M. J. Park, J. Choi, and S. S. Kim, "Wide bandwidth pyramidal absorbers of granular ferrite and carbonyl iron powders," IEEE transactions on magnetics, Vol. 36, No. 5, pp. 3272-3274,2000.

[7] Y. Naito, and K. Suetake, "Application of ferrite to electromagnetic wave absorber and its characteristics," IEEE Trans. Microwave, Theory Tech, Vol.19, No.1, pp.65-72,1971.

[8] I. H. Baek, S.Y. Choi, H.W. Lee, W. B. Cho, V. Petrov, A. Agnesi, V. Pasiskevicius, D. Yeom, K. Kim, and F. Rotermund, "Single-walled carbon nanotube saturable absorber assisted high-power mode-locking of a Ti: sapphire laser," Optics Express, Vol. 19, No. 8, pp.7833-7838,2011.

[9] J. Yang, and Z. Shen, "A thin and broadband absorber using double-square loops," IEEE Antennas and Wireless Propagation Letters, Vol.6, pp.388-391,2007.

[10] Y. Shang, Z. Shen, and S. Xiao, "On the design of single-layer circuit analog absorber using double-square-loop array," IEEE Transactions on Antennas and Propagation, Vol.61, No.12, pp. 6022-6029,2013.

[11] O. Ayop, M. K. A. Rahim, N. A. Murad, and N. A. Samsuri, "Dual band polarization insensitive and wide angle circular ring metamaterial absorber," The 8th European Conference on Antennas and Propagation (EuCAP 2014), IEEE, pp. 955-957,2014.

[12] J. Chen, X. Huang, G. Zerihun, Z. Hu, S. Wang, G. Wang, X. Hu, and M. Liu, "Polarization-independent, thin, broadband metamaterial absorber using double-circle rings loaded with lumped resistances,"Journal of Electronic Materials, Vol. 44.No. 11, pp. 4269-4274,2015.

[13] T. K. Suchu, A. Sahu, R. Panwar, and R. Khanna, "Chip Resistor Loaded Fractal Frequency Selective Surface Based Miniaturized Broadband Microwave Absorber from 2 to 18 GHz," In International Conference on Intelligent Computing and Smart Communication 2019, Springer, Singapore, pp. 513-521,2020.

[14] S. Ghosh, S. Bhattacharyya, and K. V. Srivastava, " Design, characterization and fabrication of a broadband polarization-insensitive multi-layer circuit analogue absorber," IET Microwaves, Antennas & Propagation, Vol. 10, No.8, pp. 850-855,2016.

[15] M. Karaaslan, M. Bağmancı, E. Ünal, O. Akgol, and C. Sabah, "Microwave energy harvesting based on metamaterial absorbers with multi-layered square

split rings for wireless communications," Optics Communications, Vol. 392, pp. 31-38,2017.

[16] J. Chen, Y. Shang, and C. Liao, "Double-layer circuit analog absorbers based on resistor-loaded square-loop arrays," IEEE Antennas and Wireless Propagation, Vol. 17, No.4, pp. 591-595,2018.

[17] S. Bhattacharyya, S. Ghosh, D. Chaurasiya, and K. V. Srivastava, "Bandwidth-enhanced dual-band dual-layer polarization-independent ultra-thin metamaterial absorber," Applied Physics A, Vol. 118, No.1, pp. 207-215,2015.

[18] R. J. Langley, and E. A. Parker, "Equivalent circuit model for arrays of square loops," Electron Letters, Vol. 18, No. 7, pp. 294–296, 1982.

[19] R. J. Langley and E. A. Parker, "Double-square frequency-selective surfaces and their equivalent circuit," Electron Letters, Vol. 19, No. 17, pp. 675–676,1983.

[20] M. I. Hossain, N. Nguyen-Trong, K. H. Sayidmarie, and A. M. Abbosh, " Equivalent-Circuit Design Method for Wideband Nonmagnetic Absorbers at Low Microwave Frequencies," IEEE Transactions on Antennas and Propagation, Vol. 68, No.12, , pp. 8215 – 8220, ,2020.

[21] G. I. Kiani, A. R. Weily, and K. P. Esselle, "A novel absorb/transmit FSS for secure indoor wireless networks with reduced multipath fading," IEEE Microwave and Wireless Components Letters, Vol. 16, No. 6, pp.378-380, 2006.

[22] L.H. Tao, C. H. Feng, C.Z. Yong, and Z. D. Yong, "Absorbing properties of frequency selective surface absorbers with cross-shaped resistive patches," Materials & design, Vol. 28, No. 7, pp 2166-2171,2007.

[23] G. I. Kiani, K.L. Ford, K.P. Esselle, A.R. Weily, and C. J. Panagamuwa, "Oblique incidence performance of a novel frequency selective surface absorber," IEEE Transactions on Antennas and Propagation, Vol. 55, No. 10, pp.2931-2934,2007.

[24] C. Zhang, Q. Zhang, and M. Hu, "Frequency Selective Surface absorber loaded with lumped-element," 2007 International Symposium on Electromagnetic Compatibility, IEEE, pp. 539-542,2007.

[25] F. Costa, A. Monorchio, and G. Manara, "Analysis and design of ultra-thin electromagnetic absorbers comprising resistively loaded high impedance surfaces," IEEE transactions on antennas and propagation. Vol.58, No.5, pp.1551-1558, 2010.

[26] U. Rafique, G. I. Kiani, M. M. Ahmed, and S. Habib, "Frequency selective surface absorber for WLAN security," Proceedings of the 5th European Conference on Antennas and Propagation (EUCAP), IEEE, pp.872-875, 2011.

[27] Y. Liu, S. Gu, C. Luo, and X. Zhao, "Ultra-thin broadband metamaterial absorber," Applied Physics A, Vol.108, No.1, pp.19-24.,2012.

[28] M. Li, S. Q. Xiao, Y.Y. Bai, and B.Z. Wang, "An ultrathin and broadband radar absorber using resistive FSS," IEEE Antennas Wireless Propagation, Letters, Vol. 11, pp. 748–751, 2012.

[29] H.B. Zhang, P.H. Zhou, H.P. Lu, Y.Q. Xu, D.F. Liang, and L.J. Deng, "Resistance selection of high impedance surface absorbers for perfect and broadband absorption," IEEE Transactions on Antennas and Propagation, Vol.61, No.2, ,pp.976-979,2012.

[30] O. Ayop, M. K. A. Rahim, and N. A. Murad, "Double layer circular ring metamaterial absorber for dual-directional application at 10 GHz," 2013 IEEE International RF and Microwave Conference (RFM), IEEE, pp. 405-408,2013.

[31] W. Yuan, and Y. Cheng, "Low-frequency and broadband metamaterial absorber based on lumped elements: design, characterization and experiment," Applied Physics A, Vol.117. No.4, pp. 1915-1921,2014.

[32] D. Kundu, A. Mohan, and A. Chakrabarty, "Single-layer wideband microwave absorber using array of crossed dipoles," IEEE Antennas and Wireless Propagation Letters, Vol.15, pp. 1589-1592,2016.

[33] T. Liu, and S.S. Kim, "Design of wide-bandwidth electromagnetic wave absorbers using the inductance and capacitance of a square loop-frequency selective surface calculated from an equivalent circuit model," Optics Communications, Vol.359 pp.372-377,2016.

[34] S. Ghosh, S. Bhattacharyya, and K. V. Srivastava, "Design and analysis of a broadband single layer circuit analog absorber," 2016 46th European Microwave Conference (EuMC), IEEE, pp. 584-587,2016.

[35] T.T. Nguyen, and S. Lim, "Angle-and polarization-insensitive broadband metamaterial absorber using resistive fan-shaped resonators," Applied Physics Letters, Vol.112, No.2, pp. 021605,2018.

[36] H. Ahmad, M.U. Khan1, F. A. Tahir, R. Hussain, and M. S. Sharawi, "Microwave absorber using single-layer FSS with wideband operation above the x-band," 12th European Conference on Antennas and Propagation (EuCAP 2018), IET, pp. 1-3, 2018.

[37] L. V. Abdulhakim, and C. K. Aanandan, "A novel polarization independent wideband circuit analog absorber using crossed loops," Radio engineering, Vol. 27, No. 3, pp. 738-745, 2018.

[38] G. Haitao, W. Jianjiang, X. Baocai, L. Ze, and S. Qingtao, "Broadband metamaterial absorber based on magnetic substrate and resistance rings," Materials Research Express, Vol.6, No.4, pp. 045803,2019.

[39] K. Chen, X. Luo, G. Ding, J. Zhao, Y. Feng, and T. Jiang, "Broadband microwave metamaterial absorber with lumped resistor loading," EPJ Applied Metamaterials, Vol.6, No.1, pp.1-7,2019.

[40] S. Kalraiya, R. K. Chaudhary, and M. A. Abdalla, "Design and analysis of polarization independent conformal wideband metamaterial absorber using resistor loaded sector shaped resonators," Journal of Applied Physics.Vol.125, No.13, pp.134904,2019.

[41] D. Youssef, A. Shaker, and K. R. Mahmoud, "Double Layer-Resistive FSS Ultra Wideband Absorber with Improved Thickness to Bandwidth Ratio," 2019 7th International Japan-Africa Conference on Electronics, Communications, and Computations, (JAC-ECC), IEEE, pp. 140-143, 2019.

[42] P. Zhou, Q. Huang, L. Ji, and X. Shi, "Design of a thin broadband metamaterial absorber based on resistance frequency selective surface," The Applied Computational Electromagnetics Society Journal (ACES), Vol. 34, No. 10, pp. 1494-1499,2019.

[43] T. Q. H. Nguyen, T.K. T. Nguyen, T. N. Cao, H. Nguyen, and L. G. Bach, "Numerical study of a broadband metamaterial absorber using a single split circle ring and lumped resistors for X-band applications," AIP Advances, Vol.10, No.3, pp.035326, 2020.

[44] R. Liu, B. Zhang, J. Duan, L. Dong, J. Yu, and Z. Zhang, "Composite structure-based transparent ultra-broadband metamaterial absorber with multi-applications," Materials Research Express, Vol. 7, No. 4, pp. 045803,2020.

[45] Z. Khan, T. Ejaz, T. Zaidi, and H. Imtiaz, " design of FSS based microwave absorber for wideband absorption applications," EURASIAWEB, International Conference At: Kopavogur, Iceland, pp. 1-6,2020.

[46] G. Deng, K. Lv, H. Sun, Y. Hong, X. Zhang, Z. Yin, and J. Yang, "Wideband absorber based on conductive ink frequency selective surface with polarization insensitivity and wide-incident-angle stability," Nanomaterials and Nanotechnology, Vol. 10, pp. 1847980420935718,2020.

[47] S. Fan, and Y. Song, "Ultra-wideband flexible absorber in microwave frequency band," Materials Vol. 13. No. 21, pp. 4883, 2020.

[48] E.P.d. Santos, A. L. P. S. Campos, A. G. Neto, and M. W. B. Silva, "Proposed Technique of Analysis for Absorber/Transmitter Frequency Selective Surfaces," Journal of Microwaves, Optoelectronics and Electromagnetic Applications, Vol. 20, No. 2, pp. 435-444,2021.

[49] G. Singh, A. Bhardwaj, K.V. Srivastava, J. Ramkumar, and S. A. Ramakrishna, "Perforated lightweight microwave metamaterial broadband absorber with discontinuous ground plane," Applied Physics A, Vol. 127, pp. 1-9,2021.

[50] S. Liao, "microwave device and circuit," 3rd Edition, 1996.

[51] A. T. Mayouf, K. H. Sayidmarie, and Y.E Mohammed Ali, "A Dual stopband two-sided frequency selective surface for mobile shielding applications," IOP Conference Series: Materials Science and Engineering. Vol. 1152. No. 1. IOP Publishing, 2021.

[52] E. Martini, F. Caminita, M. Nannetti, and S. Maci, "Fast analysis of FSS radome for antenna RCS reduction," IEEE Antennas and Propagation Society International Symposium, pp. 1801-1804, 2006.

[53] C. H. Tong, "Interference theory of metamaterial perfect absorbers," Optics express, Center for Integrated Nanotechnologies, Los Alamos National Laboratory, Los Alamos, New Mexico 87545, USA, Vol. 20, No. 7, pp. 7165-7172, 2012.

[54] H. Wakatsuchi, J. Paul, and C. Christopoulos, "Performance of customizable cut-wire-based metamaterial absorbers: Absorbing mechanism and experimental demonstration," IEEE transactions on antennas and propagation, Vol. 60, No. 12, pp. 5743-5752, 2012.

[55] F. Bayatpur, "Metamaterial-Inspired Frequency-Selective Surfaces," PhD diss, University of Michigan, 2009.

[56] E. A. Parker, and A.N.A. El Sheikh, "Convoluted array elements and reduced size unit cells for frequency-selective surfaces," IEE Proceedings H-Microwaves, Antennas and Propagation, Vol. 138. No. 1. IET, 1991.

[57] W. Zuo, Y. Yang, X. He, D. Zhan, and Q. Zhang, "A miniaturized metamaterial absorber for ultrahigh-frequency RFID system," IEEE Antennas and Wireless Propagation Letters, Vol. 16, pp. 329-332, 2016.

[58] X. Zhang, S. Liu, Q. Yu, L. Wang, and K. Liao, "A miniaturized high-performance broadband absorber based on 2.5-D meander lines and magnetic materials at low frequencies," International Journal of RF and Microwave Computer-Aided Engineering, Vol. 31, No. 5, p.e22601, 2021.

[59] P. Munaga, S. Ghosh, S. Bhattacharyya, and K.V. Srivastava, "A fractal-based compact broadband polarization insensitive metamaterial absorber using lumped resistors," Microwave and Optical Technology Letters, Vol. 58, No. 2, pp. 343-347,2016.

[60] M. W. B. Silva, A. L. P. S. Campos, and L. C. Kretly, "Design of thin microwave absorbers using lossy frequency selective surfaces," Microwave and Optical Technology Letters, Vol. 57, No. 4, pp. 928-933,2015.

[61] T. Liu, and S.S. Kim, "Ultrawide bandwidth electromagnetic wave absorbers using a high-capacitive folded spiral frequency selective surface in a multilayer structure,"Scientific reports, Vol. 9, No. 1, pp. 1-10, 2019.

[62] M. Basravi, M. Maddahali, Z. H. Firouzeh, and A. Ramezani, "Design of a novel ultra broadband single-layer absorber using double fractal square loops," 2016 24th Iranian Conference on Electrical Engineering (ICEE), IEEE, pp. 621-625, 2016.

[63] F. Li, C. Meng, F. Meng, D. Fan, and P. Chen, "A thin broadband microwave absorber with hexagonal resistive frequency selective surface," IEEE Antennas and Wireless Propagation Letters, 2018.

[64] Liu, Tian, and Sung-Soo Kim, "Ultrawide bandwidth electromagnetic wave absorbers composed of double-layer frequency selective surfaces with different patterns," Scientific reports, Vol. 8, No. 1, pp. 1-10,2018.

[65] A. Sharma, S. Ghosh, and K.V. Srivastava, "A polarization-insensitive band-notched absorber for Radar Cross Section reduction," IEEE Antennas and Wireless Propagation Letters, Vol. 20, No. 2, pp. 259-263,2020.

[66] A. Sharma, S. Malik, S. Ghosh, and K. V. Srivastava, "A Miniaturized Band-Notched Absorber for Wideband RCS Reduction," 2020 International Symposium on Antennas and Propagation (ISAP). IEEE, pp. 813-814, 2021.

[67] A. Bhardwaj, G. Singh, K. V. Srivastava, J. Ramkumar, and S. A. Ramakrishna, "Polarization Insensitive Optically Transparent Microwave Metamaterial Absorber using Complementary Layer," IEEE Antennas and Wireless Propagation Letters, pp. 1536-1225, 2021.

[68] R.T. Cock, "Design of a two Design of a two-Layer, Capacitively Coupled, Microstrip Patch Antenna Element for Broadband Applications," Thesis, University of Central Florida, 1986.

[69] R.T. Cock, and C. Christodoulou, "Design of a two-layer, capacitively coupled, microstrip patch antenna element for broadband applications," 1987 Antennas and Propagation Society International Symposium. IEEE, Vol. 25, pp. 936-939, 1987.

[70] Balanis, Constantine A, " Advanced engineering electromagnetics". John Wiley & Sons, New York, 1989.

الخلاصة

تقدم هذه الرسالة استخدام طبقة ماصة للموجات الكهرومغاطيسية متحسسة للترددات من خلال اقتراح ودراسة عدة تصاميم من السطوح الممتصة للترددات. اظهرت نتائج التحكم بالمعالم الهندسية للتصاميم امكانية الحصول على سطح ماص ذي حزمة امتصاص عريضة التي يمكن الاستفادة منها في تطبيقات تجميع الطاقة والحماية من الموجات الكهرومغناطيسية.

تم اقتراح تصميم سطح حساس مكون من حلقة متصلة من النحاس مثبته على طبقة عازلة تفصلها فجوة هوائية عن طبقة ارضية مستوية من النحاس لمنع مرور الاشارة عبر السطح الحساس للتردد. تم تنفيذ التصميم واستحصال النتائج باستخدام برنامج CST. تم تحليل واشتقاق صيغة لمعامل الانعكاس بواسطة موديل الدائرة المكافئ ومن ثم فحصها باستخدام برنامج MATLAB. تمت ايضا دراسة خسارة السطح الممتص نظريا ومقارنتها بتلك المقدرة من محاكاه النظام.

تم عرض دراسة تاثير سطح ممتص باستخدام حلقة متصلة بأربع مقاومات بجميع الاتجاهات لتعزيز اداء الامتصاص. اظهرت نتائج التصميم ذو الاربع مقاومات تحسننا في عرض النطاق الترددي بتغير عدة بارامترات مختلفة. تم استخلاص دائرة مكافئة للسطح المقترح مع اشتقاق وتخمين انعكاسية التصميم ضياع الامتصاص.

تم اقتراح تصميم يتضمن حلقة مقاومية متصلة وطبقة مقاومية ارضية لتعزيز الامتصاص. تم التحقق من تأثير كل من ابعاد الحلقة والفجوة الهوائية. بينت النتائج تحسنا كبيراً بالامتصاص بمقدار 29 dB مقارنة مع حالة الحلقة الموصلة.

تم تطوير التصميم بإضافة شريط مقاومي للحلقة وربطه بالاتجاه الافقي للهيكل ذي الحلقة المقاومية المتصلة وطبقة مقاومية الارضية. تم التحقق من تأثير تغير المجال الكهربائي الموازي والافقي و توزيع التيار الكهربائي, دراسة تاثير عدة معالم. اظهرت النتائج تقدما ملحوظة في عرض النطاق الترددي للامتصاص.

إقرار لجنة المناقشة

نشهد بأننا أعضاء لجنة التقويم والمناقشة قد اطلعنا على هذه الرسالة الموسومة (دراسة السطوح المنتقية للترددات الكهرومغناطيسية (FSS) ذات خصائص امتصاص) وناقشنا الطالبة (آمنه جمال رشيد) في محتوياتها وفيما له علاقة بها بتاريخ ٢٠٢٢/٤/٢٥ وقد وجدناها جديرة بنيل شهادة الماجستير/علوم في اختصاص هندسة الاتصالات.

التوقيع:

رئيس اللجنة: أ.د. جعفر رمضان محمد

التاريخ: / / ٢٠٢٢

التوقيع:

عضو اللجنة: أ.م.د. ياسر احمد فاضل

التاريخ: / / ٢٠٢٢

التوقيع:

عضو اللجنة: د. ادهم معن صالح

التاريخ: ٢٠٢٢/٥/٨

التوقيع:

عضو اللجنة/المشرف:أ.د. خليل حسن سيد مرعي

التاريخ: / / ٢٠٢٢

قرار مجلس الكلية

اجتمع مجلس كلية هندسة الالكترونيات بجلسته المنعقدة بتاريخ: / / ٢٠٢٢

وقرر المجلس منح الطالبة شهادة الماجستير علوم في اختصاص هندسة الاتصالات

مقرر المجلس: أ.م.د. صدقي بكر ذنون

التاريخ: / / ٢٠٢٢

رئيس مجلس الكلية: أ.د. خالد خليل محمد

التاريخ: / / ٢٠٢٢

إقرار المشرف

أشهد بأن هذه الرسالة الموسومة (دراسة السطوح المنتقية للترددات الكهرومغناطيسية (FSS) ذات خصائص امتصاص) تم اعدادها من قبل الطالبة (أمنه جمال رشيد) تحت اشرافي في قسم هندسة الاتصالات / كلية هندسة الالكترونيات / جامعة نينوى، وهي جزء من متطلبات نيل شهادة الماجستير علوم في اختصاص هندسة الاتصالات.

التوقيع:

الاسم: أ.د. خليل حسن سيد مرعي

التاريخ: /   / ٢٠٢٢

إقرار المقوم اللغوي

اشهد بأنه قد تمت مراجعة هذه الرسالة من الناحية اللغوية وتصحيح ما ورد فيها من أخطاء لغوية وتعبيرية وبذلك أصبحت الرسالة مؤهلة للمناقشة بقدر تعلق الأمر بسلامة الأسلوب أو صحة التعبير.

التوقيع:
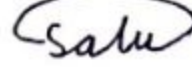
الاسم: م.د. صالح عبد الله عبد الرحمن

التاريخ: /   / ٢٠٢٢

إقرار رئيس لجنة الدراسات العليا

بناءً على التوصيات المقدمة من قبل المشرف والمقوم اللغوي أرشح هذه الرسالة للمناقشة.

التوقيع:

الاسم: أ.م.د محمود احمد محمود

التاريخ: /   / ٢٠٢٢

إقرار رئيس القسم

بناءً على التوصيات المقدمة من قبل المشرف والمقوم اللغوي ورئيس لجنة الدراسات العليا أرشح هذه الرسالة للمناقشة.

التوقيع:

الاسم: أ.م.د. محمود احمد محمود

التاريخ: /   / ٢٠٢٢

دراسة السطوح المنتقية للترددات الكهرومغناطيسية (FSS)

ذات خصائص امتصاص

رسالة تقدمت بها

آمنه جمال رشيد

مجلس كلية هندسة الالكترونيات
جامعة نينوى

كجزء من متطلبات نيل شهادة الماجستير في

هندسة الاتصالات

بأشراف

الأستاذ الدكتور خليل حسن سيد مرعي

وزارة التعليم العالي والبحث العلمي

جامعة نينوى

كلية هندسة الالكترونيات

قسم هندسة الاتصالات

دراسة السطوح المنتقية للترددات الكهرومغناطيسية (FSS)

ذات خصائص امتصاص

آمنه جمال رشيد

رسالة ماجستير علوم في هندسة الاتصالات

بأشراف

الأستاذ الدكتور خليل حسن سيد مرعي

1443 هـ   2022 م